UNIVERSITY OF OKLAHOMA

GRADUATE COLLEGE

ONLINE CLOSED-LOOP tACS-fMRI FOR BRAIN MODULATION

A DISSERTATION

SUBMITTED TO THE GRADUATE FACULTY

in partial fulfillment of the requirements for the

Degree of

DOCTOR OF PHILOSOPHY

in Electrical & Computer Engineering

By

BENI MULYANA
Norman, Oklahoma
2022

ONLINE CLOSED-LOOP tACS-fMRI FOR BRAIN MODULATION

A DISSERTATION APPROVED FOR THE SCHOOL OF ELECTRICAL AND COMPUTER ENGINEERING

BY THE COMMITTEE CONSISTING OF

Dr. Samuel Cheng, Chair

Dr. Yuan Yang, Co-chair

Dr. Hamed Ekhtiari

Dr. Sahib Khalsa

Dr. Gregory MacDonald

This is dedicated to my mother who always gives motivation and prays for my goodness. Also, to Eni Puji Lestari and Qalesya Mulya, my wife and my lovely daughter who faithfully accompanies me in any situation during study and always gives joy and enthusiasm to everything.

Acknowledgments

Struggling for something we desire will surely be filled with challenges. However, facing challenges will feel lighter because of the support of many people around us. This dissertation is the work of numerous people. Firstly, I would like to express my deepest gratitude and respect to Dr. Samuel Cheng and Dr. Jerzy Bodurka for their support, both academic and non-academic, during my life and study in the US and their incredible support and guidance. I am grateful to Dr. Jerzy Bodurka for his kindness and cheers since I came to the US until the end of his life. Dr. Jerzy Bodurka had opened up new perspectives for thought and created the seed of invaluable research space on brain imaging. He is an unforgettable person in my life. Likewise, Dr. Samuel Cheng is always willing to help me pave the way and offer advice, support, and generosity at all times serving my questions and outpourings through long chats at any time and unconditionally for going through this study. I also want to express my deepest gratitude to Dr. Hamed Ekhtiari for all the ideas and help to develop great ideas about combining tES and fMRI and for providing literature to support the thesis that is being built. This is an invaluable support and help because ideas are the essence of all creativities. My gratitude also must go to other committee members: Dr. Yang Yuan, Dr. Sahib Khalsa, and Dr. Gregory MacDonald, for their comments, feedback, and tremendous encouragement in going through all of this study. During my study, experiments, and writing manuscript, I obtained great teamwork from Dr. Jerzy Bodurka's lab. Therefore, I am grateful to Dr. Masaya Misaki, Dr. Aki Tsuchiyagaito, Jared Smith, Julie Arterbury, Bill Alden, Julie DiCarlo, and Greg Hammond. I have gained so much experience, and they are very patient people to help me in the manuscript writing and experiment with all sincerity. My gratitude also to Dr. Ghazaleh Soleimani and Dr. Rayus Kuplicki for online meeting with me regularly and

providing me feedback and comments, which nourish my academic growth. Thanks to the Laureate Institute for Brain Research, including all staff who have offered support and training opportunities. This work would not have been possible without generous access to the state of the art of the online closed-loop tES-fMRI devices, datasets, and high-quality facilities. In particular, my gratitude to Dr. Martin Paulus for his guidance and support for me and my family, especially after Dr. Jerzy Bodurka passed, who is very important for survival in the US and undergoes this study. I also thank all OU-Tulsa staff who have helped me a lot in administration during my study. Finally, I would like to thank the institution that funded my work: the William K. Warren Foundation and, in part, the Brain & Behavior Research Foundation through a NARSAD young investigator grant (#27305 to Dr. Hamed Ekhtiari).

Contents

List of Figures

Abstract

Recent studies suggest that transcranial electrical stimulation (tES) can be performed during functional magnetic resonance imaging (fMRI). The novel approach of using concurrent tES-fMRI to modulate and measure targeted brain activity/connectivity may provide unique insights into the causal interactions between the brain's neural responses and psychiatric/neurologic signs and symptoms, and importantly, guide the development of new treatments. However, tES stimulation parameters to optimally influence the underlying brain activity may vary with respect to the phase difference, frequency, intensity, and electrode montage among individuals. The dissertation proposes a protocol for closed-loop tES-fMRI to optimize the frequency and phase difference of alternating current stimulation (tACS) for two nodes (frontal and parietal regions or called as frontoparietal regions) in individual participants. It is carefully considered the challenges in an online optimization of tES parameters with concurrent fMRI, specifically in its safety, artifact in fMRI image quality, online evaluation of the tES effect, and parameter optimization method, and the protocol is designed to run an effective study to enhance frontoparietal connectivity and working memory performance with the optimized tACS using closed-loop tES-fMRI. The dissertation provides technical details of the protocol, including electrode types, electrolytes, electrode montages, concurrent tES-fMRI hardware, online fMRI processing pipelines, and the optimization algorithm. Result analyses confirmed the implementation of this protocol worked successfully to improve frontoparietal connectivity compared to the control group. However, it did not give a significant difference in working memory improvement compared to the control group. Therefore, through literature study, in the future work Chapter, a better protocol is proposed to enhance the stimulation effect by including electrode montage and electric current optimization.

Chapter 1: Primer on tES-fMRI analysis

1.1 Introduction

Functional neuroimaging facilitates the study of the neural correlates of behavior and its underlying processes. However, functional neuroimaging cannot establish causality for brain-behavior relationships by itself. A combination of non-invasive brain stimulation techniques, such as transcranial electric stimulation (tES) combined with functional neuroimaging allows researchers to modulate neural activity patterns and establish causal relationships between specific brain regions and cognitive processes (Clark et al., 2012; Ligneul, Obeso, Ruff, & Dreher, 2016). Initially, tES combined with fMRI was recorded sequentially in order to study the neural mechanisms involved in the offline effects of tES (Esmaeilpour et al., 2020; Ruttorf, Kristensen, Schad, & Almeida, 2019).

The latest advancements in tES technology have enabled concurrent tES-fMRI (where acquired fMRI data during tES) to be technically feasible in principle so that we can monitor the immediate (online) effects of tES. The novel approach of using concurrent tES-fMRI to modulate and measure targeted brain activity/connectivity may provide unique insights into the causal interactions between the brain's neural responses and psychiatric/neurologic signs and symptoms and, importantly, guide the development of new treatments. However, tES stimulation parameters to optimally influence the underlying brain activity may vary with respect to phase, frequency, intensity, and electrode placement. We delineate how a closed-loop tES-fMRI study of frontoparietal network modulation can be designed and performed. The dissertation also discusses

the challenges of running a concurrent tES-fMRI, describing how we can distinguish clinically meaningful physiological changes caused by tES from tES-related artifacts.

One of the main challenges in transcranial electrical stimulation (tES) studies is inter-and intra-individual variability in behavioral and neural responses to tES. Brain-function, as well as brain-structure, can be considered as the two main sources of inter-and intra-individual variations in response to tES. To minimize variations emerge a large methodological parameter space including; electric current intensity, electrode placement, and tES parameters that should be carefully optimized for closed-loop tES-fMRI brain modulation. Therefore, in chapter six, the dissertation proposes a new pipeline regarding individual parameters optimization in the general form, which would work better than one-size-fits-all paradigms. The dissertation provides technical details on how to test and monitor the safety and quality of tES-fMRI settings during the study to ensure they do not exceed safety standards. It also reports the results of the feasibility and applicability of closed-loop tES-fMRI, and it discusses the potential hypotheses for the outcomes.

1.2 Transcranial electrical stimulation

Transcranial electrical stimulation (tES) provides electric current stimulation over the scalp to modulate specific brain regions' neural activity or their functional connectivity (Bikson et al., 2019). This method can be concurrently combined with functional magnetic resonance imaging (fMRI). Such a tES-fMRI combination has several technical advantages (Saiote, Turi, Paulus, & Antal, 2013; Williams et al., 2017) compared with 1) sequential fMRI-tES-fMRI in terms of the ability to investigate ongoing brain activity, and 2) simultaneous tES-electroencephalography (EEG) in terms of higher spatial resolution and fewer problems with stimulation artifacts. A major advantage of concurrent tES with fMRI is: that we can stimulate several regions of the brain by

tES (i.e., two nodes of a network with conventional or high definition (HD) electrode montages) and evaluate its online stimulation effect by fMRI to reveal associations between brain stimulation and whole-brain activity/connectivity (Bächinger et al., 2017; Cabral-Calderin, Williams, Opitz, Dechent, & Wilke, 2016; Violante et al., 2017; Vosskuhl, Huster, & Herrmann, 2016).

tES is a non-invasive brain stimulation (NIBS) technique including direct (tDCS), alternating current (tACS) and random noise stimulation (tRNS) as shown in Figure 1-1 (Bikson et al., 2019; Yavari, Nitsche, & Ekhtiari, 2017). Although all tES methods can target large scale brain networks, tACS has the unique potential to modulate oscillations within or between the large-scale brain networks using alternating currents at a chosen frequency and phase difference between network nodes to interact with synchronization-based functional connectivity (Ruffini, Fox, Ripolles, Miranda, & Pascual-Leone, 2014). In this study will use tACS device and do online closed-loop tACS parameters optimization concurrent with fMRI to find the highest frontoparietal connectivity.

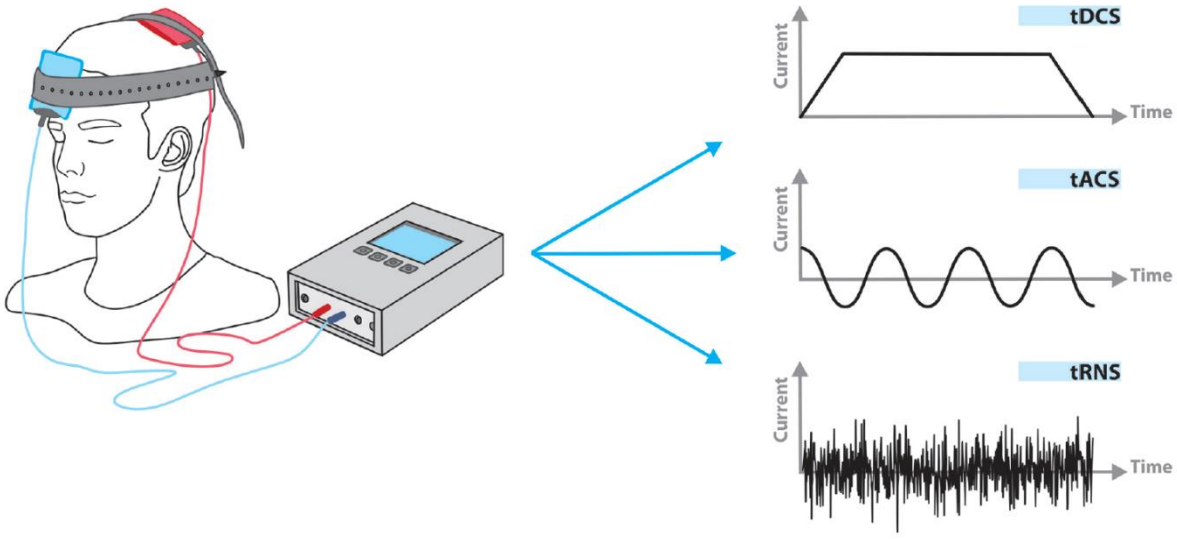

Figure 1-1: Schematic of tES modalities

1.3 Functional Magnetic Resonance Imaging

Functional magnetic resonance imaging (fMRI) is a non-invasive and safe technique for monitoring and imaging brain activity. An increasing number of studies are using it to understand better how the healthy brain functions and how the normal function is impaired in disease. Brain activity is measured using fMRI, which detects changes in blood flow. The fact that cerebral blood flow and neuronal activation are linked is used in this approach. When a part of the brain is used, blood flow to that part of the brain increases as well (Logothetis, Pauls, Augath, Trinath, & Oeltermann, 2001). The main form of fMRI uses blood-oxygen-level-dependent (BOLD) contrast. The signal-to-noise ratio (SNR) limits the spatial resolution of fMRI. The standard fMRI voxel size is 2–4 mm to keep an acceptable SNR (Glover, 2011). The spatial resolution of fMRI is significantly improved over EEG/MEG, which has a resolution of more than 10-20 mm. Moreover, EEG / MEG imaging is worse because it has a confounding that scalp recording can be spatially distorted by heterogeneous electrical conduction paths in the brain and skull.

However, fMRI's temporal resolution is limited by the hemodynamic response time; typically, the BOLD response is 5-6 s wide after the onset of a brief neural stimulus. It moves at a much slower rate than the underlying neural processes, so the temporal information is unclear. Therefore, to improve fMRI temporal resolution, a multimodal approach combining fMRI and EEG might be applied to reconstruct electrophysiology with high temporal resolution using fMRI maps as a spatial priority, resulting improvement in resolution in spatial and temporal dimensions.

1.4 tACS-fMRI

The blood oxygenation level-dependent (BOLD) fMRI signal relies on the blood flow response to neuronal activity, which is much slower than the activity of the individual neuron. The BOLD response starts to increase some seconds after the respective change in neural activation. However, cofluctuations of the BOLD signal across brain areas may result from oscillatory synchronization facilitating communication between those regions (Buzsáki & Draguhn, 2004; Canolty & Knight, 2010). Findings from concurrent EEG-fMRI studies supported the above statement. Concurrent EEG-fMRI studies demonstrated the association of inter-area oscillatory and BOLD signal synchronization (Mantini, Perrucci, Del Gratta, Romani, & Corbetta, 2007; Whitman, Ward, & Woodward, 2013). Therefore, functional connectivity across various brain regions may serve as an indirect marker to measure the functional connectivity established by the internal oscillatory synchronization of those regions. External oscillatory stimulation above several cortical regions using multi-site tACS has been demonstrated to increase internal oscillatory synchronization and functional connectivity between brain regions as well as cognitive function (Cabral-Calderin et al., 2016; Kuo & Nitsche, 2012; Moisa, Polania, Grueschow, & Ruff, 2016; Violante et al., 2017; Weinrich et al., 2017; Williams et al., 2017; Zoefel, Archer-Boyd, & Davis, 2018). Moreover, the flow of information between brain areas may also be flexibly reconfigured through phase synchronization (Akam & Kullmann, 2014; Womelsdorf et al., 2007), and functional connectivity across distant brain regions is modulated in a phase-dependent manner (Violante et al., 2017). However, determining the ideal configuration of a multi-site tACS system aimed at modulating brain networks is complex as the effects of tACS are highly dependent on the stimulation parameters such as stimulation intensity, frequency, and inter-regional phase differences, selection of electrode locations and individual differences in brain structure (Antal & Paulus, 2013). For example, a plausible range of stimulation frequencies (0.1-100 Hz) and phase differences (0-359°)

between stimulation sites (Lorenz et al., 2019) result in a wide range of possibilities. Establishing optimization algorithms might aid in the clinical application of tACS. Therefore, concurrent tACS-fMRI can be used to verify the changes of brain networks targeted by tACS. More precisely, an online fMRI measurement will enable us to establish empirically an optimization algorithm by identifying the stimulation parameters (i.e., frequency and phase differences in this study) which

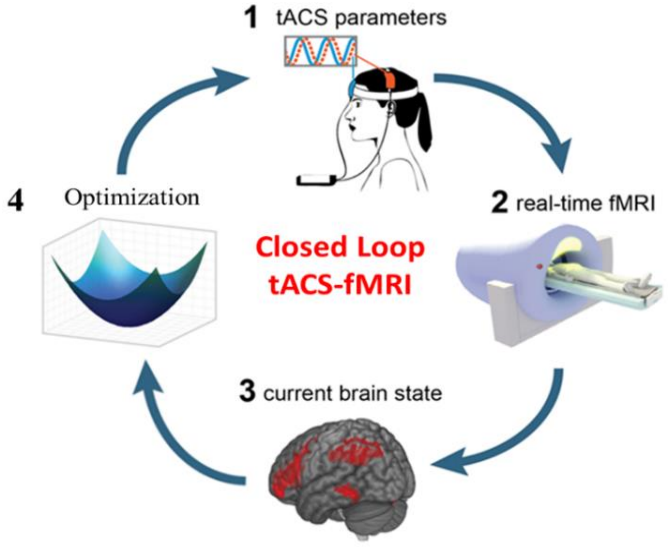

Figure 1-2: Online closed-loop tACS-fMRI.

(1). After subject capped by two electrodes sites and ready for fMRI scanning, the initial stimulus with specific tACS parameters is given to the electrode's sites. (2) and (3). During fMRI scanning, the online real-time functional connectivity (brain-state) between two sites is calculated using a sliding window. (4). The online real-time target functional connectivity is fed to the optimizer, which calculates the best values of both stimulation parameters (frequency and phase difference) to increase/decrease target functional connectivity, and the optimizer will update the tACS parameters device for the next stimulation trial. This process runs online and in a closed-loop approach.

maximize the targeted brain network activity/connectivity (i.e., temporal correlations between BOLD signal changes in two target regions). Figure 1-2 is the concept of online closed-loop tACS-fMRI to optimize tACS parameters in maximizing the two targeted brain network connectivity.

1.5 Summary of Contribution

The following points summarize the contribution of this work:

- The dissertation reports recently developed MRI-conditional high-definition tACS (HD-tACS) setup using two sites 4×1 ring montages for frontoparietal synchronization (FPS) (Saturnino, Madsen, Siebner, & Thielscher, 2017) in combination with an optimization algorithm to achieve, for the first time, a fully closed-loop tACS-fMRI. The dissertation provides the details of the online FPS closed-loop tACS-fMRI experimental protocol to test the feasibility of this intervention, expected outcomes, hypotheses, and experiment data.
- Moreover, the dissertation shows how the effect of tACS on brain activity, as inferred from the BOLD signal, can be measured, and validated, while excluding technical artifacts in fMRI signals related to tACS. It also discuss the safety aspects (i.e., temperature under electrodes and patient comfort, sensation, and side effects) of the closed-loop tACS-fMRI setting.
- Pipelines of individualized treatments through the online closed-loop brain stimulation approach have the potential to work better compared with one-size-fits-all approaches. The novel innovations of this method include (1) Individual electrodes' placement selection based on a task-based fMRI protocol. This method might find the precise stimulation site that can optimally decrease the symptoms of a specific disorder selectively. (2) Individual electric current dose based on individualized brain segmentation using CHM potentially improves efficacy. (3) Online closed-loop concurrent tACS-fMRI can find the optimal

tACS parameters (within subject) which can increase/decrease task-based functional connectivity, also it potentially can improve treatment efficacy of the disorder. (4) The method can be used for various psychiatric disorders by customizing/designing the PPI task related to the target disorder at the beginning.

1.6 Dissertation Outline

Chapters 2 - 4 are reproduced and adapted from Mulyana, Beni, et al. "Online Closed-Loop Real-Time tES-fMRI for Brain Modulation: Feasibility, Noise/Safety and Pilot Study." BioRxiv, 2021.04.10.439268. https://doi.org/10.1101/2021.04.10.439268. This dissertation is organized as follows.

Chapter 2. Closed-loop tACS-fMRI setup

This chapter describes the online closed-loop system overview and tACS device used in this study, electrode and montage design, and electric field simulation due to the montage selection.

Chapter 3. tACS-fMRI quality check and safety

This chapter provides technical details on how safety and quality of tACS-fMRI settings can be tested, and how these settings can be monitored during the study to ensure they do not exceed safety standards.

Chapter 4. Study design

It needs to design carefully the protocol experiment to engage the brain activation refers to objective study. Besides that, it must ensure the experiment is safe for participants in the prepared protocol. This chapter describes the design of protocol of online closed-loop tACS-fMRI, hypotheses, and expected outcomes

Chapter 5. Experiment results and analyses.

This chapter investigates whether the online closed-loop tACS-fMRI optimization approach can optimize the tACS parameters in terms of enhancing the target functional connectivity and improving cognitive function measured by the working memory task compared to the control group.

Chapter 6. Conclusion and Future Work

This chapter integrates all analyses presented in this dissertation and provides recommendations for further studies involving online closed-loop tACS concurrent fMRI.

Chapter 2: Closed-loop tACS-fMRI setup

2.1 System overview

Figure 2-1 shows an overview of the closed-loop tACS with a concurrent fMRI system. The tACS stimulation was applied using a battery-driven MRI-compatible Starstim AC-Stimulator (https://www.neuroelectrics.com/products/starstim/starstim-r32/). The tACS device is positioned outside the magnetic field in the operator room (Figure 2-1). The stimulation current is channeled into the scanner bore via a filter box (MECMRI-Series, 2018) attached to the penetration panel that filters out radio frequency (RF) noise (7–1000 MHz) and high magnetic fields from the scanner.

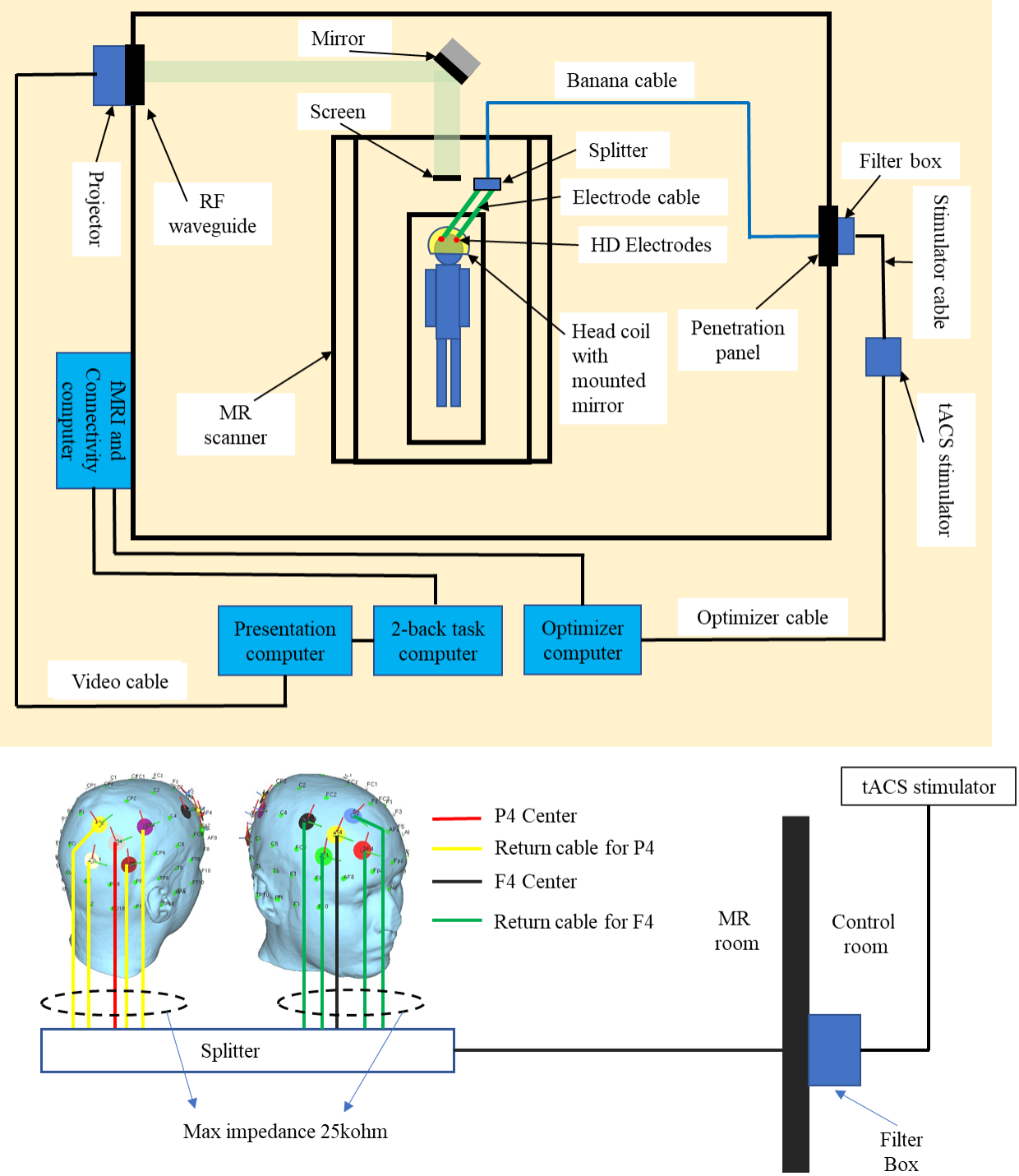

Figure 2-1: Closed-loop tACS-fMRI setup.

The participant is capped with 10 high definition (HD) electrodes in a frontoparietal montage, then lying inside the MRI room to get tACS stimulation concurrent with fMRI scanning. During fMRI scanning, the fMRI connectivity computer sends frontoparietal connectivity to the 2-back task

computer and the optimizer computer. 2-back task computer connected to the presentation computer to display 2-back task on the screen inside the MRI room for the participant. The optimizer calculates the optimal tACS parameters for improving participant frontoparietal functional connectivity. Then, the optimizer sends the tACS parameters through the optimizer cable to the tACS device. The tACS device is connected to the filter box that is attached on the penetration panel using a stimulator cable. Then, the filter box is connected through a banana cable to the participant's frontoparietal sites via 10 HD electrodes to give the stimulation.

2.2 tACS electrodes

The Starstim R32 tACS device uses rubber electrodes embedded in sponge pockets with saline solution as a conductive material between the electrode and scalp. Although this electrode solution is more comfortable for participants compared to conductive gel, using saline solution has many disadvantages, such as; (1) saline solution evaporates quickly, which makes it difficult to maintain safe and low impedance during long duration experiments; (2) saline solution easily spreads out and has a greater risk to short-circuit electrodes, which will not provide accurate stimulation over the desired sites of cortical area; and (3) the sponge is made of textile sponge and the contact with the carbon rubber could be loose.

To overcome these potential disadvantages of saline solution and also to take advantage of the focality of HD electrodes, we created MRI compatible rubber HD electrodes (circular pad with radius 10 mm and 1 mm thickness, electrode material: carbon rubber and plastic shell) (Figure 2-2A). We removed the carbon rubber cores from MRI Sponstim (model: NE026MRI, brand: Neuroelectrics) and placed them inside next-generation (NG) Pistim's shells (model: NE029, brand: Neuroelectrics) to replace the metal part (Ag/AgCl) of the shells. We applied highly conductive gel/paste (Piervirgili, Petracca, & Merletti, 2014) (model: Abralyt HiCl, brand:

Easycap) between those MRI-compatible electrodes and the scalp to improve contact conductivity. Our electrode shell construction has a dome structure so that it avoids gel spreading out over the scalp and will be a better setting compared with electrodes embedded in sponge pockets soaked with saline solution. The electrode is made from a nonmagnetic material (carbon rubber), and it connects to an MRI electrode cable that is also made from carbon rubber (model: NE046c, brand: Neuroelectrics) with distributed low-conductivity to reduce stray fields in magnetic resonance current density imaging (MRCDI) (Gregersen et al., 2021). This setting will allow us to minimize the possibility of a spurious electric field. We used textile caps with holes indicating places for electrode positioning (model: Neoprene Headcap/ NE019, brand: Neuroelectrics).

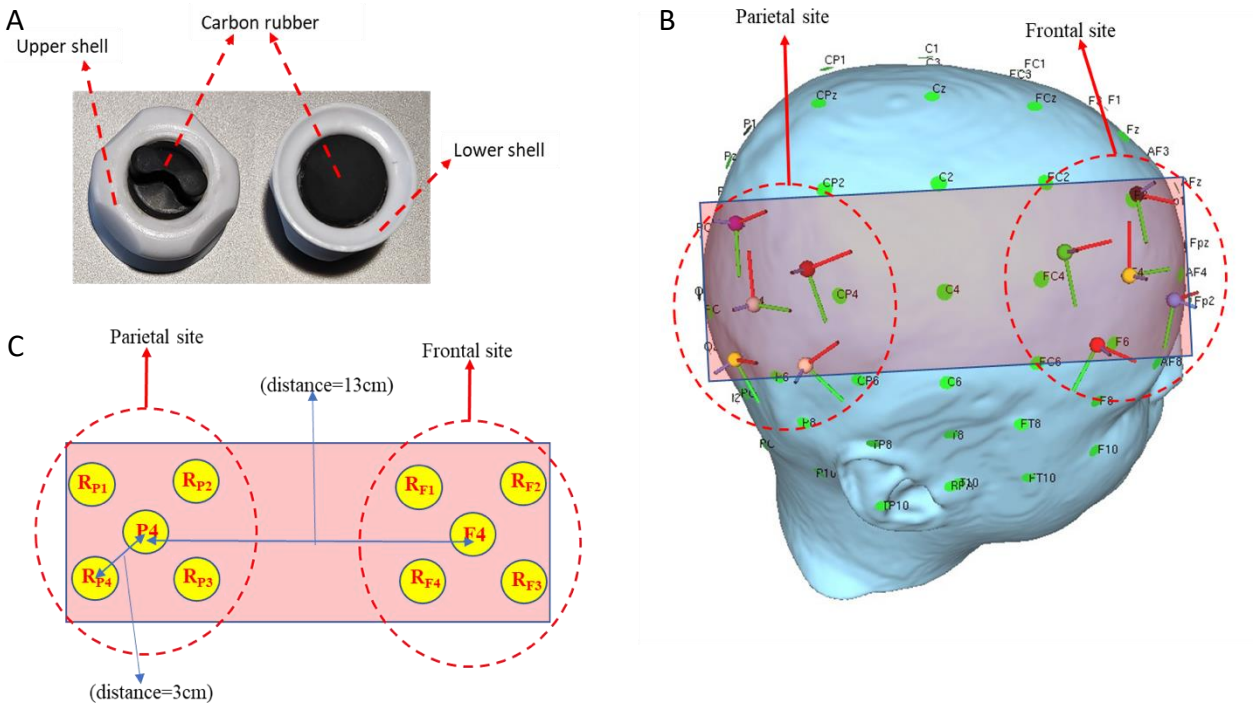

Figure 2-2: MR compatible HD electrodes and montage settings.

A) MR compatible high definition (HD) electrodes; B) Head model of equidistance center-return (3cm) electrode placement; C) Plane surface of equidistance (3cm) electrode placement, with a distance of 13 cm between sites. To simplify analyses, we ignored the head curvature, but drew

the surface of the head on which the electrodes are positioned as a plane surface, as shown in Figure 2-2B and C above, and the electrodes side view as shown in Figure S1 at Supplementary Materials A where the peripheral electrodes aligned in the direction of view and occluding each other being and combined into one electrode.

2.3 Electrode montage

We targeted the frontoparietal network to maximize the FPS with tACS stimulation. This network is within the executive control network (ECN) and is involved in sustained attention, complex problem-solving, and working memory (Menon, 2011). Specifically, the present protocol targeted the right middle frontal gyrus and right inferior parietal cortex as important nodes of the frontoparietal network, which are approximated by electrode positions at F4 [49.65, 53.71, 72.15] (mm in MNI space) and P4 [48.73, -84.52, 66.10] of the 10-10 EEG system using Ernie model in the SimNIBS software (Saturnino, Madsen, & Thielscher, 2019).

The current of the center electrodes was fixed to a 1 mA-peak value. Although higher stimulation intensities (up to 4 mA) could result in a higher neural response (dose-response relationship) (Karabanov, Saturnino, Thielscher, & Siebner, 2019; Kessler, Turkeltaub, Benson, & Hamilton, 2011; O'connell et al., 2012), we used a lower current intensity (1 mA) in this first closed-loop tACS-fMRI pilot study. Previous tACS-fMRI studies used similar current (i.e., 1 mA) or even lower (Antal et al., 2008; Moliadze, Atalay, Antal, & Paulus, 2012; Splittgerber, Suwelack, Kadish, & Moliadze, 2020; Violante et al., 2017b). Higher doses could be evaluated after confirming the subjects' tolerance.

The current of each return electrode (4 return electrodes on each side) was set to 0.25 mA. Return-electrode placement for F4 and P4 sites was designed to be at an equal center-return distance (3cm)

in order to reduce gel bridging (short circuit) and to reduce the electrical shunt effect in the anti-phase condition, explained in section 2.5. Return-electrode coordinates for the F4 site are: RF1 = [51.35, 28.51, 86.09], RF2 = [25.05, 58.87, 87.63], RF3 = [42.95, 74.26, 51.96], and RF4 = [64.83, 41.57, 52.64] (Figure 2-3) and return-electrode coordinates for P4 site are: (RP1 = [49.02, -95.93, 38.49], RP2 = [25.63, -89.69, 84.28], RP3 = [52.57, -62.68, 85.96], and RP4 = [65.54, -67.52, 51.97] (Figure 2-3A) in the MNI coordinates aligned from the Ernie model from SimNIBS software. Care was taken to avoid placing the return electrodes around PO4, as this electrode site would result in uncomfortable pressure on the back of the subject's head when lying on the MRI table (the red area in Figure 2-3A).

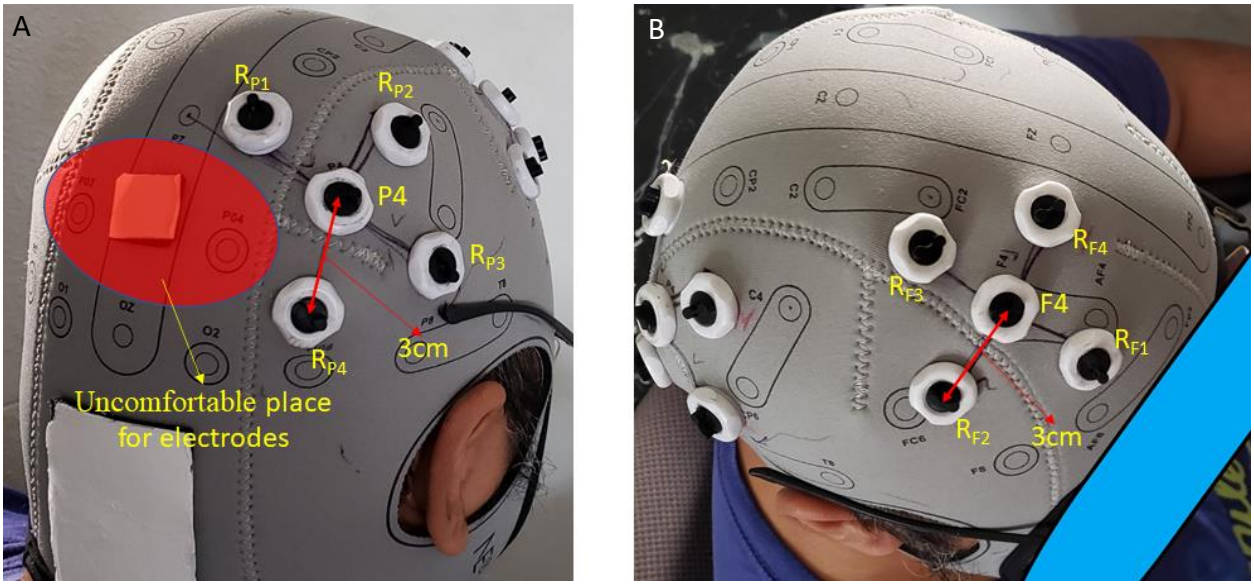

Figure 2-3: Overview of the frontoparietal montage with 10 HD electrodes.

A) Montage of 5 high definition (HD) electrodes on the parietal site with equidistant (3 cm) center and return electrodes. The red highlighted area is a subject uncomfortable area where we need to avoid placing the electrodes due to the constant head pressure when subjects lie down on the MRI table; B) Montage of 5 HD electrodes on the frontal site with equidistant (3 cm) center and return electrodes.

2.4 tACS capping

Before applying gel, we checked that there were no tattoos, scars, or active skin irritation around the electrode location. Afterward, we cleaned the scalp area in the electrode shell with isopropyl alcohol (IPA) using a cotton swab. This is to clean the scalp area where the electrodes will be installed, so that dust and oil in the area will be removed to make a low impedance contact between the electrode and the scalp. We dipped the cotton swab into the IPA, then swabbed the scalp under the electrode shell with the cotton swab evenly and gently (Figure 2-4A). We repeated these procedures three or four times. Then we applied Abralyt HiCl gel to the scalp area inside the electrode's shell so that the amount of gel avoids a short circuit between the electrodes. If a short circuit occurs between electrodes, tACS will not work as intended. The gel must be spread evenly across the scalp inside the shell, and the gel level should not exceed the thickness shown in Figure 2-4B, which is about 1 mm or the amount of 0.5 ml.

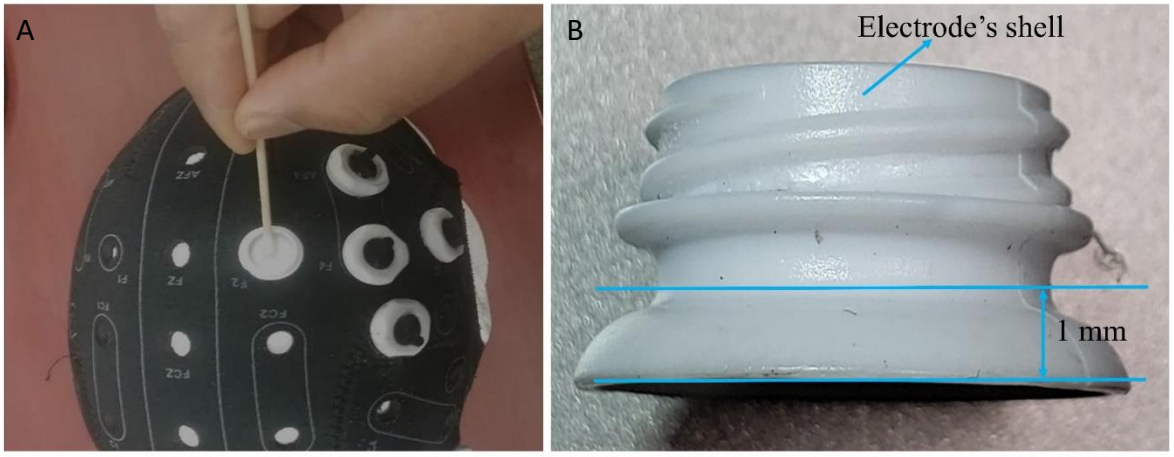

Figure 2-4: Peripheral cautions for dual-site HD montage capping.
A) Swab evenly and gently using a cotton swab with isopropyl alcohol on the scalp area inside the electrode shell. Repeat three or four times. B) After 10 high definition (HD) electrodes' shells are attached to the holes on the cap referring to the montage location, the gel is spread evenly across

the scalp inside the shell. The layer of gel should not exceed 1 mm thickness or 0.5 ml gel volume to reduce excessive leakage of gel, which could make a short circuit to nearby electrodes.

2.5 The electric field of the montage

Electric field derivation for in-phase and anti-phase conditions in the frontoparietal montage can be found in Supplementary Materials A. Derivations show that the electric field on the in-phase condition from our montage will appear under the frontal and parietal electrodes but not between them. Any appearance of the electric field between the sites is the electric shunt effect (Saturnino et al., 2017). Electric shunt increases the stimulated area and decreases focality. This is not desirable if we need to focus stimulation over a specific region (e.g., frontal and parietal areas in the frontoparietal network). Therefore, the in-phase condition is relatively safe from the shunt condition. Our montage with 13 cm distance between each site does not show the electric shunt effect between their sites (Figures 2-5A, B). During the anti-phase condition, there is a possibility of the electric shunt effect between each site (see equation 6 in Supplementary Materials A). Therefore, based on equation 6, and to avoid the shunt effect, we need to pay attention to (i) ensuring sufficient distance between the return electrodes of the two sites and (ii) positioning the return electrodes as close as possible to their center electrode ($d_1 \approx d_2 \approx d_3$) but not too close to prevent too much shunting effect via the skin between the center and surround electrodes (Neri et al., 2020).

In the montage, it is feasible to establish a return-to-center distance of 3 cm, resulting in a gap of 1 cm between the edges of the center and return electrodes (each of them having a diameter of 2 cm). With this montage, the return-to-center electrode distance is relatively small, and the return-to-return electrode distance between frontal and parietal sites is relatively large so that the shunt

effect between frontal and parietal sites in the anti-phase condition is minimized. From our montage, by using equation 6 (in Supplementary Materials A) and data; 2d2 = distance from F4 to P4 around 13cm (https://www.biosemi.com/headcap.htm), 2d2 = d1+ d3 = 13 cm and gray matter conductivity = 0.275 S/m (Wagner, Zahn, Grodzinsky, & Pascual-Leone, 2004), the maximum electric field in the gray matter midway between the two sites was 0.04 V/m in the anti-phase condition, which is below than 0.1 V/m. The electric field intensity as 0.1 V/m is considered as the threshold for measurable physiological effects in neurons (Ivry et al., 2017; Jefferys et al., 2003; Ozen et al., 2010), and with this montage, the electric field between the sites can be negligible even in the anti-phase condition.

The electric field in the cortical target regions of interest in the frontal and parietal cortex was provided by SimNIBS. The top percentiles of the electric field intensity in 99.9% was 9.22e-02 V/m or close to 0.1 V/m, which appeared on the cortical surface under the center electrode for each site (frontal and parietal) (Figure 2-5). Our simulation results indicate that the electric field obtained on the cortical areas under each site was high to capture measurable physiological effects in neurons and the shunting effect between the center and their surrounding return electrodes can be negligible. To test these hypotheses in more detail in silico, we simulated the electric field in the brain using SimNIBS 3.2 software (Saturnino, Puonti, et al., 2019; Thielscher, Antunes, & Saturnino, 2015). SimNIBS 3.2 uses the finite element mesh (FEM) method to calculate the electric field on every tetrahedron element mesh in every brain segmentation. It can be interpolated onto the cortical surface (surface-based electric field distribution) or interpolated into a NIfTI volume and transformed to MNI space (volume-based electric field distribution). Therefore, we can analyze the electric field in each voxel. SimNIBS also provides information about the focality of the stimulated area, which is defined as the grey matter volume with an electric field greater or

equal to 75% of the peak value. To avoid the effect of outliers, we defined the peak value as the 99.9th percentile. The smaller the value of this volume metric, the more focal the electric field in the brain.

Figures 2-5A and B depict the intensity of the electric field on the cortical surface, on volumetric sagittal view, and the stimulated area for F4-P4 in-phase. Meanwhile, Figures 2-5C and D show the intensity of the electric field on the cortical surface, on volumetric sagittal view and the stimulated area for F4-P4 anti-phase. Figures 2-5A, B, C, and D indicate that the electric field was focused under frontal and parietal sites as predicted by equation 4. However, in the anti-phase condition, the electric field between sites appears stronger than in the in-phase condition, and also the stimulated area was wider than the in-phase condition (in-phase stimulated area = 5.34×103 mm^3, anti-phase stimulated area = 5.56×103 mm^3, percent change anti-phase to in-phase = 4.12%). This is caused by the electric shunt effect. As predicted by equation 6, the maximum shunt effect on the cortical surface was less than 0.05V/m (Figure 2-5C). However, the electric shunt effect for the anti-phase condition was not overly large (the stimulated area only increases by 4.12% compared to the in-phase condition), so the shunt effect can be neglected.

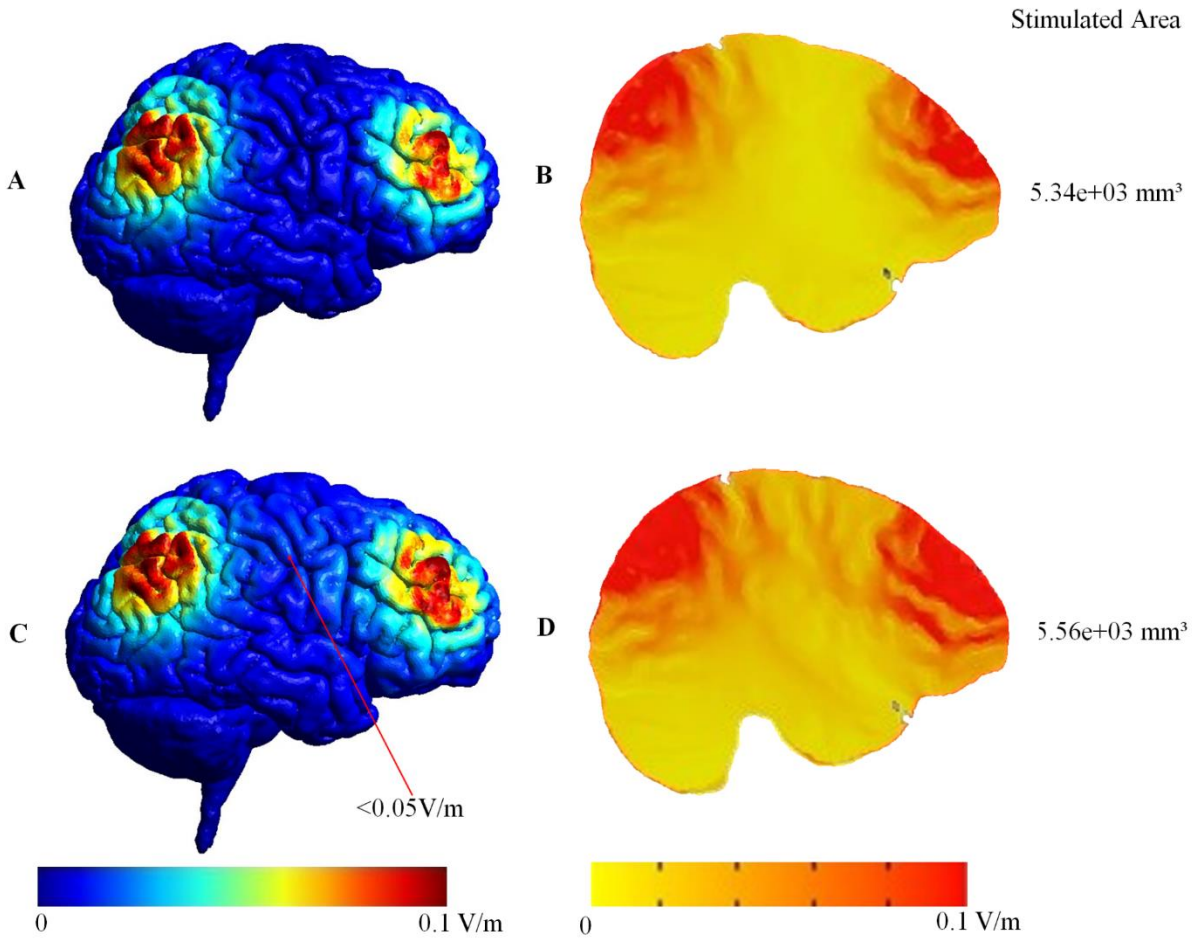

Figure 2-5: Surface- and volume-based comparison of in- and anti-phase conditions.

The cortical surface (surface-based electric field distribution) is calculated by SimNIBS (A and C) and could be interpolated into a NIfTI volume and applied to transform it to MNI space (volume-based electric field distribution). Therefore, we can analyze the electric field in each voxel using AFNI software (B and D). A) and B) Surface and volume-based simulation result of the in-phase condition; C) and D) Surface and volume-based simulation result of the anti-phase condition. The stimulated area in the anti-phase is 4.12 % wider than in the in-phase condition due to the electric shunt effect. In anti-phase condition, the electric shunt effect can be seen as a stronger electric field (red color) in between sites (D) and more electric field dots of less than 0.05V/m on the cortical surface in between sites (C).

Chapter 3: tACS-fMRI quality check and safety

3.1 Background

Before applying tACS-fMRI, it is necessary to verify the impact of tACS-fMRI on fMRI image quality and safety. Reliable and safe setups for the application of simultaneous tACS-fMRI are well known (Chaieb et al., 2014; Frank et al., 2010; Gbadeyan, Steinhauser, Mcmahon, & Meinzer, 2016; Loo et al., 2011; Poreisz, Boros, Antal, & Paulus, 2007; Williams et al., 2017). However, there is no published evidence on the safety of simultaneous tACS-fMRI with dual-site HD montages. Therefore, we first scanned a watermelon (in Supplementary Materials B) to test for MRI artifacts and noise, and then conducted a human scan to measure the temperature changes during tACS-fMRI in order to prove that combined tACS-fMRI has no aversive impact on human safety and image quality. We aimed to: (1) examine whether tACS stimulation significantly induces any artifacts or increases noise on MRI/fMRI images, and (2) to conduct a tACS safety test regarding the scalp temperature under the stimulation electrodes during concurrent tACS stimulation during fMRI. Details of MRI artifacts, fMRI noise testing methods, and a temperature test can be found in Supplementary Materials B.

3.2 MRI/fMRI noise

We scanned a watermelon with concurrent tACS-fMRI to evaluate the tACS noise that is free from the effect of a neural activation signal. Detailed procedures of this artifact and noise test can be found in Supplementary Materials B. We first obtained k-space data without RF excitation pulse. Since no echo signal was emitted without RF excitation, we could measure only the tACS noise

received by seeing the k-space data. We collapsed the phase encoding direction by averaging and made a frequency-by-slice k-space image for each volume. Figure 3-1A shows the FDR-corrected p-values for the t-test for the received signals between the stimulation ON and OFF period. The smallest FDR-corrected p-value was 0.35, indicating that tACS did not produce significant noise in the received signal.

Second, we scanned a watermelon in the same way but with a RF excitation pulses. We performed GLM analysis to test the signal difference between the stimulation ON and OFF period in the signal time-course. We found no voxel had a significant difference between the stimulation ON and OFF period (the smallest FDR corrected p-value was 0.312). We also compared mean value of time series in each voxel within the ROIs (F4 and P4) and its SD, and found no significant difference between tACS ON and OFF (ON: mean=1210.70 and OFF: mean=1210.50, t[223]=0.4, p=0.72; ON: SD=2.24 and OFF: SD=2.55, F[150,75]=1.14, p=0.27). The temporal signal-to-noise ratio (TSNR) map is shown in Figure 3-1B. These results indicated that tACS did not produce significant noise in the echo signal and the fMRI image time-series.

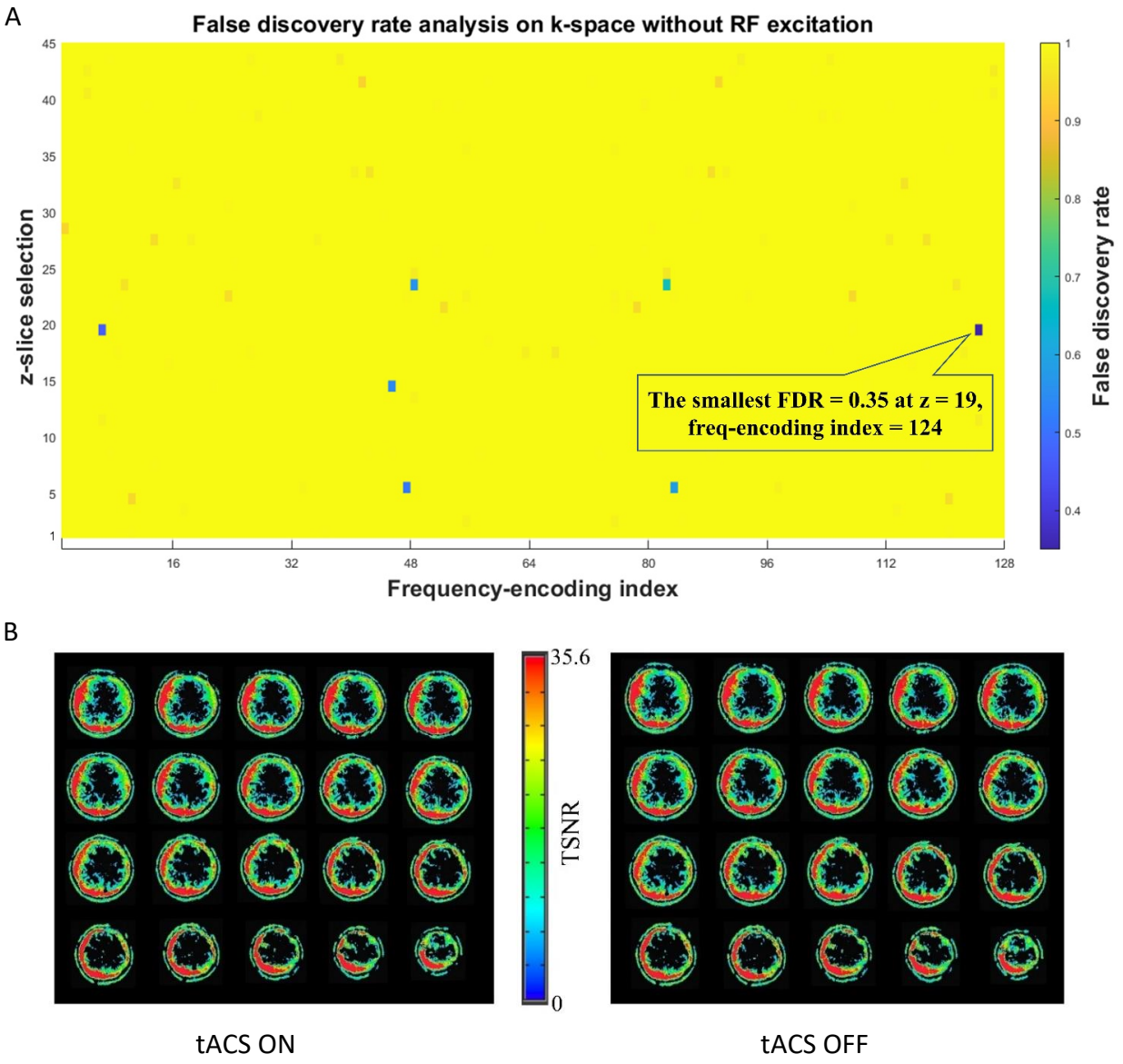

Figure 3-1: Results of the noise test influencing fMRI signal (EPIs).

A) FDR-corrected p-value in the k-space without-RF excitation. The smallest FDR corrected voxel-wise p value = 0.35 which is bigger than 0.05, it means tACS stimulation did not create significant artifacts. B) Voxel-wise temporal signal-to-noise ratio (TSNR) from stimulation ON and OFF. A visual inspection corroborates there is no tACS-related artifact are observed in the EPI images. It is also confirmed by the voxel-wise analysis (with-RF) which found the smallest FDR corrected voxel-wise p value = 0.312 > 0.05.

3.3 Temperature measurement results

Next, we scanned a human subject to examine the temperature change due to tACS during fMRI. Details of the test procedure can be found in Supplementary Materials B. The normal human body temperature is typically observed in a range from 36.5 to 37.5 ℃ (Hutchison et al., 2008; Mackowiak, Wasserman, & Levine, 1992). The baseline scalp temperatures prior to scanning and tACS stimulation were stable below 33 ℃ (F4: mean = 30.30, SD = 0.003; P4: mean = 32.22, SD = 0.05) (Figure 3-2A). The EPI scan did not cause a substantial heating effect at the tACS electrodes (F4: mean = 30.37, SD = 0.08; P4: mean = 32.05, SD = 0.05) (Figure 3-2B). Moreover, the temperatures did not significantly change with the tACS stimulation (F4 ON; mean = 30.39, SD = 0.11: F4 OFF; mean = 30.35, SD = 0.05; z = 0.68, p = 0.49: P4 ON; mean = 32.04, SD = 0.04: P4 OFF; mean = 32.07, SD = 0.05; z = -0.59, p = 0.56). Furthermore, the scalp temperatures under the electrodes are below 37.5^{o} C during a 12 min EPI scan, confirming that there is no issue with patient safety in term of temperature change during concurrent tACS-fMRI in the current experimental set-up.

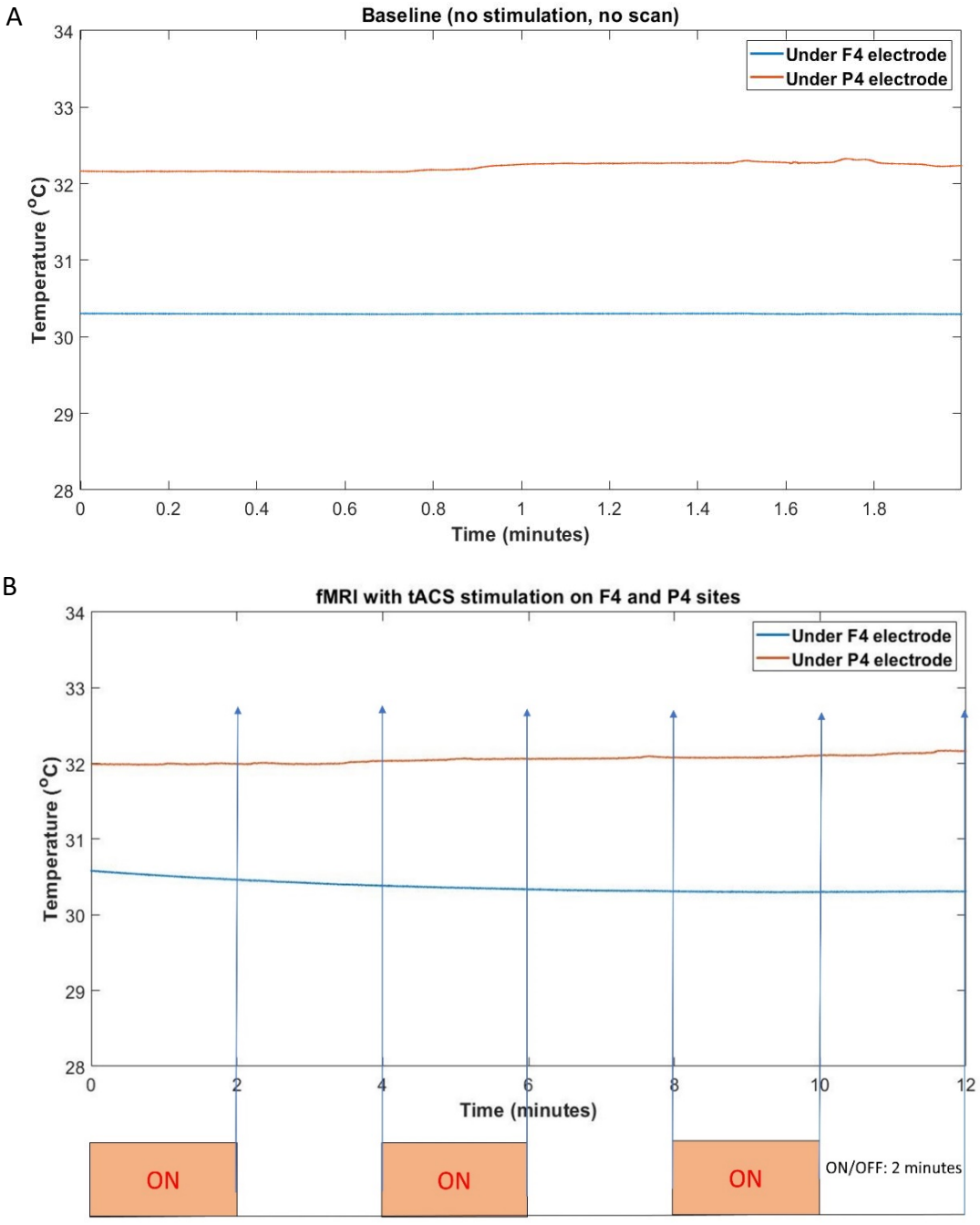

Figure 3-2: Safety test using temperature records under the electrodes.

A) Baseline temperature on the scalp at F4-P4 electrodes when there is no tACS scan. The baseline scalp temperatures prior to scanning and tACS stimulation are stable below 33° C; B) Temperature during fMRI with and without tACS under F4-P4, 2 minutes ON/2 minutes OFF for 12 minutes. The temperatures did not significantly change regardless of the tACS stimulations ON or OFF.

Furthermore, the scalp temperatures under the electrodes are below the upper limit human body temperature (37.5^{o} C) during a 12 min fMRI (EPI) scan. There is no issue with patient safety in terms of temperature changes during tACS-fMRI.

Chapter 4: Study design

Here we propose a possible study design to examine closed-loop online tACS-fMRI optimization performance. We aim to investigate (i) whether the closed-loop online tACS-fMRI optimization can find the tACS parameters in terms of enhancing the target functional connectivity during the training runs (the optimization run), and (ii) whether the optimized (i.e., personalized) tACS can influence (i.e., increase) the target functional connectivity during the testing run, compared to a control condition.

The study aims cannot be tested without a control condition since we cannot exclude non-specific changes in functional connectivity (e.g., due to boredom, habituation with MRI environment, alertness, etc.). We propose and summarize all possible control conditions for this study in Figure 4-1. To test study aims (i) and (ii), we decided to apply the control condition described in Figure 4-1, condition no.7. In short, during the testing run, a participant in the experimental condition will receive tACS with the parameters that maximize FPS in the training runs, while a participant in the control group will receive tACS with the parameters that minimize FPS. Future studies might like to try other control conditions based on their study questions.

Condition		Training runs		Testing runs		Factors to be controlled for to establish the causality				Hypotheses test	
		Optimization method	Stimulation type	Parameter settings	Stimulation type	Equal stimulus sensations	Maintained blindness	Exclude potential carry over effects of Optimization phase	Demonstrate optimization specificity	Study Aim (i)	Study Aim (ii)
Experimental group											
		Optimization	Real	Optimized	Real						
Control group											
Require randomization from Testing run	1	Optimization	Real	Conservative	Real	✓	✓	✗	✓	✗	✓
	2	Optimization	Real	Arbitarily	Real	✓	✓	✗	✓	✗	✓
	3	Optimization	Real	Lowest	Real	✓	✓	✗	✓	✗	✓
	4	Optimization	Real	Optimized	Sham	✗	✗	✗	✗	✗	✓
Require randomization from Training runs	5	Optimization	Sham	Conservative	Sham	✗	▲	✓	✗	✓	✓
	6	Optimization	Sham	Optimized	Sham	✗	▲	✓	✗	✓	✓
	7	Min-optimization	Real	Min-optimized	Real	✓	✓	✓	▲	✓	✓
	8	Min-optimization	Sham	Min-optimized	Sham	✗	▲	✓	✗	✓	✓

Figure 4-1: Selection of the control condition and pros and cons.

Optimization: Optimizer searches the parameter space to maximize the target functional connectivity (FC). Min-optimization: Optimizer searches the parameter space to minimize the

target FC. Real: each block is composed of 20-sec stimulation and 10 sec resting alternatively and repeated for 15 blocks. Sham: each block is composed of 2-sec sham stimulation (i.e., 1-sec ramp up and 1-sec ramp down) and 18 sec resting alternatively and repeated for 15 blocks. Conservative: use parameter settings considered to influence target FC based on the literature (e.g., 6 Hz and 0-degree phase). Arbitrarily: use completely opposite parameter settings with optimized parameters (e.g., frequency * 3.7 modulo 150 - and 180-degree phase difference). Lowest: using the parameter settings demonstrating the poorest (i.e., lowest) target FC during the training runs. Optimized: use optimized parameter settings defined by the training runs. Min-optimized: use min-optimized parameter settings defined by the training runs. Remarks: Control group; 1. Require strong evidence to support the parameter settings. 2. There are no established methods to generate parameter settings completely outside of the optimized parameters. 3. We cannot investigate whether the training runs actually increased target FC compared with other approaches. Study aim (i) cannot be tested. 4. We can only investigate the effect of tACS itself compared with the sham stimulation. Highly doubtful to maintain the blindness since subjects will explain the real stimulation during the training runs. 5. There is a chance that the subject will notice the sham stimulation even if they do not experience the real stimulation. 6. There is a chance that the subject will notice the sham stimulation even if they do not experience the real stimulation. 7. We can conclude that the group difference is specified by the optimization method because subjects will experience a min-optimization approach during the training runs, which may affect the target FC. Therefore, we can test both study aims (i) and (ii). 8. There is a chance that the subject will notice the sham stimulation even if they do not experience the real stimulation.

4.1 Experiment protocol

Figure 4-2 shows the protocol of the experiment for the experimental (optimized; maximize FPS) and the control (min-optimized; minimize FPS) groups. For the two training FPS sessions, participants are randomly assigned to either an optimized (experimental) group or a control group (Figure 4-3). For the optimized group (experimental group), the optimizer searches the tACS parameters that can achieve the highest FPS, while for the control group, the optimizer searches

the tACS parameters that can achieve the lowest FPS during the training runs. Then participants undergo a testing scan, in which they are stimulated with the optimized (in the experimental group) or min-optimized parameters (in the control group) during the training runs. The testing run tests the optimized parameters' ability to directionally modulate the FPS. The testing run is similar to the training runs, which is divided into 15 blocks (Figure 4-3B), while the parameters are fixed to that obtained in the training 1 and 2 runs. Resting-state scans (rsfMRI) are applied before and after the FPS optimization sessions and after the test session. Each rsfMRI scan lasted 6 min 50 sec.

A small but growing body of evidence suggests the washout period should be at least half of the stimulation period. For example, Beeli, Casutt, Baumgartner, & Jäncke (2008) used 3.5 min rest between different stimulation conditions as their washout period (each condition lasted for 5 min). Considering the whole training run (17 min 8 sec) as a stimulation period, about 7 min intervals with a rest scan between the training and test scans could be safe for settling the aftereffects (Nitsche & Paulus, 2001; Shafi, Westover, Fox, & Pascual-Leone, 2012). Then, in the test scan, we would be able to evaluate the stimulation effect with an optimized parameter set apart from the aftereffects.

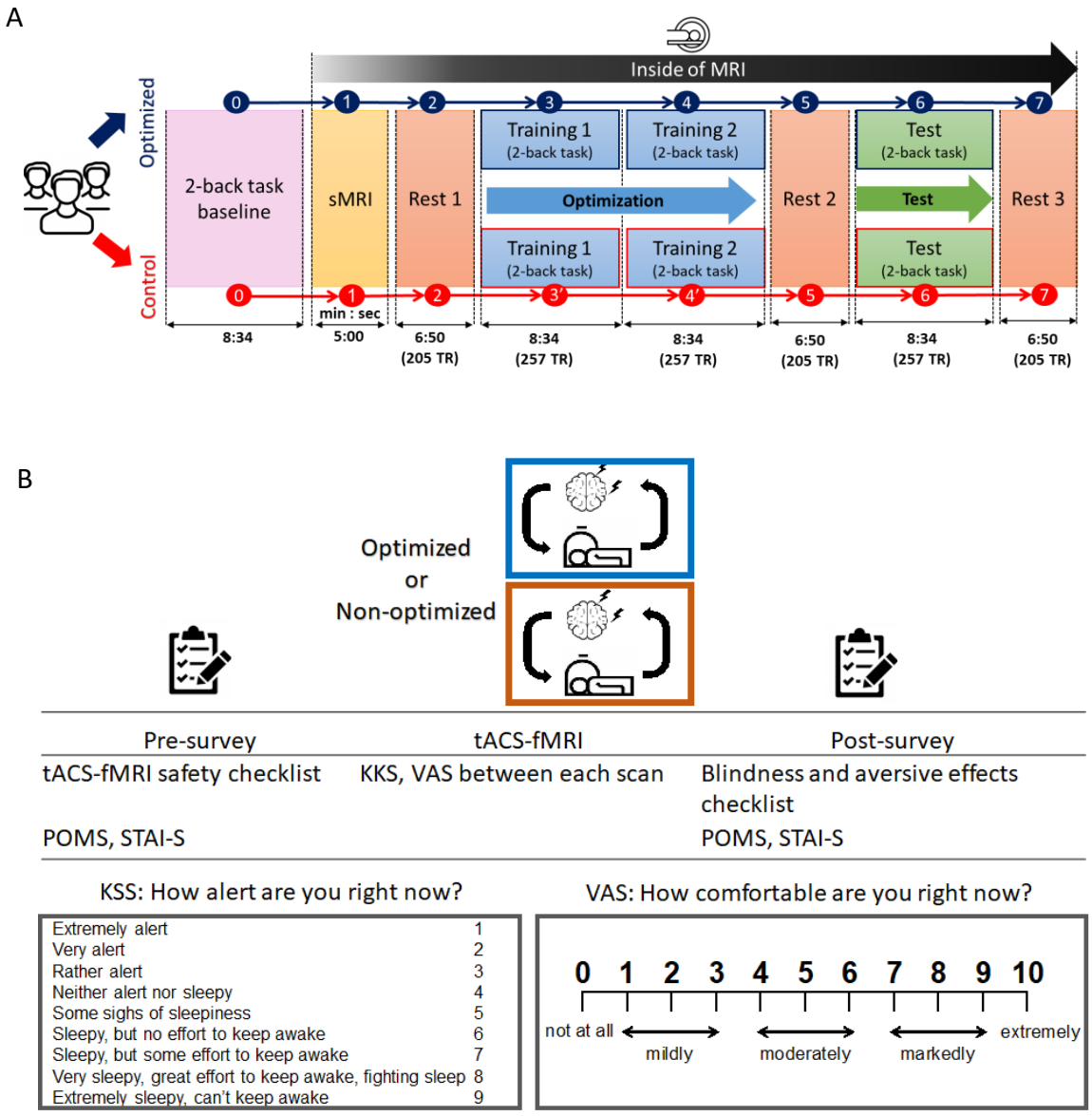

Figure 4-2: Study design.

A) A procedure of the online frontoparietal synchronization optimization protocol with a closed-loop tACS-fMRI. TR = time repetition, 2 secs. B) An overview of the session. POMS: Profile of Mood States Scale, STAI-S: State-trait Anxiety Inventory-State version, KSS: Karolinska Sleepiness Scale, VAS: Visual Analogue Scale asking one's comfortableness.

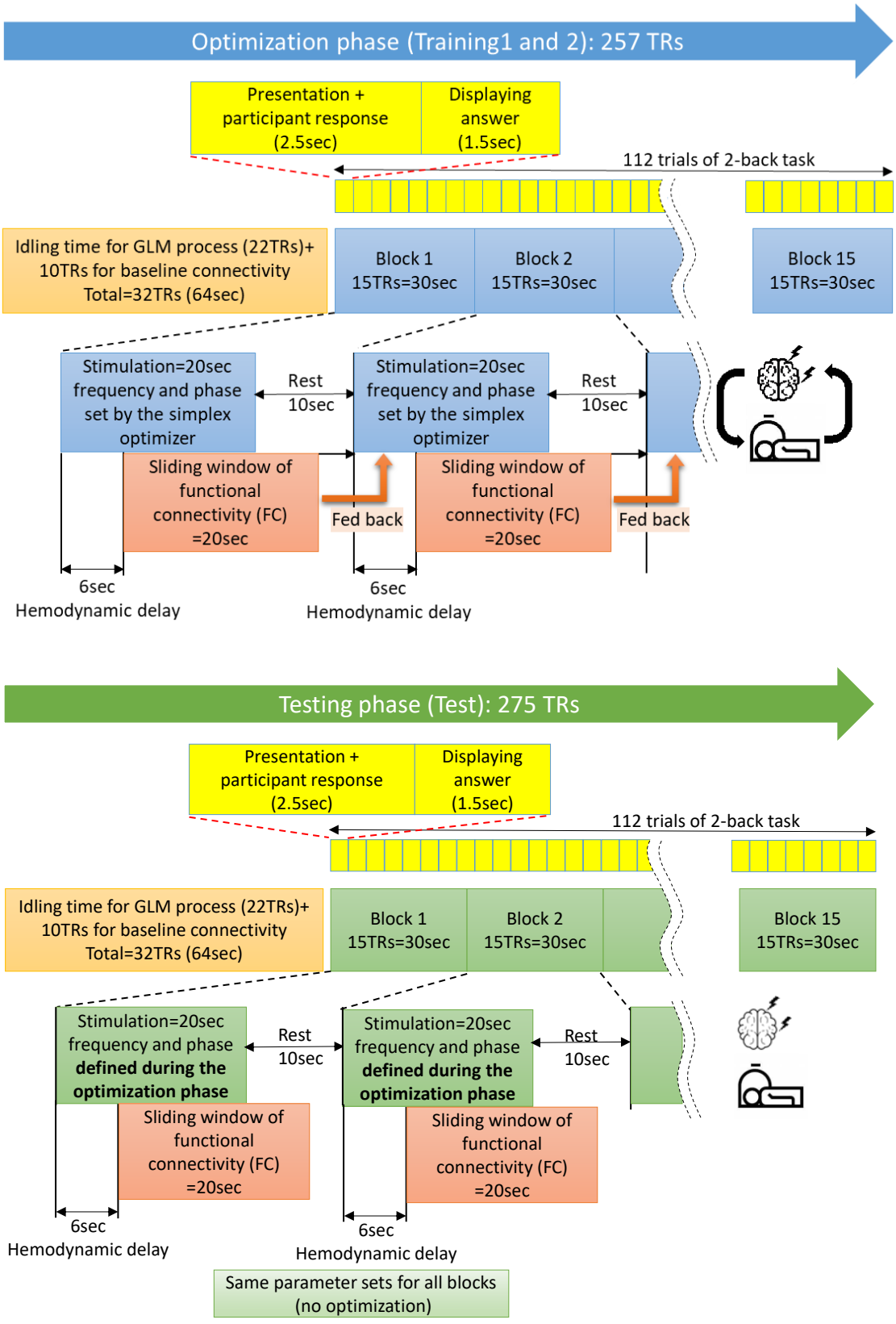
Optimization phase (Training1 and 2): 257 TRs
Presentation + participant response (2.5sec)
Displaying answer (1.5sec)
112 trials of 2-back task
Idling time for GLM process (22TRs)+ 10TRs for baseline connectivity Total=32TRs (64sec)
Block 1 15TRs=30sec
Block 2 15TRs=30sec
Block 15 15TRs=30sec
Stimulation=20sec frequency and phase set by the simplex optimizer
Rest 10sec
Stimulation=20sec frequency and phase set by the simplex optimizer
Rest 10sec
Sliding window of functional connectivity (FC) =20sec
Fed back
Sliding window of functional connectivity (FC) =20sec
Fed back
6sec Hemodynamic delay
6sec Hemodynamic delay
Testing phase (Test): 275 TRs
Presentation + participant response (2.5sec)
Displaying answer (1.5sec)
112 trials of 2-back task
Idling time for GLM process (22TRs)+ 10TRs for baseline connectivity Total=32TRs (64sec)
Block 1 15TRs=30sec
Block 2 15TRs=30sec
Block 15 15TRs=30sec
Stimulation=20sec frequency and phase defined during the optimization phase
Rest 10sec
Stimulation=20sec frequency and phase defined during the optimization phase
Rest 10sec
Sliding window of functional connectivity (FC) =20sec
Sliding window of functional connectivity (FC) =20sec
6sec Hemodynamic delay
6sec Hemodynamic delay
Same parameter sets for all blocks (no optimization)

Figure 4-3: Details of the training and test runs.

A) Training 1 and 2 runs in order to find optimal tACS parameters. Real-time calculation of functional connectivity (FC) within the frontoparietal network (under F4 and P4) is conducted and is fed back to the optimizer. The optimizer searches through the parameters based on the real-time FC to maximize its value. The optimizer keeps searching the parameters to maximize FC values in the optimized subject, while the optimizer keeps searching the parameters to minimize FC values in the control subject. B) Testing run to test the optimal parameters which is found by training runs. During the testing run, subjects in the optimized group will receive the optimized parameters defined to maximize the FC in the training runs, while subjects in the control subject will receive the parameters defined to minimize the FC in the training runs. There are 112 2-back task trials across runs (4sec for each trial) in order to stabilize the cognitive or subject state changing. The purpose of 2-back task also for cognitive performance measurement (accuracy and response-time of the correct answer).

4.2 Hypotheses and expected outcomes

The hypotheses and expected outcomes of the study with this protocol are the following.

Hypothesis 1: Regarding the first study aim, we hypothesize that a participant in the experimental condition will show increased frontoparietal functional connectivity, while the participant in the control condition will show decreased frontoparietal functional connectivity on the course of training2 respect to training1. We looked for the best tACS parameters within each subject's training runs (intra-individual variability) without any comparison to other subjects.

Hypothesis 2: Regarding the second study aim, we hypothesize that the optimized (i.e., personalized) tACS parameter settings will increase the fMRI connectivity between the tACS targets (under the electrodes of F4-P4) during the testing run for the experimental condition while will decrease the connectivity for the control condition.

Hypothesis 3: The experimental group will show improvement in the accuracy and response-time on the 2-back task from training to the testing run, compared to the control group.

Chapter 5: Experiment results and analyses

We perform a pilot experiment for twenty healthy participants to confirm the feasibility of the protocol implementation. Twenty participants are divided into two groups (10 participants as the experimental and the other 10 participants as the control group). The study is approved by the Western Internal Review Board (WIRB #20200192) and the participants give informed consent. The experiment is performed according to the protocol presented in Chapter 4. One of the participants from the control group has a number of censors more than the censors' threshold number. Therefore, that participant is removed from analyses in this Chapter with 10 participants as the experimental and the other 9 participants as the control group. Regarding how to define the number of censors, the consort flow diagram of participants before the experiment, demographics, and the aversive effect after the experiment can be checked in Supplementary Materials C.

5.1 Linear mixed effect of PPI

fMRI allows one to study task-based regional responses and task-dependent connectivity analysis using psychophysiological interaction (PPI) methods. The latter affords the additional opportunity to understand how brain regions interact in a task-dependent manner (McLaren et al., 2012; Di et al., 2017). The task-based waveform is the stimulation protocol presented in Chapter 4 (Stimulation ON: 20 seconds and Stimulation OFF: 10 seconds repeated 15 times). The description of PPI method can be seen in Supplemental Materials D.

Figure 5-1 shows the linear mixed effect for visualizing changes in the target functional connectivity (Frontal as the seed ROI and Parietal as the observation ROI) across runs between experimental and control groups with the motion as a covariate and each subject as a random effect.

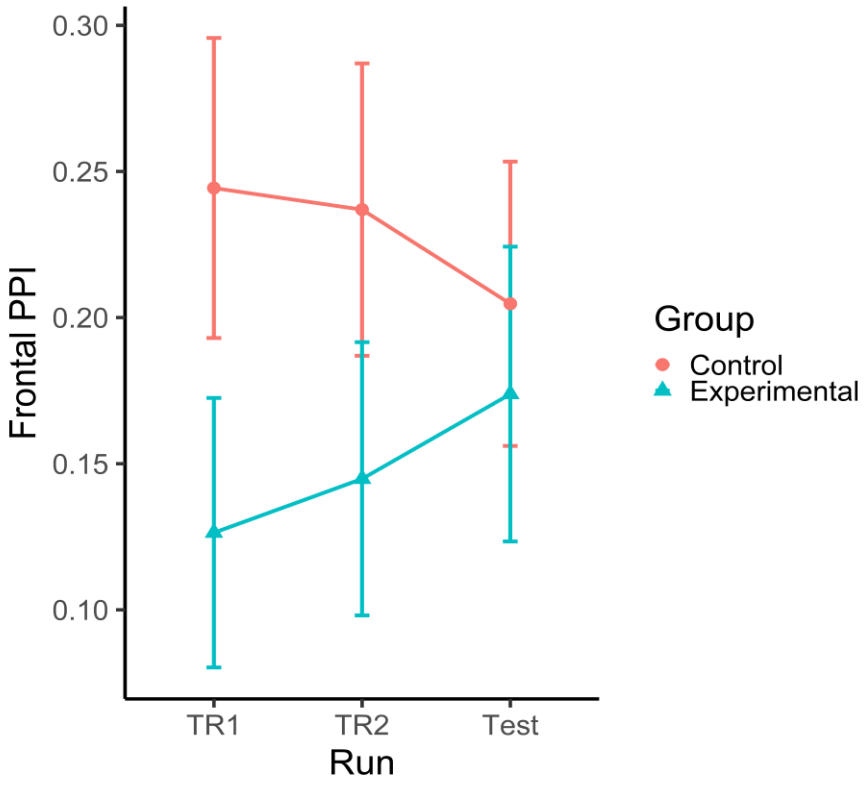

Frontal PPI ~ run * group + motion + (1|Subj)

Figure 5-1: Linear mixed effect of PPI connectivity across the runs shows connectivity change for each run between groups.

There is uptrend PPI connectivity in comparison between Test - TR1 for Experimental, meanwhile downtrend PPI connectivity in comparison between Test - TR1 for control group.

However, there is a slightly significant difference between the group in TR1 (Exp vs Cont at TR1: dF= 32.9, t=1.71, p=0.09). It means there is a difference baseline connectivity at TR1 for each

group. It is not expected because we suppose to find a similar baseline connectivity at TR1. It indicates there is an insufficient sample size which is by accidental the tail of distribution from each group created error type II and separated the baseline. The power analysis is done to PPI connectivity in between-group at TR1 by using Bayesian estimation BEST script (Kruschke, 2013) to ensure the above statement. Figure 5-2 shows the portion of the Highest Density Interval (HDI) of the posterior distribution that is covered by the region of practical equivalent [ROPE] corresponds to the number of participants used (sample size of experimental=10, control=9) is apparently so small (<1%), or the current sample size only give less than 1% of the effect size. This fact supports the above statement that the sample size is insufficient. Therefore, it creates error type II, which can be seen as the baseline PPI connectivity difference at TR1 between groups. We need to simulate a sufficient number of sample size that can give an appropriate effect size. Cohen stated the appropriate effect size should more than 80% (Cohen, 1988). Figure 5-3 shows the simulation result using BEST script that the effect size would be 92% if the number of samples is 175 participants for each group. Simulation suggests the number of participants for experimental=control=175 so that the effect size will become 92%. It will make the baseline difference go to zero (PPI conn Experimental and Control at TR1 will be merged), and PPI conn Experimental vs Control at Test will be significantly separated difference. The Figure in which the effect size is to be made more than 80% is hypothesized would be like in Figure 5-4. It is created using the current PPI Conn by removing out the difference in TR1. In that Figure, the difference between groups in the Test run was insignificant. However, in the future experiment, the result with the effect size>80% of the HDI might create a significant difference between PPI conn experimental vs control at Test run because the error type II will be significantly reduced.

Figure 5-4 has supported hypotheses 1 and 2 that the PPI connectivity is improved across runs compared to TR1 for experimental, otherwise for the control group.

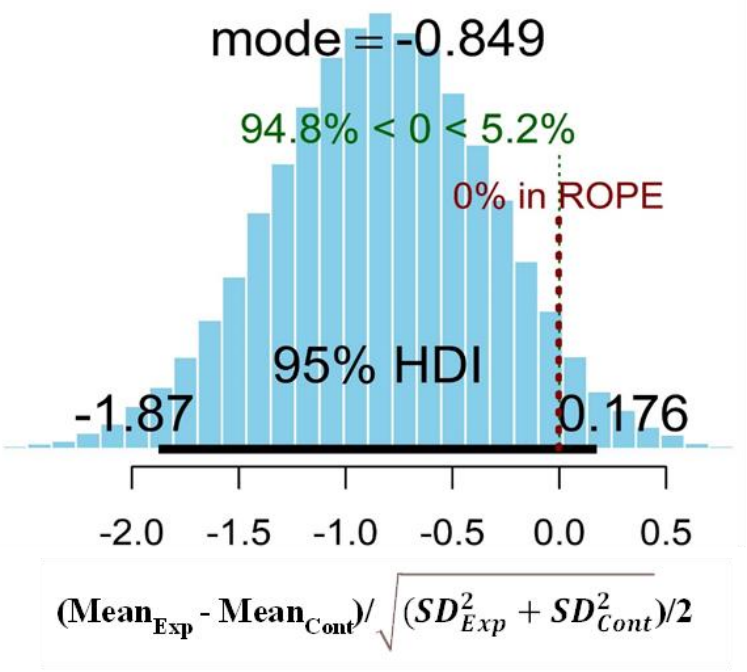

Figure 5-2: Bayesian estimation analysis.

It shows the current sample size (experimental=10participants, control=9participants) only gives the effect size less than 1%. Referring to Cohen, 1988, the proper effect size should be more than 80%.

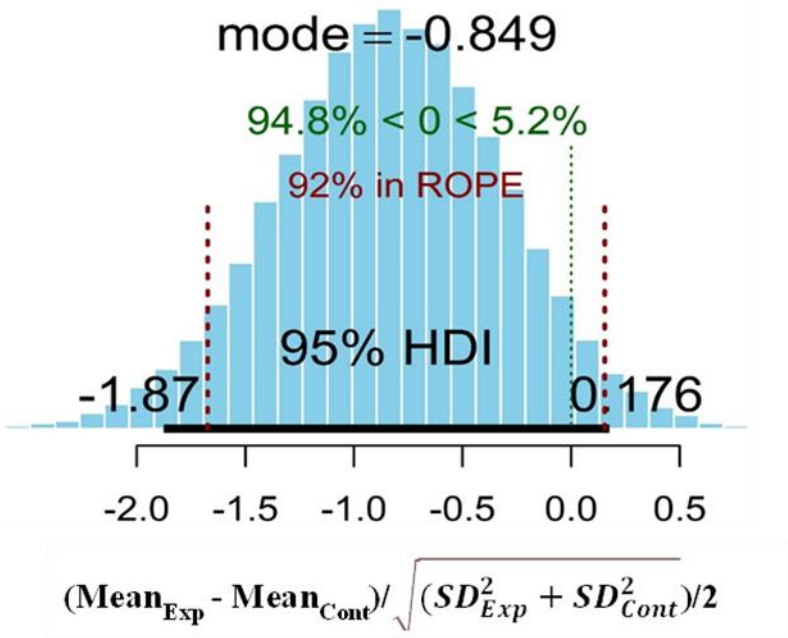

Figure 5-3: The Bayesian power analysis simulation shows the sample size of experimental=control=175participants gives the effect size=92%.

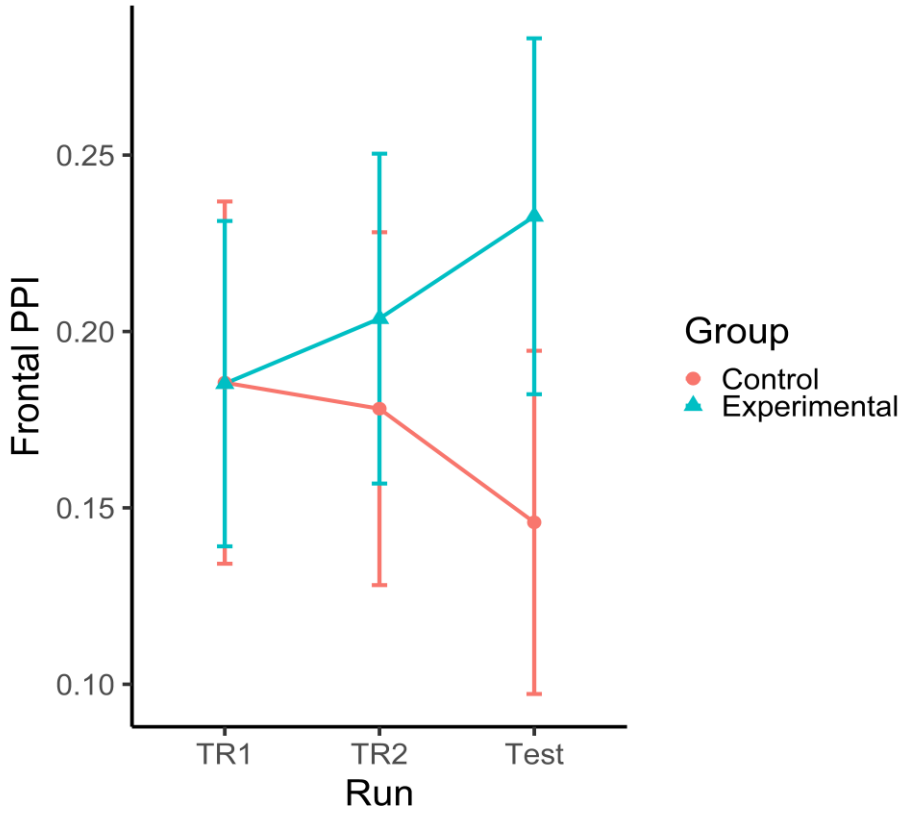

Figure 5-4: Linear mixed effect of PPI connectivity without baseline difference at TR1 across the runs.

It supports hypotheses 1 and 2 that the PPI connectivity improved across runs for experimental. Otherwise, the PPI connectivity decreased across runs for the control group.

5.2 Cognitive analyses

Accuracy

Accuracy is the percentage of the correct answers number of 2-back task (working memory task) from 112 data points during each TR1, TR2, Test. Figure 5-5 is the linear mixed effect analysis of accuracy across runs to show the effect of stimulation. Figure shows the significant increases across the runs for both experimental and control groups (Experimental in Test - TR1: $dF=39.2$, $t=5.21$, $p<0.0001$; Control in Test - TR1: $dF=36.0$, $t=4.72$, $p=0.001$). However, there is no significant difference between group in Test run (experimental - control: $dF=28.6$, $t=-0.16$, $p=0.87$).

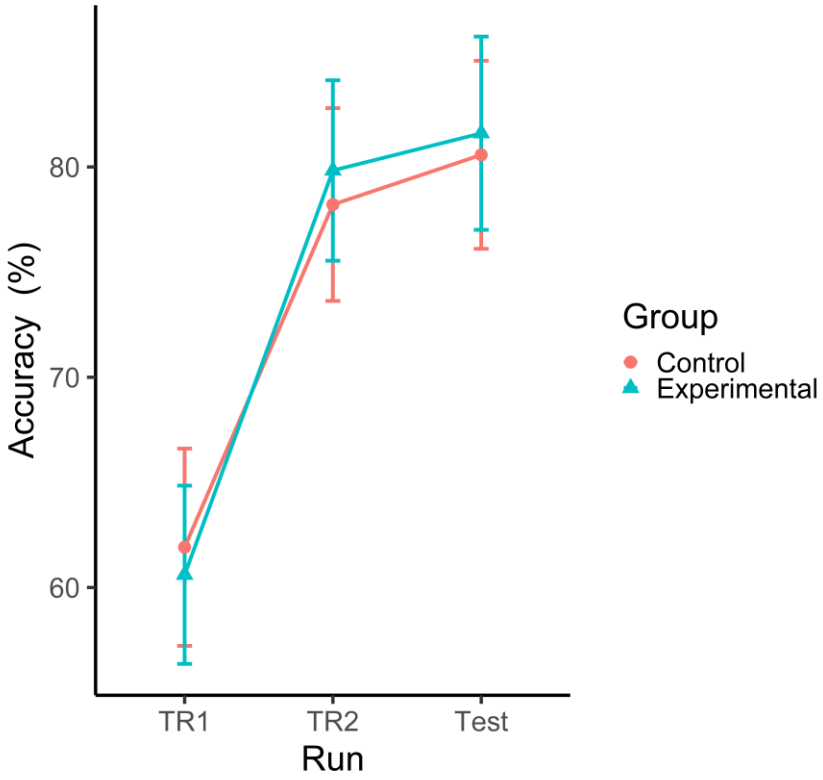

Figure 5-5: Linear mixed effect of accuracy across the runs.

It significantly increases the accuracy across the runs. However, it does not have a significant difference between groups.

Response-time

Response-time is the average time (in seconds) response of the correct answer of 2-back task (working memory task) from 112 data points during each TR1, TR2, Test. Figure 5-6 is the linear mixed effect analysis of response-time across runs to show the stimulation effect. Figure shows the significant decreases across the runs for both experimental and control groups (experimental in Test - TR1: dF=35.8, t=-3.5, p=0.002; control in Test - TR1: dF=34.4, t=-3.46, p=0.003). Also,

there is no significant difference between the group in the Test run. However, the experimental group is a slightly faster response than the control group in all runs.

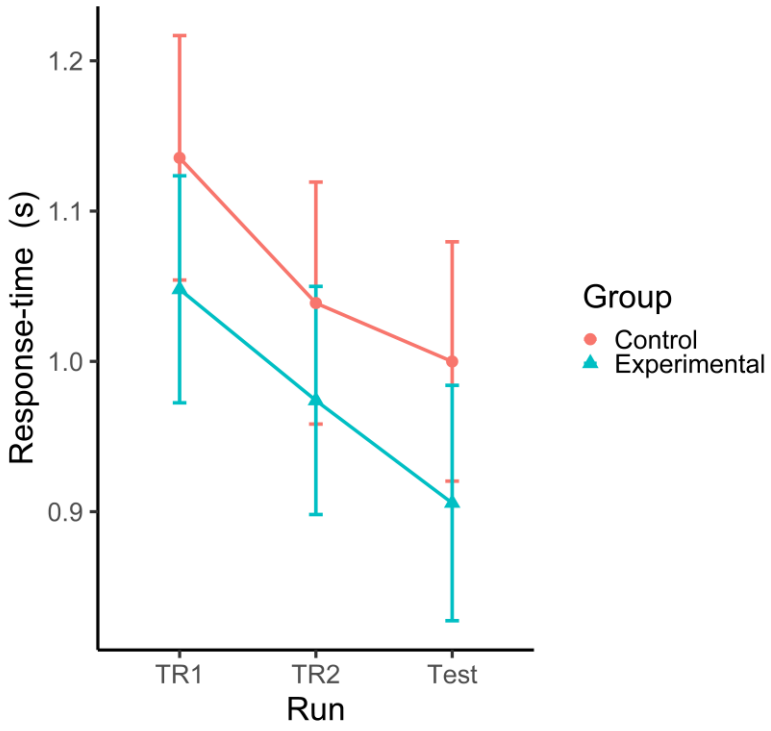

Figure 5-6: Linear mixed effect of response-time across the runs.

It significantly decreases the accuracy across the runs. However, it does not have a significant difference between groups.

There is no difference between the experimental and control group from the linear mixed effect of accuracy and response-time results. It means these results do not support hypothesis 3. Meanwhile, the PPI analysis in subchapter 5.1 supported hypotheses 1 and 2.

5.3 Limitation

The linear mixed effect of PPI and cognitive result analysis shows that increasing or decreasing PPI by stimulation at the same ROI location for all participants does not mean will be fitted for all participants to increase or decrease of working memory (cognitive function). The variation of brain function (state), as well as brain structure, can be considered as the two main sources of inter-and intra-individual variation in response to tACS (Kasten, Duecker, Maack, Meiser, & Herrmann, 2019; Yavari, Nitsche, & Ekhtiari, 2017). The recent protocol study tried to reduce brain function and structure variation by using individualized electrode placement stimulation selection (montage optimization) (Soleimani et al., 2021). Moreover, the earlier studies stated there was a threshold electrical field intensity required to produce measurable physiological effects on neurons (Ivry et al., 2017; Jefferys et al., 2003; Ozen et al., 2010). Therefore, a computational head model (CHM) is essentially needed to simulate how much an electrical dose on the scalp can fulfill at least the minimum electric field (EF) intensity in the target brain. Regarding it, I have designed a procedure to cover not only tACS parameters optimization (individualized tACS parameters) but also consider the montage optimization and electric current (individualized montage and electric current). Those optimizations are described in the future work's chapter.

There are behavioral analyses (alertness and comfortability) in which the data are collected by asking questionnaires to the participant after each run. Those analyses are placed in **Supplementary Materials E** because that data did not collect during stimulation. However, collect by questionnaires which are subjective participant evaluations.

Chapter 6: Conclusion and future work

6.1 Conclusion

The summary of the current protocol and other potential options in designing a closed-loop tACS-fMRI system is illustrated in Figure 6-1. It introduced an online frontoparietal stimulation closed-loop tACS-fMRI protocol. It described the concurrent tACS-fMRI equipment settings, including HD electrodes and montages, online connectivity evaluation with real-time fMRI, and the optimization algorithm. The simulation analysis shows that the focality of electric current stimulation can be obtained under each frontal and parietal site during different phase conditions. Furthermore, by the specific return electrode placement, we can reduce the shunt effect of different phase stimulations to minimal values (stimulated area only increases 4.12% in the anti-phase stimulation compared to the in-phase stimulation). It conducted a safety/noise test for this proposed protocol using watermelon and a single human subject and confirmed that the concurrent tACS-fMRI setting does not cause any adverse heating effects or image artifacts.

Also, it suggested the Simplex optimizer (Nelder-Mead technique) as a simple optimization algorithm with a light computational burden, which is suitable for real-time closed-loop experimental settings with a limited number of parameter search steps. With a task requiring the cognitive load (instead of resting-state), we could expect less fluctuation in the frontoparietal functional connectivity. Utilizing a cognitive task (e.g., 2-back task) to stabilize functional connectivity during the course of stimulation would help the Simplex optimizer search parameter space efficiently.

While the present protocol optimized the tACS frequency and phase difference parameters, optimizing the electrode placement stimulation (montage optimization) may further improve the

efficacy of the stimulation. Although the stimulation coordinates in the present protocol were determined based on previous tACS studies (Jaušovec et al., 2014; Violante et al., 2017b), a newly developed method attempted to optimize the stimulation coordinates utilizing fMRI (Soleimani, Kupliki, Bodurka, Paulus, & Ekhtiari, 2021) can be incorporated in the future studies. Therefore, It proposes a procedure for a future study involving montage and electric current optimization.

However, it confirmed the present protocol could be implemented in practice and worked as expected for a **pilot project**. Also, the experiment result confirms and supports hypotheses 1 and 2 that the current protocol improves frontoparietal PPI connectivity in the experimental group, otherwise decreasing frontoparietal PPI connectivity in the control group. Another finding that based on Bayesian estimation power analysis, the current sample size is not sufficient to be mentioned as a credible result (number of experimental group = 10 participants, control group = 9 participants). Further simulation, Bayesian power analysis suggest that needs 175 participants for each group (total=350 participants) to make the credible effect size. Because of the lack of sample size, therefore, we can see there is a difference baseline at TR1 between group as the effect of insufficient of sample size. However, if we go back to the aims of the experiment as the pilot project, the feasibility of this experiment has been achieved.

The experiment result failed to support the hypothesis to increase/decrease working memory performance in between groups, as mentioned in hypothesis 3. The variation of brain function and brain structure can be considered as the two main sources of inter-and intra-individual variation in response to tACS. These individual variations suspected to be the root cause of there is no significant cognitive function difference between group. Therefore, for the future work, I propose two other optimizations protocol in order to improve cognitive functions. Please find those two other optimizations protocol description in the next future work's sub-Chapter.

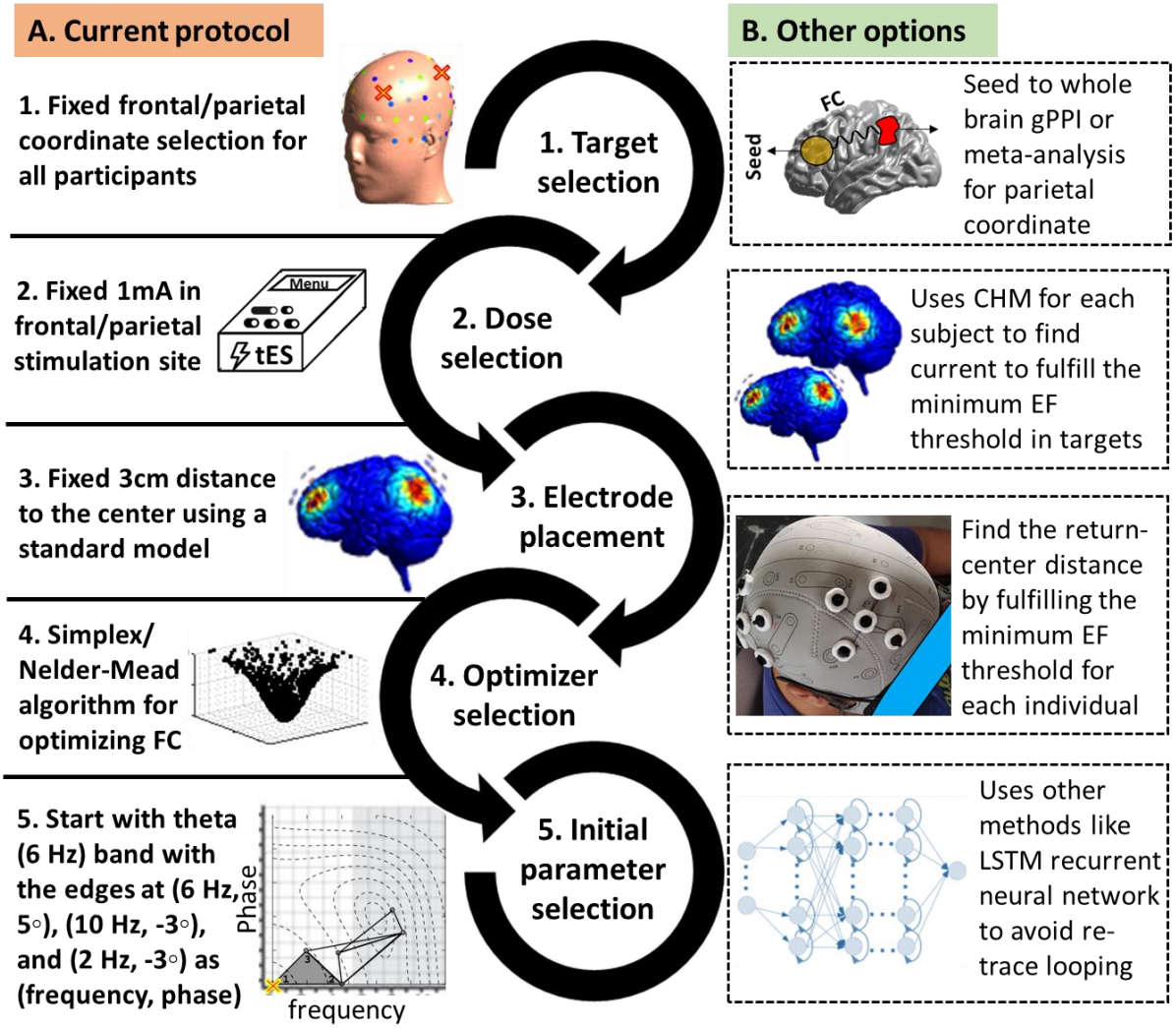

Figure 6-1: Current protocol and other potential options in designing a closed-loop tES-fMRI system.

A) Current protocol. In the current proposed pipeline, there are 5 main steps: (1) fixed frontal and parietal coordinates were used for all participants based on the 10-10 EEG standard system and previous studies with a similar purpose (working memory enhancement), (2) Fixed 1 mA peak-to-peak current intensity is used in both frontal and parietal sites for all subjects refer to the previous study and by considering safety inside the scanner. (3) Fixed 3 cm between electrode distance (between the center and peripheral electrodes) is used based on electric field calculations to have a satisfying focality in the targeted brain region. (4) Simplex/Nelder-Mead optimizer is used for

finding optimized stimulation parameters because of fast and simple computation and fairly robust searching algorithm. (5) Starting point for the Simplex optimizer is in the theta band with the edges at (frequency in Hz, phase difference in degree): (6, 5), (10, -3), and (2, -3) to have a faster search in the optimization. (6) Defining training and testing runs for stimulation protocols. Training 1 and 2: 20 sec Stim, 10 sec no-Stim, and repeated 15 times. There are 7 min rsfMRI time to washout aftereffects stim in between training 1 and training 2 and testing. Experimental group will find the best tES parameters to highest increase functional connectivity (FC), otherwise the Control. B) Other options: There are many other options for the decisions made in the current protocol. For example, seed to whole-brain analysis can be performed for finding connected regions, and computational head models (CHMs) can be used for determining optimized current intensity for each individual based on personalized brain structure to fulfill the minimum EF threshold in order to engage the brain target activity. Between electrode distance can be determined based on personalized skull shape and simulated electric fields, other optimization algorithms like Long-Short Term Memory (LSTM) network or Bayesian optimization can be used for finding optimized stimulation parameters. It would be possible to optimize timing in the application of electrical stimulation, data collection or task-fMRI task design.

6.2 Future work

Pipeline for fMRI Informed Montage Optimization in Dual Site tACS

To optimize functional and anatomical targeting for each individual in a network-level frontoparietal synchronization trial using tACS, There are three kinds of optimization that need to do: (1) Montage optimization (Figure 6-2). (2) Electric current optimization (Figure 6-2). (3) tACS parameters (frequency and phase) optimization (Figure 1-2). Based on Soleimani et al., and Mulyana et al (Mulyana et al., 2021; Soleimani et al., 2021), here are a step-by-step pipeline:

A. Determination of the first stimulation site

1 The first stimulation site could be determined based on the previous studies for stimulating neural targets of interest (e.g., dorsolateral prefrontal cortex (DLPFC) in frontoparietal stimulation).

2 A set of electrodes will be placed over the neural target (e.g., high definition (HD) electrodes over F3 with a more focal DLPFC targeting compared to the conventional large electrode pads). EF distribution patterns will then be calculated based on CHMs.

B. Definition of the fMRI-informed activated/connected regions.

1 A seed region will be defined based on a predefined threshold over the EFs (e.g., a sphere with a specific focality around the maximum EFs).

2 Seed-to-whole-brain connectivity analysis will be performed during rest or task-based fMRI to find brain regions that are currently activated/connected with respect to the seed region (e.g., changes in functional connectivity during the rest obtained from correlation analysis or task-based (e.g., a cue-reactivity task) connectivity obtained from psychophysiological (PPI) interaction).

C. Selection of the second stimulation site.

1 Association between behavioral/cognitive outcomes (e.g., craving score before and after a cue-reactivity task) and changes in connectivity (between seed region and currently activated/connected significant cluster) could support validation of the neural target.

2 The best electrode location for modulating the significant cluster will be determined over the scalp based on the center of the cluster coordinate that is projected to the scalp or using the approximately method on EEG 10-20 standard coordinates that are closest in Euclidean distance to the center of the cluster.

D. Determination of the current amplitude in each stimulation site

Following Tan et al., (Tan et al., 2020b) and the low edge of the intensity (EF threshold = 0.1 V/m) needed for generating measurable physiological effects in neurons (Ivry et al., 2017; Jefferys et al., 2003; Ozen et al., 2010), CHMs and focality area in each site (frontal and parietal sites) can be used for determining the current amplitude and ratio at the anodes and cathodes in a way that averaged EF becomes similar in all stimulation sites.

E. tACS parameters optimization

The online closed-loop tACS-fMRI optimization has been described in Chapters 2 until 4 with the aim to find an optimal tACS oscillation and phase difference between the frontal and the second cluster site, which is most improves or decreases its functional connectivity in order to synchronize/desynchronize level of internal brain activity. The optimization algorithm is needed to seek the vector of parameters corresponding to the maximum or minimum two-dimensional function of space (frequency and phase), searching through the parameter space. The optimizer can use any machine learning algorithm or even use the Simplex algorithm. The ease of deployment in real-time setup and robustness are critical factors in selecting the optimization algorithm and closed-loop protocol design because it is limited by the human maximum time scan and stimulation.

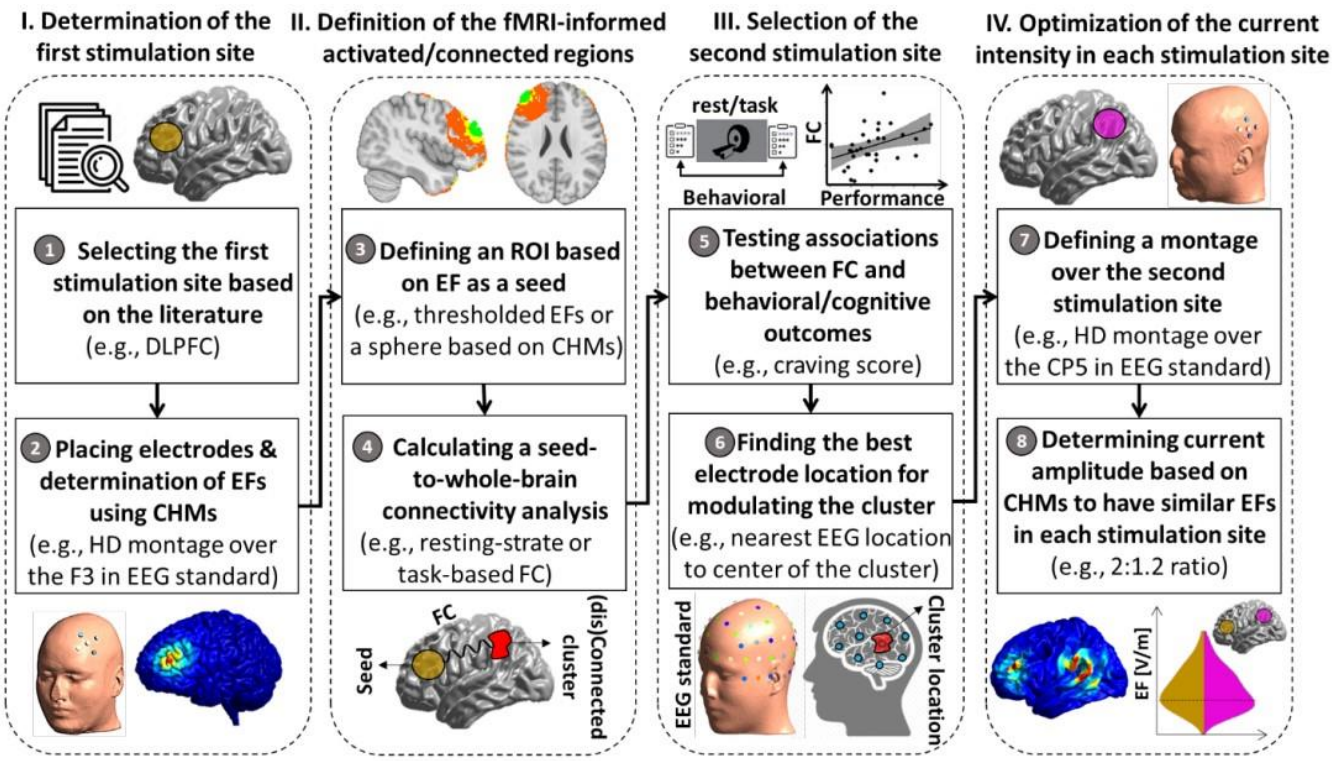

Figure 6-2: An analytic Pipeline for fMRI Informed Montage Optimization in Dual Site tACS

Practical example for the integrating CHM with closed-loop concurrent tACS-fMRI

As a practical example for the integrating CHM with closed-loop concurrent tACS-fMRI, we are going to run a trial to modulate brain response to negative emotional cues to reduce the negative feeling these cues can induce among a group of people with depression.

A. Determination of the first stimulation site

According to the pipeline above, the first neural target/site could be determined based on previous studies. Based on Kuo et al., major depression pathologically reduced/increased activity of the left/right dorsolateral prefrontal cortex (DLPFC) (Kuo et al., 2014). These alterations are compatible with a neuroelectrical/local level intervention approach according to the

spatiomechanistic framework (Yavari et al., 2017). Therefore, we decide the first stimulation site is the left DLPFC which the center coordinate is under F3 on EEG 10-20 standard coordinate. We use a high-definition tACS (HD-tACS) setup site 4 x 1 ring montages with F3 electrode is the center node of the frontal network with electric current = 2mA. Four return-electrodes are placed surrounding the main node at F1, F5, AF3, FC3 (Figure 6-3A) with the electric current for each return electrode is 0.5mA and a phase of 180^{o} is added to fulfill Kirchhoff's law. For electrode, we use MRI compatible rubber HD electrodes that used in Mulyana et al., experiment (Mulyana et al., 2021) (circular pad with radius 1cm and 1mm thickness, electrode material: carbon rubber and plastic shell) (Figure 6-3B) and use Abralyt HiCl highly conductive gel (Piervirgili et al., 2014) as a conductor. We use SimNIBS software as the CHM tool in this study (Saturnino et al., 2019; Thielscher et al., 2015). A seed region will be defined based on a predefined EF threshold (>0.1 V/m) (Ivry et al., 2017; Jefferys et al., 2003; Ozen et al., 2010). For example, a hemisphere radius=10mm around F3 is the volume with an EF greater or equal than = 0.1 V/m (Figure 6-3C).

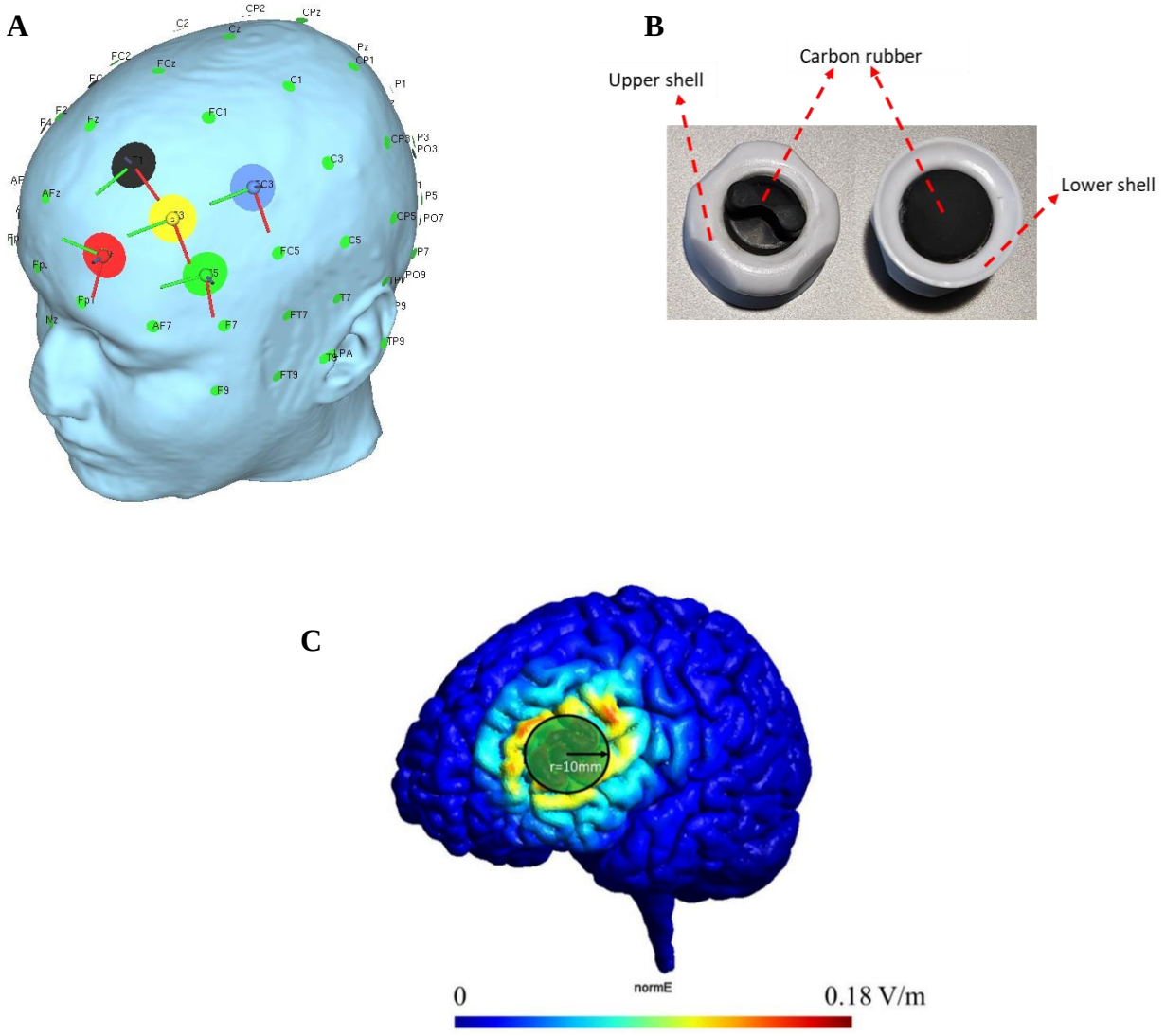

Figure 6-3: The first stimulation site selection.

A) Based on literatures, the first stimulation site is at the left DLPFC which the center coordinate is under F3 on EEG 10-20 standard coordinate. B) MR compatible HD electrodes. C) Frontal site's EF on the cortical surface.

B. Determination of the second stimulation site

The next step is to find the second stimulation site. Seed-to-whole-brain connectivity analysis will be performed on the task-based fMRI to determine the second stimulation site that is currently

activated/connected with respect to the seed region determined in first step. Task-based (in this case is a negative-feeling-reactivity) fMRI follows the psychophysiological interaction (PPI) protocol. The PPI's protocol (Figure 6-4) is adopted from Goodin et al., (Goodin et al., 2019). The blocked design of negative-feeling reactivity task consisted of 20 blocks recorded in two runs (10 blocks per run). Each block was 20 s in length and consisted of 5 trials, with each trial made up of a 2.5 s presentation of the stimuli and 1.5 s presentation of result, either faces (male or female faces displaying sad expressions in odd block indices and neutral expressions in even block indices). Participants were asked to determine whether the sex of the faces on the currently presented image. Responses for the sex of the face were obtained through a button box. Presentation of result will consist of; (1) "Correct" if participant's answer is correct, (2) "Wrong" if participant's answer is wrong, and (3) "Missed to answer" if participant did not press any button during 2.5 s presentation of the stimuli. Assumed, after Seed-to-whole-brain connectivity analysis, we found the second stimulation site at right DLPFC with F4 in EEG 10-20 standard coordinate as the center of the second site (Figure 6-5). This montage in the previous study corresponds to bihemispheric stimulation (bilateral-balanced/bipolar-balanced montage) to simultaneously increased left hypoactive stimulation; also it reduced stimulation of hyperactive right DLPFC in depression subjects treatment using tACS (Nitsche et al., 2009). Supposed, the region of connectivity of the second site has a similar radius with the first site (r=10mm). Furthermore, in group analysis using linear mixed-effect (LME), assumed there is negative association between change behavioral outcomes (depression score before and after a negative-feeling-reactivity task) and PPI connectivity between the seed region and the second stimulation site. Higher score in HAM-D scoring means higher depression level. This is also support validation of the second stimulation site (Figure 6-6). It determines the way of treatment that by decreasing the connectivity between

seed region and currently activated/connected significant cluster reaching to zero or lowest PPI connectivity's value might improve depression score.

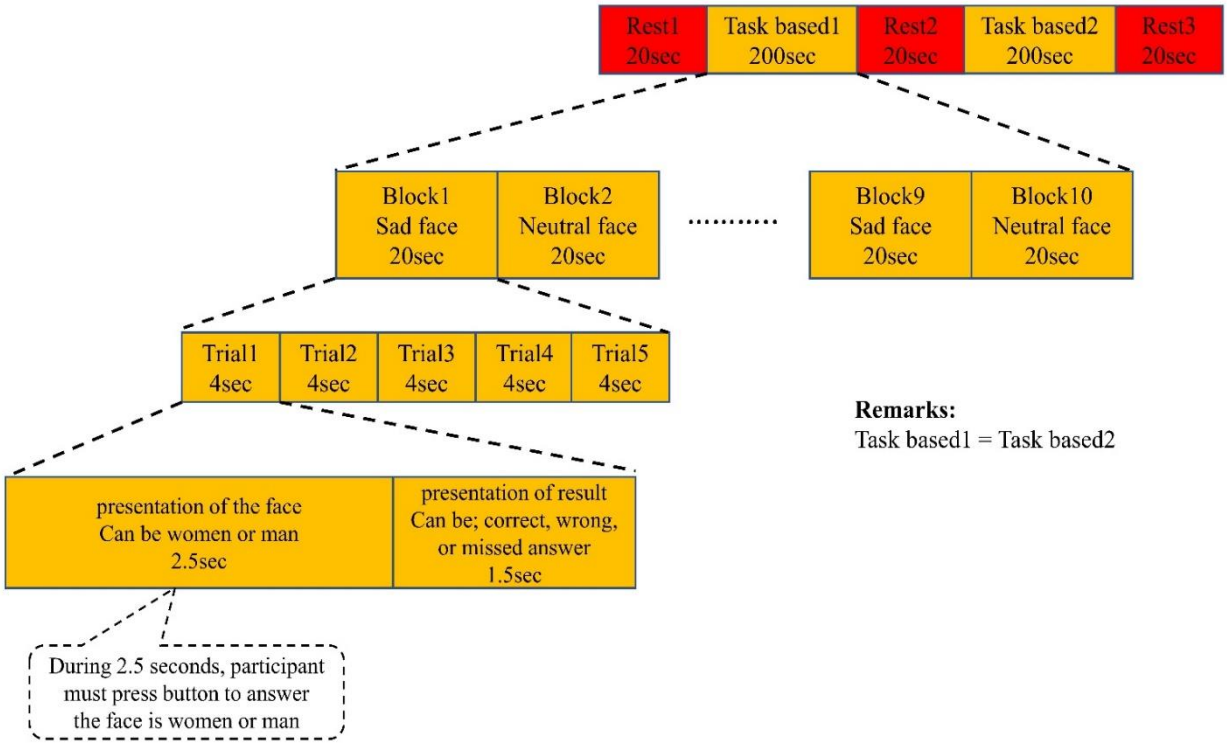

Figure 6-4: Task-based/Psychophysiological interaction (negative-feeling-reactivity) protocol

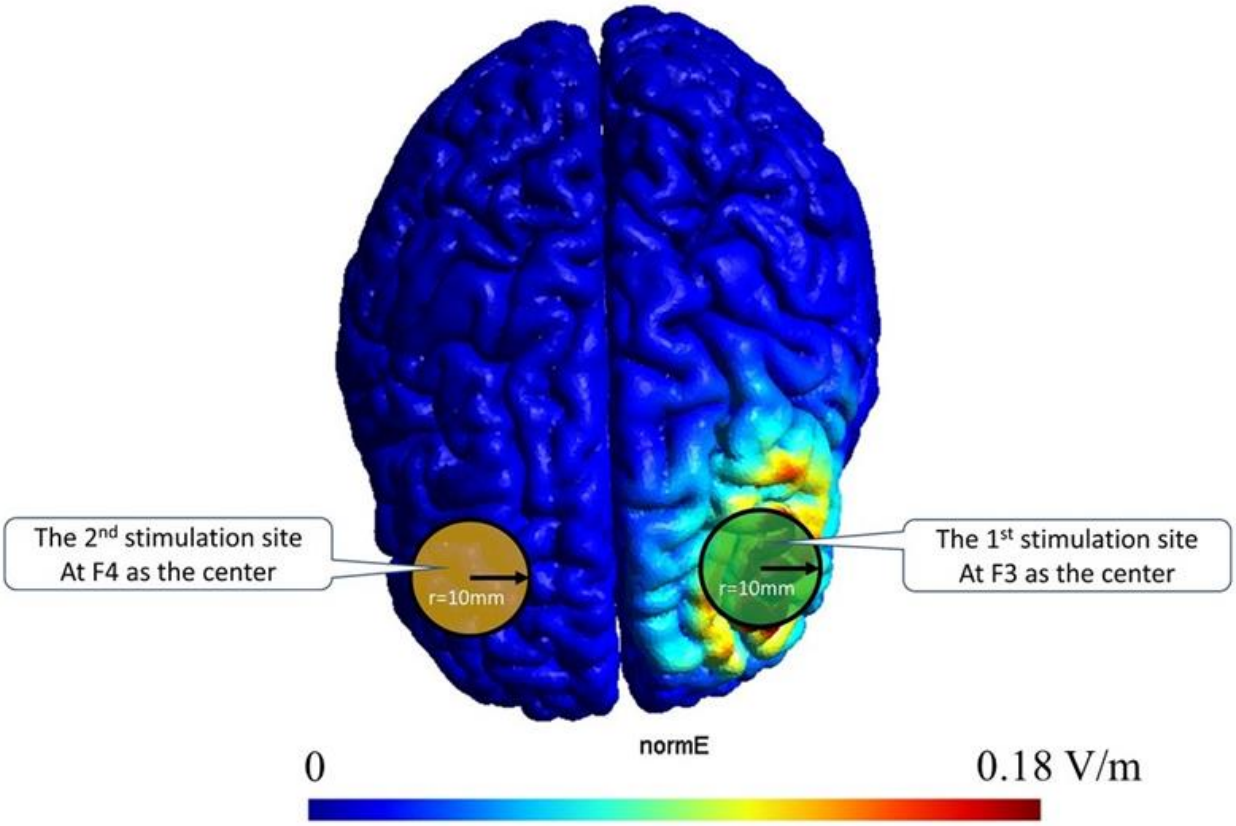

Figure 6-5: The second stimulation site selection.

Based on the seed-to-whole-brain connectivity analysis on the task-based fMRI, the second stimulation site found at right DLPFC with F4 in EEG 10-20 standard coordinate as the center of second site

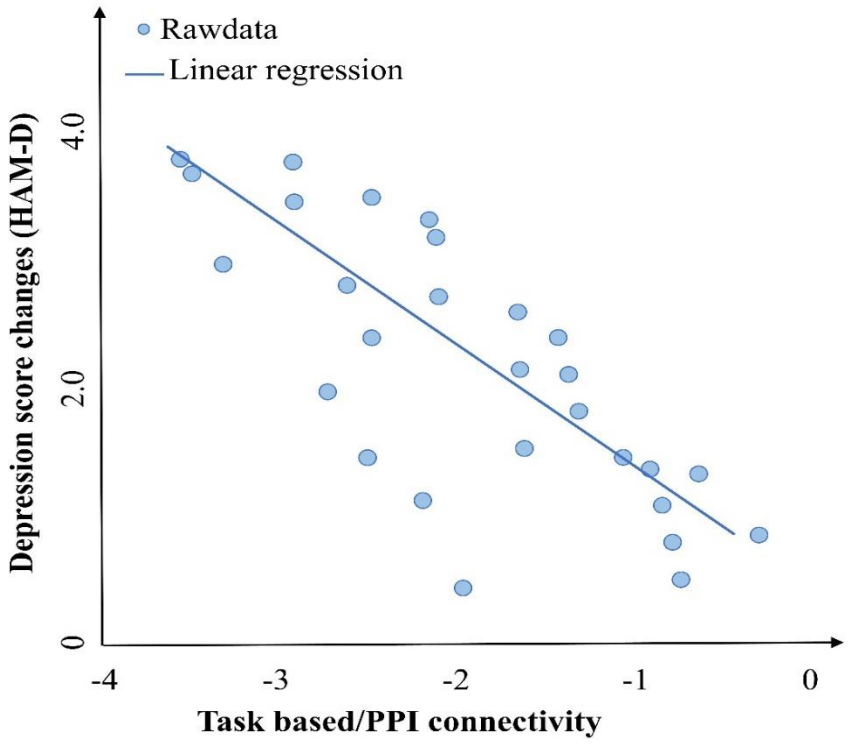

Figure 6-6: Group analysis using linear mixed effect (LME).

Supposed, there is an association between change behavioral outcomes (depression score before and after a negative-feeling-reactivity task) and PPI connectivity between seed region and currently activated/connected significant cluster, this is also support validation of the second stimulation site. Higher score in HAM-D scoring means higher depression level. Minus of PPI connectivity values means the connectivity due to negative-feeling reactivity is less than connectivity in neutral-feeling reactivity. Also, it determines the way of treatment that by increasing the connectivity between seed region and currently activated/connected significant cluster reaching to zero PPI connectivity's value might improve depression score.

C. Determination of electric current for each site

To create a focal area of EF stimulation on the second stimulation area, we need also to use HD electrodes in the second site. The center of site is at F4 coordinate, then 4 return-electrodes at: F2, F6, AF4, FC4 (Figure 6-7A). Dual site HD montage would be like shown in Figure 6-7B. By using

headreco function in SimNIBS and MRI structural brain data from an individual patient, we can create an individualized segmentation and meshing head model. The benefit of individualized segmentation and meshing head model is high accuracy of EF's modeling for each patient because EF are calculated directly from individualized head model properties. Therefore, it needs individualized MRI structural brain data to create an individualized segmentation and meshing head model. For example, from Ernie's head model that available in SimNIBS, we could find EF average in F3 ROI's site = 0.154 V/m when applied electric current 2mA, meanwhile, EF peak in F4 ROI's site = 0.141 V/m in the same electric current. The average of EF between two sites are relatively balanced; however, to make it more balance, the electric current ratio between F3 and F4 ROI's site should be 2:2.15 mA. EFs on cortical surface of two sites shown on Figure 6-7C.

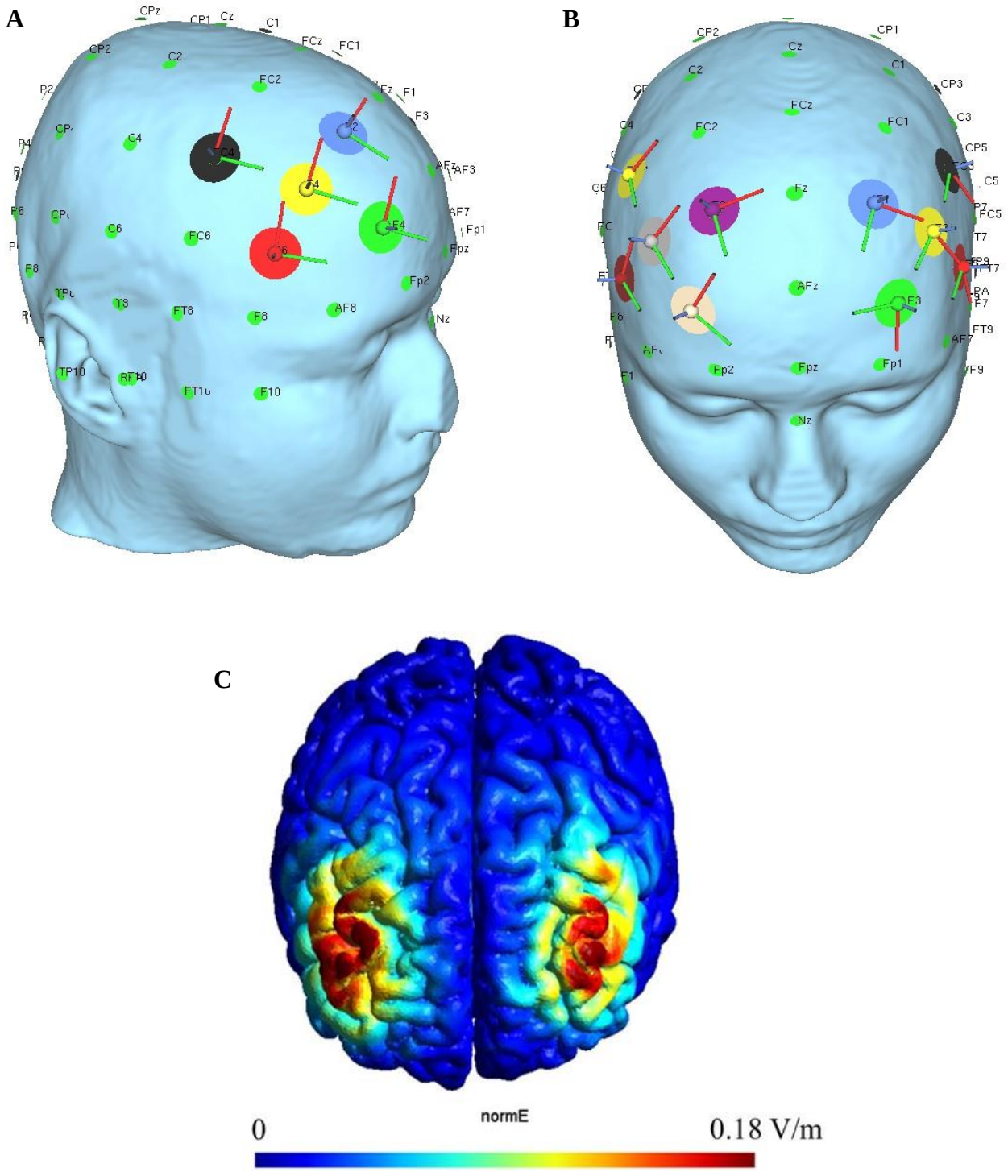

Figure 6-7: The second stimulation site on EEG 10-20 standard coordinate and EFs.

A) The center of second stimulation site is at F4 coordinate, then 4 return-electrodes at; F2, F6, AF4, FC4. B) Dual site HD montage. C) EFs on cortical surface of two stimulation sites.

D. tACS parameters optimization

Finally, we will optimize tACS parameters in order to obtain the lowest PPI connectivity as our goal by using the online closed-loop concurrent tACS-fMRI following Mulyana et al., (Mulyana et al., 2021). The protocol can be shown in Figure 6-8A, the stimulation is divided into two stages (training and testing). Firstly, the MRI anatomical image is aligned to one fMRI echo planar image (EPI) image on Rest1 and then converted to MNI space. Then the frontal-frontal reference mask in MNI space that is obtained from 1 and 2 points (F3 and F4) are multiplied to that result to create an individual mask for calculating the online frontal-frontal connectivity (FFC). The training stage determines the optimum frequency and phase difference parameters that produce the highest online FFC while subjects perform a negative-feeling-reactivity (NFR) task. In here, we hypothesize online FFC has significant positive association with PPI connectivity; therefore, to find the highest online FFC will same as to find the highest PPI connectivity. Directly measuring PPI connectivity is not feasible for online real-time tACS-fMRI because it needs many blocks tACS stimulation and longer time. Meanwhile, the sliding-window online FFC can be measured in one block tACS stimulation in a few seconds, therefore we use it instead of PPI connectivity. The training run is divided into 15 blocks (Figure 6-8B) where each block consists of 20 seconds tACS with parameters (frequency and phase) derived from the Simplex optimizer rules. This is followed by 20 seconds of rest. During each block, the Simplex optimizer searches the optimized parameter of the combination of frequency and phase from the parameters' field (i.e., two-dimensional parameters' field of the frequency (1-150Hz) and phase difference (0–359°)) based on the fMRI FFC measurements. The optimizer uses the Simplex algorithm or the Nelder-Mead technique. Details of this method are explained in (Mathews & Fink, 2004; Nelder & Mead, 1965; Singer & Nelder, 2009). Briefly, it is a simple optimization algorithm seeking the vector of parameters,

which, in this study, are frequency and phase difference between F3 and F4 sites, that correspond to the maximum online FFC. Online FFC calculates using the sliding-window method with the length of window = 20seconds (10TRs). The online FFC is calculated in real-time and analyzed by the Simplex optimizer to predict what frequency and phase cause the highest increase in online FFC. Before the first stimulation block, there is an idling time for a general linear model (GLM) process to regress noise from the fMRI signal for 22 TRs (1 TR = 2 seconds, 22 TRs = 44 seconds). The optimization phase takes approximately 11 minutes and is repeated twice (training 1 and 2), to reduce the burden for the participant and give them a short break between scans. Moreover, the second training is the continuation of the first training which the initial tACS parameters in the second training is the best tACS parameters that achieved from the first training. The testing phase (testing run) tests the optimized parameters' ability to modulate the FFC. The testing run is similar to the training, which is divided into 15 blocks (Figure 6-8C).

A

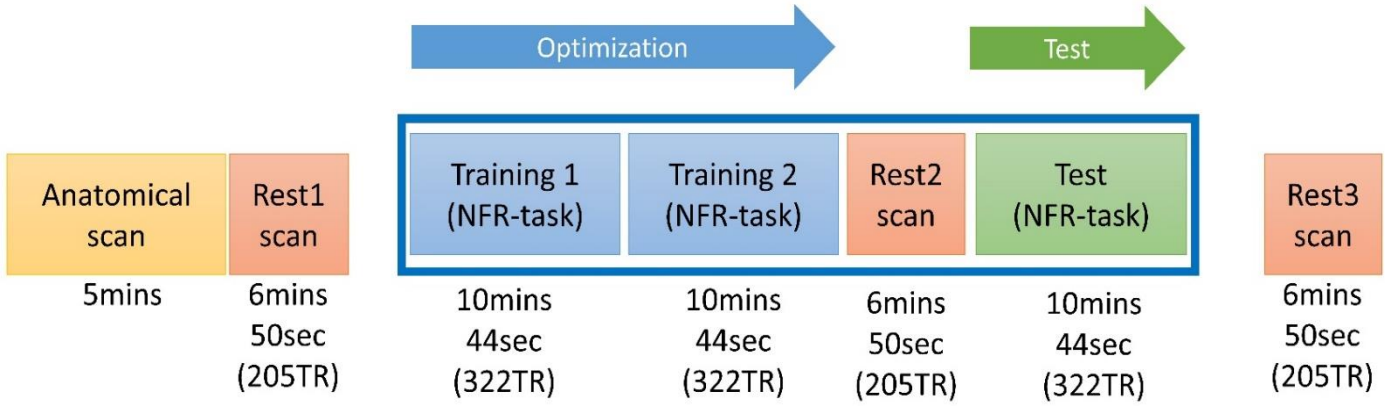

B

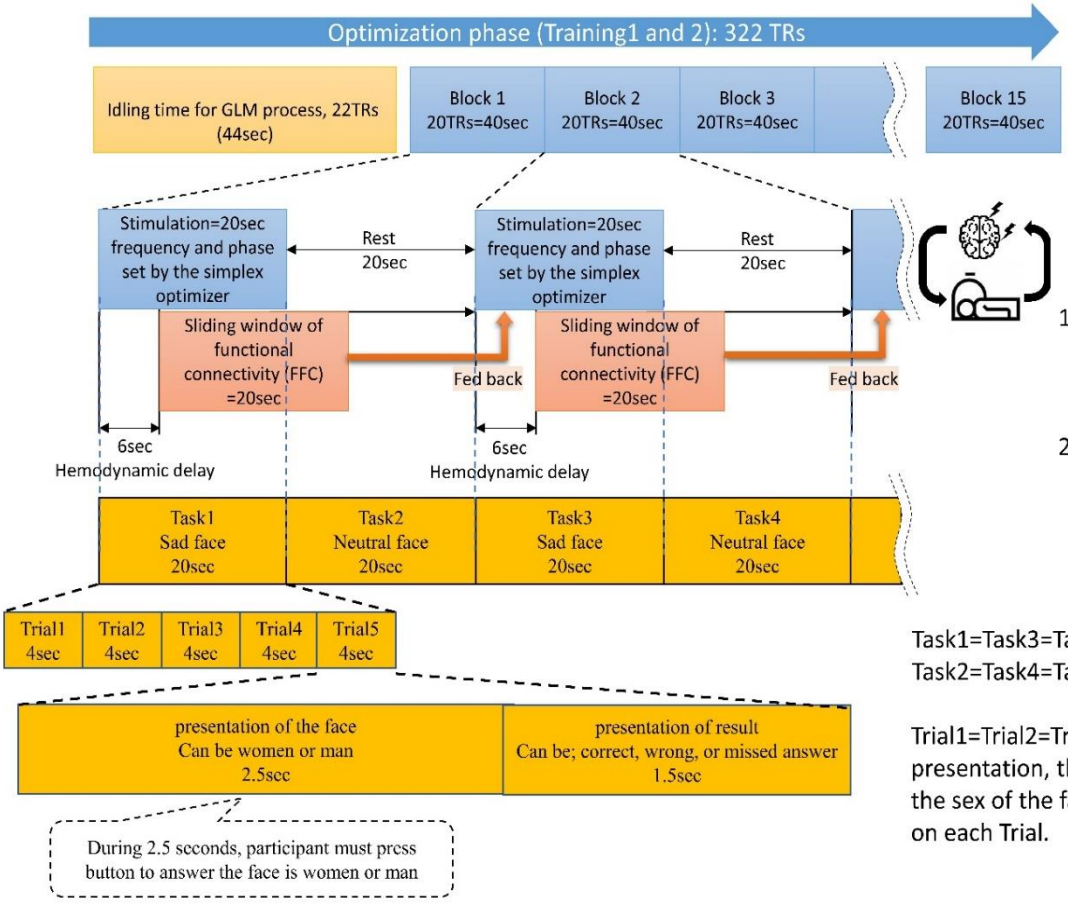

1. Real-time calculation of bilateral frontal-frontal connectivity (FFC) (under F3 and F4) is conducted and is fed back to the optimizer.
2. The optimizer searches through the parameters based on the real-time FFC to maximize its value.

Task1=Task3=Task5=.... (Odd indices are Sad faces)
Task2=Task4=Task6=.... (Even indices are Neutral faces)

Trial1=Trial2=Trial3=Trial4=Trial5 are Sad/Neutral face presentation, then ask patient to determine whether the sex of the faces on the currently presented image on each Trial.

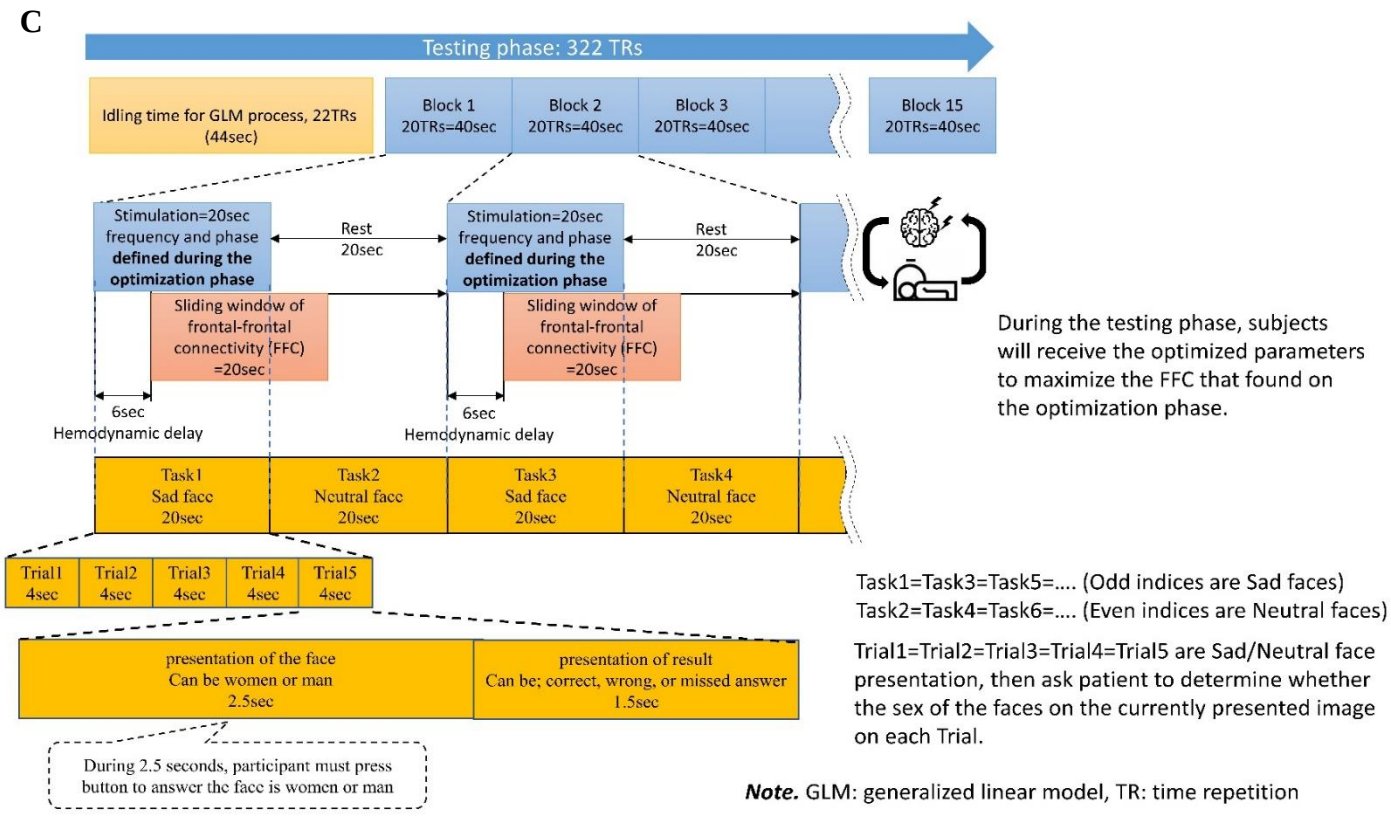

Figure 6-8: A) The online closed-loop concurrent tACS-fMRI protocol.

Stimulation is divided into two stages (training and testing). B) Training/optimization phase. The training run is divided into 15 blocks where each block consists of 20 seconds tACS with parameters (frequency and phase) derived from the Simplex optimizer rules. This is followed by 20 seconds of rest. During each block, the Simplex optimizer searches the optimized parameter of the combination of frequency and phase from the parameters' field. C) The testing phase (testing run) tests the optimized parameters' ability to modulate the FFC. The testing run is the same with the training, which is divided into 15 blocks, however the tACS parameters are fixed using the best tACS parameters obtained from training phase.

Supplementary Materials

A. Electric field derivation in-phase and anti-phase condition

F4 and P4 electrodes in the 10-20 system are the centers of stimulation, with the current function of $F4 = A \times \sin(2\pi \times freq_{F4} \times t + phase_{F4})$, and of $P4 = A \times \sin(2\pi \times freq_{P4} \times t + phase_{P4})$. To reduce space complexity in finding optimal parameters and to reduce training time, the electric current $'A'$ will not become a parameter that will be searched by the optimizer, but it will be fixed to 1 mA-peak value. The current function of each of the F4 returning-electrodes is such that: $\frac{A}{4} \times \sin(2\pi \times freq_{F4} \times t + phase_{F4} + 180^o)$. The current is divided by 4 and a phase of 180^o is added in order to fulfill Kirchhoff's law (Labate & Matekovits, 2016; Paul, 2001). Likewise, the electric current function on each of the P4 returning-electrodes is that: $\frac{A}{4} \times \sin(2\pi \times freq_{P4} \times t + phase_{P4} + 180^o)$. To calculate the electric field on the cortex, we use the method described by Saturnino et al., 2017. Once the electric current is applied through electrode on the scalp, then the electric field at position p inside the head and at time point t is determined by the product of the spatial component $\boldsymbol{E}$(p) and the time course of the electric current I(t) injected into the active channel (equation 1):

$$\boldsymbol{E}(\text{p,t}) = \boldsymbol{E}(\text{p}) \times I(\text{t}) \qquad [1]$$

Because we have 10 electrodes which emit the current mentioned above, the total electric field at the point p as described in equation 2:

$$\boldsymbol{E}(\text{p, t}) = \sum_{i=1}^{10} \boldsymbol{E}_i(p) I_i(t) \qquad [2]$$

For a simpler analysis, we ignore the head curvature and draw the surface of the head in which the electrodes are positioned as a plane surface, as shown in Figures S1B and C, and the electrodes side view as shown in Figure S1A (with where the peripheral electrodes aligned in the direction

of view and occluding each other being and combined into one electrode). In equation 1, the spatial component $\boldsymbol{E}$(p) is inversely proportional to conductivity (κ) at point p and the square of the distance (r) between the electrode to point p or $\left(\frac{1}{\kappa r^2}\right)$. If the $phase_{F4}$ is equal to $phase_{P4}$, termed *in-phase* condition, then the electric field at p under P4 on the y-axis, and at time t_0 using equation 2 can be written as equation 3:

$$\boldsymbol{E}(\mathrm{p}, t_0) = \boldsymbol{E}_1(p)I_1 cos\Theta_1 - \boldsymbol{E}_2(p)I_2 + \boldsymbol{E}_3(p)I_3 cos\Theta_1 + \boldsymbol{E}_4(p)I_4 cos\Theta_2 - \boldsymbol{E}_5(p)I_5 cos\Theta_3 + \boldsymbol{E}_6(p)I_6 cos\Theta_4$$

we know, $\boldsymbol{E}_i(p)$ is proportional to $\left(\frac{1}{\kappa r^2}\right)$, for simplification, we assume κ =1 at point p, and $I_1 = I_3 = 0.5I_2$, $I_4 = I_6 = 0.5I_5$, $and\ I_2 = I_5 = I_o$. If r_2 is the distance from electrode P4 to point p, then equation 3 can be written as equation 4:

$$\boldsymbol{E}(\mathrm{p}, t_0) \approx \frac{0.5I_o}{d_1^2} cos\Theta_1 sin^2\Theta_1 - \frac{I_o}{r_2^2} + \frac{0.5I_o}{d_1^2} cos\Theta_1 sin^2\Theta_1 + \frac{0.5I_o}{d_2^2} cos\Theta_2 sin^2\Theta_2 - \frac{I_o}{d_3^2} cos\Theta_3 sin^2\Theta_3 + \frac{0.5I_o}{d_4^2} cos\Theta_4 sin^2\Theta_4 \qquad [4]$$

Note components: $\frac{0.5I_o}{d_2^2} cos\Theta_2 sin^2\Theta_2 - \frac{I_o}{d_3^2} cos\Theta_3 sin^2\Theta_3 + \frac{0.5I_o}{d_4^2} cos\Theta_4 sin^2\Theta_4$ can be neglected because they are closed to zero since $\Theta_2 \approx \Theta_3 \approx \Theta_4 \approx 90^o$ or r_2 is small, then $cos\Theta_2 \approx cos\Theta_3 \approx cos\Theta_4 \approx 0$.

Therefore, $\boldsymbol{E}(\mathrm{p}, t_0) \approx \frac{0.5I_o}{d_1^2} cos\Theta_1 sin^2\Theta_1 - \frac{I_o}{r_2^2} + \frac{0.5I_o}{d_1^2} cos\Theta_1 sin^2\Theta_1$ and is only influenced by electrodes above the cortex. Likewise, when we analyze along the x-axis, the electric field in in-phase condition will be dominant from electrodes above the cortex surface. If we put the p position in between frontal and parietal (Figure S1B), the electric field on the y-axis in that point is:

$$\boldsymbol{E}(\mathrm{p}, t_0) \approx \frac{0.5I_o}{d_1^2} cos\Theta_1 sin^2\Theta_1 - \frac{I_o}{d_2^2} cos\Theta_2 sin^2\Theta_2 + \frac{0.5I_o}{d_3^2} cos\Theta_3 sin^2\Theta_3 + \frac{0.5I_o}{d_1^2} cos\Theta_1 sin^2\Theta_1 - \frac{I_o}{d_2^2} cos\Theta_2 sin^2\Theta_2 + \frac{0.5I_o}{d_3^2} cos\Theta_3 sin^2\Theta_3$$

or

$$\boldsymbol{E}(\mathrm{p}, t_0) \approx \frac{I_o}{d_1^2} cos\Theta_1 sin^2\Theta_1 - \frac{2I_o}{d_2^2} cos\Theta_2 sin^2\Theta_2 + \frac{I_o}{d_3^2} cos\Theta_3 sin^2\Theta_3 \qquad [5]$$

Once again if $\Theta_1 \approx \Theta_2 \approx \Theta_3 \approx 90^o$ or if r_2 is small, then $\boldsymbol{E}(\mathrm{p}, t_0) \approx 0$. The electric field along the x-axis is also 0 since all x-component are cancelled each other. Thus, in the in-phase condition, there is no electric field in any volume between frontal and parietal electrodes. Therefore, it can be concluded that the electric field on the in-phase condition from our montage will appear under frontal and parietal electrodes but will not appear in between under frontal and parietal electrodes. Then, what is the electric field in between sites if we change into anti-phase condition? It is anti-phase in the condition when $phase_{F4}$ and $phase_{P4}$ differ by 180°. The electric field generated from every electrode at the time t_0 for anti-phase is illustrated in Figure S1C. From Figure S1C, we derive the electric field at point p and time t_0 along x-axis such that:

$$\boldsymbol{E}(\mathrm{p}, t_0) \approx -\frac{0.5I_o}{d_1^2} sin\Theta_1 sin^2\Theta_1 + \frac{I_o}{d_2^2} sin\Theta_2 sin^2\Theta_2 - \frac{0.5I_o}{d_3^2} sin\Theta_3 sin^2\Theta_3$$

$$-\frac{0.5I_o}{d_1^2} sin\Theta_1 sin^2\Theta_1 + \frac{I_o}{d_2^2} sin\Theta_2 sin^2\Theta_2 - \frac{0.5I_o}{d_3^2} sin\Theta_3 sin^2\Theta_3$$

or

$$\boldsymbol{E}(\mathrm{p}, t_0) \approx -\frac{I_o}{d_1^2} sin\Theta_1 sin^2\Theta_1 + \frac{2I_o}{d_2^2} sin\Theta_2 sin^2\Theta_2 - \frac{I_o}{d_3^2} sin\Theta_3 sin^2\Theta_3 \qquad [6]$$

If $\Theta_1 \approx \Theta_2 \approx \Theta_3 \approx 90^o$ or r_2 is small, then $\boldsymbol{E}(\mathrm{p}, t_0) \approx -\frac{I_o}{d_1^2} + \frac{2I_o}{d_2^2} - \frac{I_o}{d_3^2}$, and $\left|-\frac{I_o}{d_1^2} + \frac{2I_o}{d_2^2} - \frac{I_o}{d_3^2}\right|$ could be larger than 0 if $d_1 \ll d_2 < d_3$, $or\ d_1 \approx d_2 \approx d_3$. The electric field along y-axis = 0, caused by every component is cancelled each other.

A

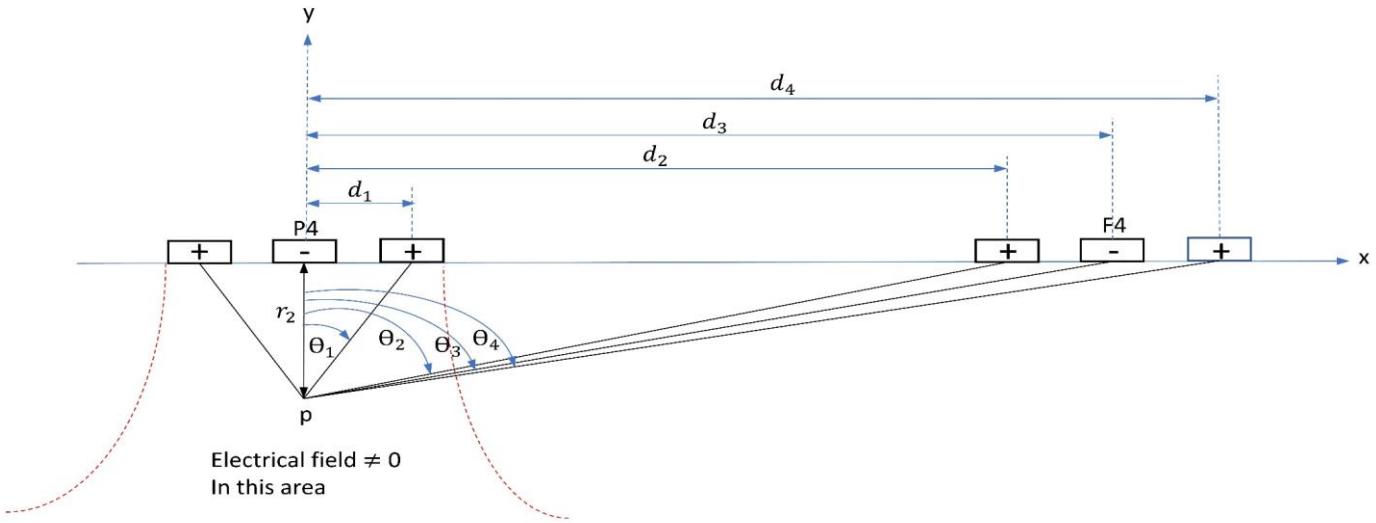
y
d_4
d_3
d_2
d_1
P4
F4
x
r_2
Θ_1
Θ_2
Θ_3
Θ_4
p
Electrical field ≠ 0
In this area

B

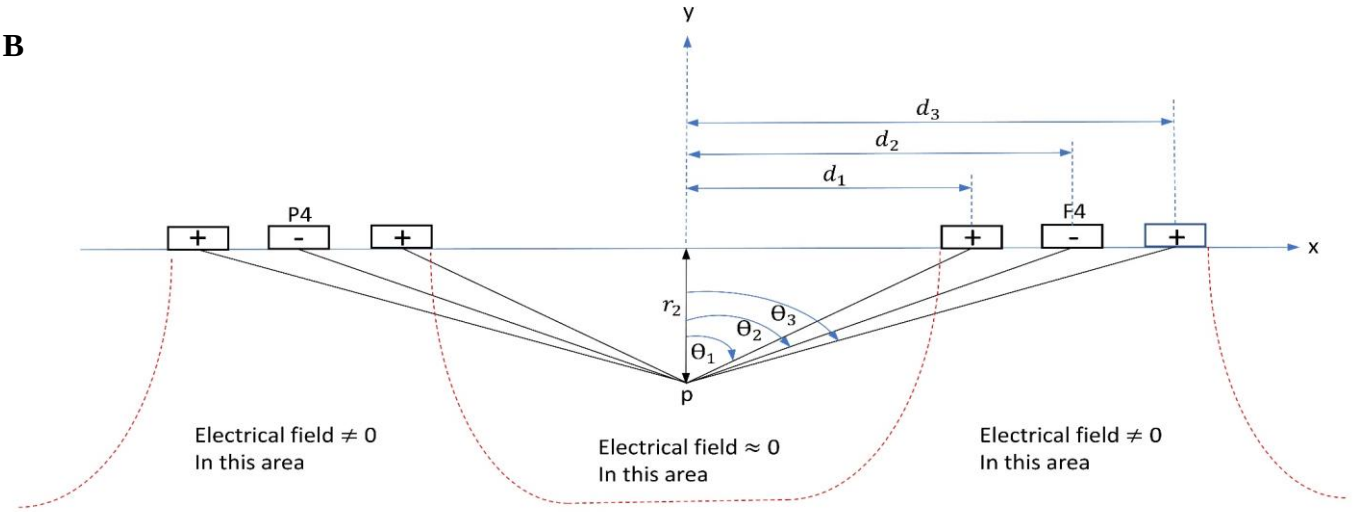
y
d_3
d_2
d_1
P4
F4
x
r_2
Θ_3
Θ_2
Θ_1
p
Electrical field ≠ 0
In this area
Electrical field ≈ 0
In this area
Electrical field ≠ 0
In this area

C

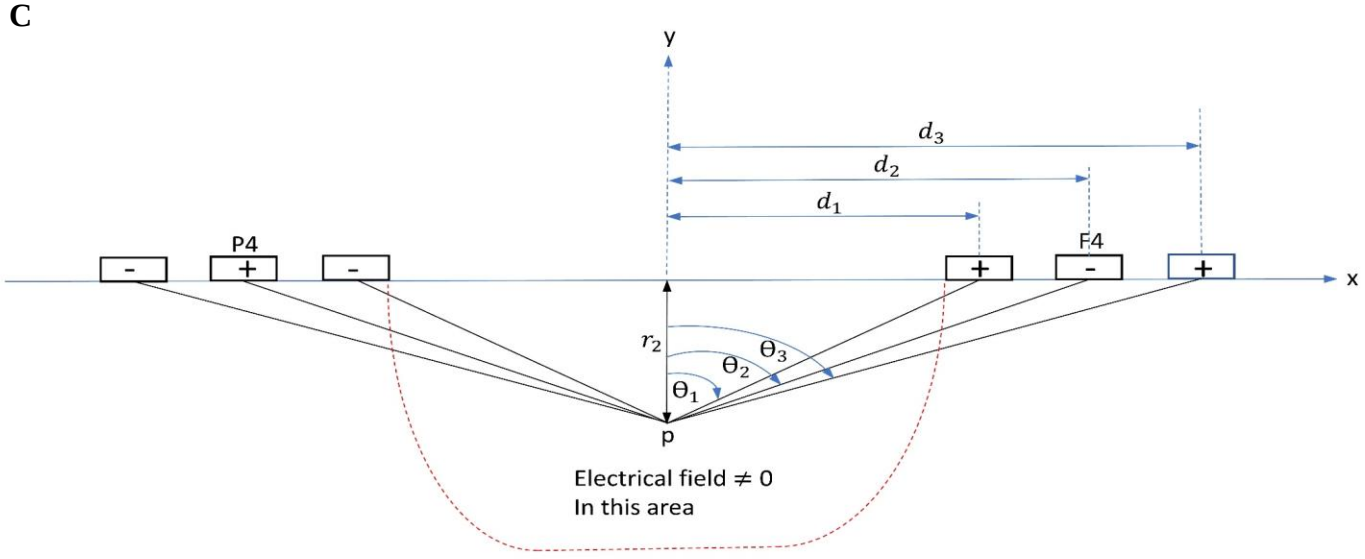
y
d_3
d_2
d_1
P4
F4
x
r_2
Θ_3
Θ_2
Θ_1
p
Electrical field ≠ 0
In this area

Figure S1: The electrodes from the sagittal side view.

d_1, d_2, d_3, d_4 and Θ_1, Θ_2, Θ_3, Θ_4 have two points of view; [1] distance and skewed angle from the center electrode to return electrodes in frontal (F4) and parietal (P4) sites which is related to point A, [2] distance and skewed angle from the center in between sites to each electrode (F4, P4 and their returns) in frontal (F4) and parietal (P4) sites which is related to point B. A) In the in-phase condition, the electric field at point p is dominant from electrodes above its point p; B) In the in-phase condition, the electric field at point p position between frontal and parietal is ≈ 0; C) The electric field generated by electrodes in anti-phase condition. The electric field at point p position between frontal and parietal is $\neq 0$. r_1 and r_2 are the distance from the scalp to point p inside the brain.

B. MRI Artifacts, fMRI Noise Testing Method

We use the same tACS stimulation device (Starstim R32; Neuroelectrics Barcelona SLU; Spain) inside the MRI (3T MRI scanner (Discovery MR750; GE Healthcare Systems, Milwaukee, WI) with an 8-channel receive-only head coil). Single-shot gradient-recalled echo-planner imaging (EPI) with sensitivity encoding (SENSE) is used for the scans with the parameters of FOV = 240 × 240 mm, matrix = 96 × 96 reconstructed into 128 × 128, SENSE acceleration factor R = 2, 45 axial slices with slice thickness = 2.9 mm, TR/TE = 2/0.025seconds, flip angle = 90^o. The tACS montage is the same as described in section 2.1, which used 10 HD electrodes with 4 × 1 ring montage at two sites (F4 and P4 are active electrodes). F4 and P4 electrodes are selected as the main nodes of the frontoparietal network (1mA, 6Hz, 0^o phase difference; Figure 2-3), and eight electrodes are used as return electrodes surrounding F4 and P4 with coordinates are described in Chapter 2.1. We use three scanning protocols for different goals. The first scan is obtained without radio frequency (RF) to evaluate the impact of tACS on the EPI k-space during no-RF excitation or only noise to draw EPI images. The second is obtained with RF excitation to evaluate the impact of tACS on voxel-wise EPI images and temporal signal to noise ratio (TSNR). And the third one

is to confirm tACS-fMRI safety. We used a watermelon phantom for the first and second scans to avoid the effect of a neural activation signal modulated by tACS stimulation. The stimulation block in the first and second scan is a 20-seconds tACS stimulation ON and following by a 10-seconds no-stimulation, then the block is repeated 15 times with a 12-seconds OFF block at the beginning. The initial 12-seconds of data are excluded from the analysis to ensure a steady-state fMRI signal. Without-RF EPI scanning data on the first scan has dimension [128 128 45] and time course = 225TRs ($10 \times 15 = 150TRs$ from Stim ON, and $5 \times 15 = 75TRs$ from Stim OFF). Data is transformed by two-dimensional fast Fourier transform (2D FFT) to obtain k-space data. Since this data is collected without-RF excitation, we can evaluate the tACS influence on the MRI system noise in the receiving signal free from the sample signal, and without having a flip angle to synchronize proton magnetization phases. Therefore, phase-encoding will be encoded randomly from 0^o until 360^o, asynchronous with tACS, ensuring that the noise amplitude in the phase encoding direction collapses once averaged, leaving the data frequency-encoding and z-slice selected along the time course (dimension: [128 45 225]). Next, ON and OFF stimulation data are separated, and a t-test is performed between ON/OFF conditions for each frequency encoding (kx-direction) and z-slice selection. All corresponding p-values are corrected for multiple hypothesis comparisons testing using the Benjamini and Hochberg procedure for False Discovery Rate (FDR) discovery (Benjamini & Hochberg, 1995). For the voxel-wise analysis in the second scan, we performed GLM analysis on the image time-course data using 3dDeconvolve in AFNI (https://afni.nimh.nih.gov/). The regressors included a boxcar time-series for the ON period and 3rd-order Legendre polynomials to remove the low-frequency fluctuation. We also compared mean value of time series in each voxel within the ROIs (F4 and P4) and its SD for the ON and OFF period. For TSNR analysis, it also uses EPI data images with-RF scan. First, ON and OFF

stimulation data of EPI data images are separated. Then TSNR is calculated for each ON and OFF stimulation data using 3dTstat to create voxel-wise TSNR.

For the fMRI safety evaluation in the third protocol, we performed a concurrent tACS-fMRI scan for a healthy female volunteer (age 38 years) to measure temperature change on the scalp under the electrodes due to concurrent tACS stimulation during fMRI. The temperature is obtained by placing MRI compatible temperature sensors (Biopac TSD202A and Biopac SKT100C, sensitivity = 100 micro °C, sample rate = 200points/seconds) under the electrodes (P4 and F4). We used the same montage (Figure 2-3), fMRI parameters, and tACS parameters as in the first and second scans. We collected a baseline temperature for 2 minutes before the scanning and stimulation. Then, 2-minutes ON and OFF blocks are repeated three times to see the tACS effect in a long time period. The temperature difference between the ON and OFF periods is tested with z statistics. This study was conducted in accordance with the Declaration of Helsinki and all methods were carried out in accordance with relevant guidelines and IRB approval.

C. Prior- and post-scannings data analysis

1. CONSORT flow diagram of participants

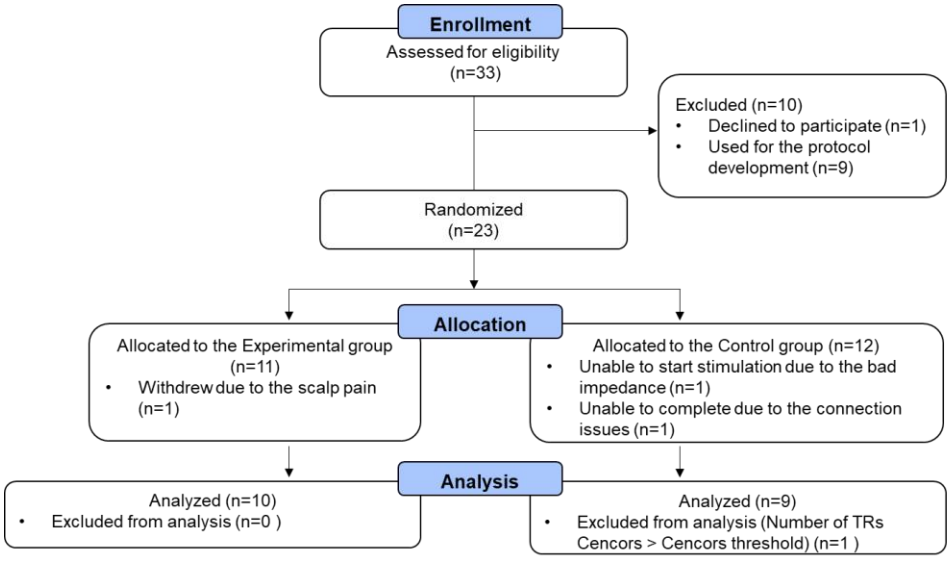

Figure S2: The process to consort participants.

2. Demographics

	Experimental group (n=10)	Control group (n=10)	Statistics
Age	38.20 (10.35)	38.60 (10.46)	$t(18)=-0.09$, $p=0.93$
Male (%)	4 (40%)	4 (40%)	$\chi^2(1)<0.001$, $p=1.00$
POMS			
Total Mood Disturbance	-7.20 (17.37)	-6.70 (9.62)	$t(18)=-0.08$, $p=0.94$
Tension	3.40 (2.99)	2.50 (1.90)	$t(18)=0.80$, $p=0.43$
Depression	2.10 (4.98)	0.20 (0.42)	*Welch's* $t(9.13)=1.20$, $p=0.26$
Anger	1.10 (2.85)	0.70 (1.57)	$t(18)=0.39$, $p=0.70$
Fatigue	2.00 (2.16)	1.40 (1.96)	$t(18)=0.65$, $p=0.52$
Vigor	18.70 (6.11)	14.10 (7.00)	$t(18)=1.57$, $p=0.13$
STAI-State	29.10 (6.84)	29.90 (7.17)	$t(18)=-0.26$, $p=0.80$

Figure S3: Participants' demographics. Data shows age, sex, profile of mood states (POMS), and state-trait anxiety inventory (STAI-State) are no different in between group.

3. Aversive effect after the experiment

	Experimental group (n=10)	Control group (n=10)	Statistics
Blindness	3 (30%)	7 (70%)	$\chi^2(1)=3.2$, $p=0.07$
Blindness response confidence	5.7 (3.13)	5 (3.43)	$t(18)=0.48$, $p=0.64$
Headache	1 (10%)	0 (0%)	$\chi^2(1)=1.05$, $p=0.30$
Scalp Pain	2 (20%)	3 (30%)	$\chi^2(1)=0.27$, $p=0.60$
Tingling	3 (30%)	3 (30%)	$\chi^2(1)=0.0$, $p=1$
Itching	1 (10%)	0 (0%)	$\chi^2(1)=1.05$, $p=0.30$
Burning Sensation	1 (10%)	2 (20%)	$\chi^2(1)=0.39$, $p=0.50$
Skin Redness	1 (10%)	0 (0%)	$\chi^2(1)=1.05$, $p=0.30$
Sleepiness	5 (50%)	6 (60%)	$\chi^2(1)=0.20$, $p=0.65$
Neck Pain	1 (10%)	1 (10%)	$\chi^2(1)=0.0$, $p=1$
Trouble Concentrating	4 (40%)	2 (20%)	$\chi^2(1)=0.95$, $p=0.33$
Acute Mood Change	0 (0%)	0 (0%)	$\chi^2(1)=0.0$, $p=1$
Other Adverse Effects	0 (0%)	0 (0%)	$\chi^2(1)=0.0$, $p=1$

Figure S4: Aversive effects after experiment.

Data shows there are no aversive effect different in between group.

4. Number of TRs censors

SubjID	Group	TR1	TR2	Test
1	Experimental	17	8	51
2	Control	7	4	6
3	Control	3	6	6
4	Experimental	0	5	14
5	Control	12	6	20
6	Experimental	12	23	70
7	Control	0	0	0
8	Experimental	7	15	14
9	Experimental	8	8	15
10	Experimental	2	2	0
11	Control	0	2	2
12	Experimental	2	6	13
13	Control	4	4	6
14	Control	0	4	15
15	Experimental	0	2	0
16	Control	118	124	130
17	Control	3	9	4
18	Experimental	14	13	15
19	Experimental	6	34	26
20	Control	12	23	29

Figure S5: The number of TRs censors.

The number of TRs censors are less than 75 (1/3 of the total TRs (225)) for each run, except SubjID 16. Therefore, in all analyses SubjID 16 is removed from analyses. TR is censored when the motion is larger than 20% from the previous TR (one step ahead TR).

5. Scatter plot with optimized frequency and phase

Figure S6 shows the optimized frequency and phase (the frequency and phase that is given on Test run after Training runs) for each subject. Plotting is in 2D scattering between frequency and phase. Then it calculates t-test the difference between group. The result of t-test for frequency: [Experimental: mean = 4.9, SD = 3.9; Control: mean = 5, SD = 4.6; t[17] = -0.05, p = 0.90]. Meanwhile the result of t-test for phase difference: [Experimental: mean = -0.4, SD = 10.1; Control: mean = -0.22, SD = 7.5; t[17] = -0.04, p = 0.96]. From those result we can conclude there is no significant difference between Experimental and Control Group in frequency and difference

phase. The range of optimized frequency and phase difference are (1 – 15Hz, -30^{o} – 20^{o}) with the mean of frequency for both groups are in theta band. It follows the literature the theta band correlates with cognitive function activation.

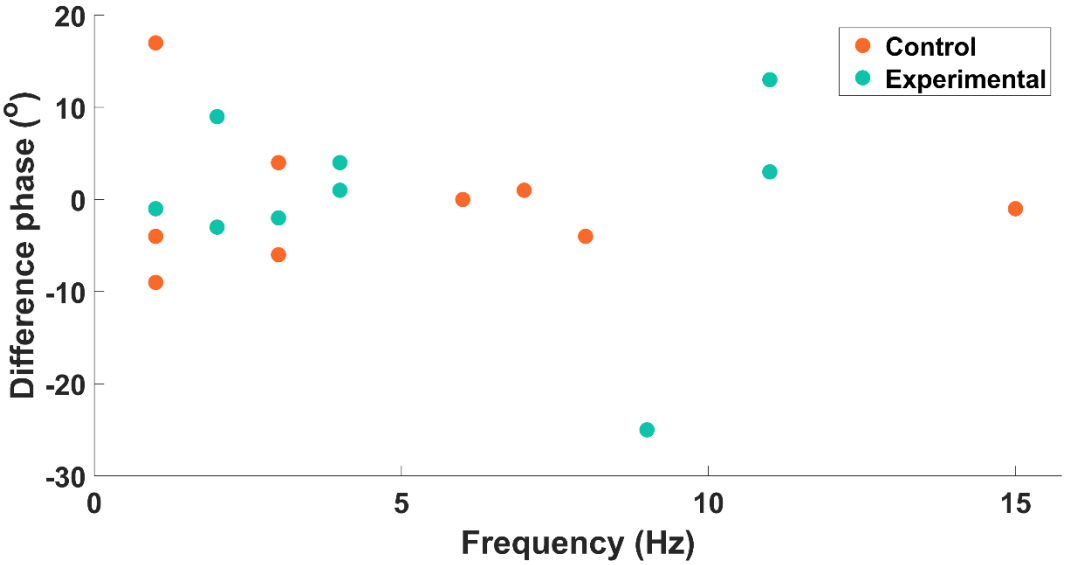

Figure S6: Scatter plot with optimized frequency and phase

D. Description of PPI method

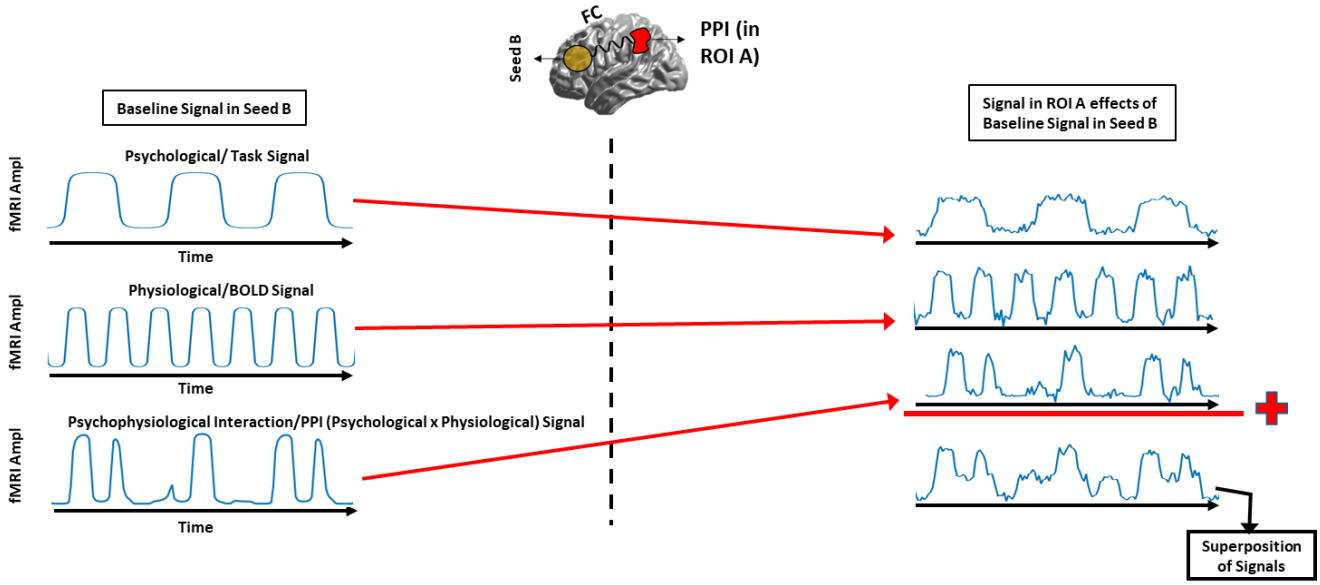

Figure S7: Illustration of the seed to an ROI brain PPI analysis.

PPI is a linear regression analysis following this formula:

$$Y_A \approx \beta_1.((HRF * tACS_{stim}).Yseed_B) + \beta_2.Yseed\_orth_B + \beta_3.(HRF * tACS_{stim}) + e$$

PPI regressor

physiological/BOLD regressor only

Psychological/Task based regressor only

Where:

- $A\ or\ B\ is\ the\ seed\ of\ interest\ that\ can\ be\ frontal\ or\ parietal\ brain\ region$
- $Yseed_B = BOLD\ signal\ from\ the\ seed's\ (ROI)\ B$
- Y_A=$Bold\ signal\ from\ the\ voxels\ or\ region\ A$
- HRF = *Hemodynamic response function*
- $tACS_{stim}$ = *tACS stimulation block (e.g., 20seconds ON, 10seconds OFF, repeated 15 times)*
- $Yseed\_orth_B$ = $BOLD\ signal\ from$ *ROI's B that orthogonal respect to* $(HRF * tACS_{stim}).Yseed_B$
- *e = residuals model*
- β_1 = *beta coefficient of the PPI regressor,* ***we need to find this value for each seed***
- From each subject and each run obtained 2 results: β_1 from Frontal, β_1 from Parietal

E. Behavior analysis

1. Linear mixed effect of alertness

Alertness is measured by Karolinska Sleepiness Scale (KSS) Questionnaire after each run. The higher scale the lesser alertness.

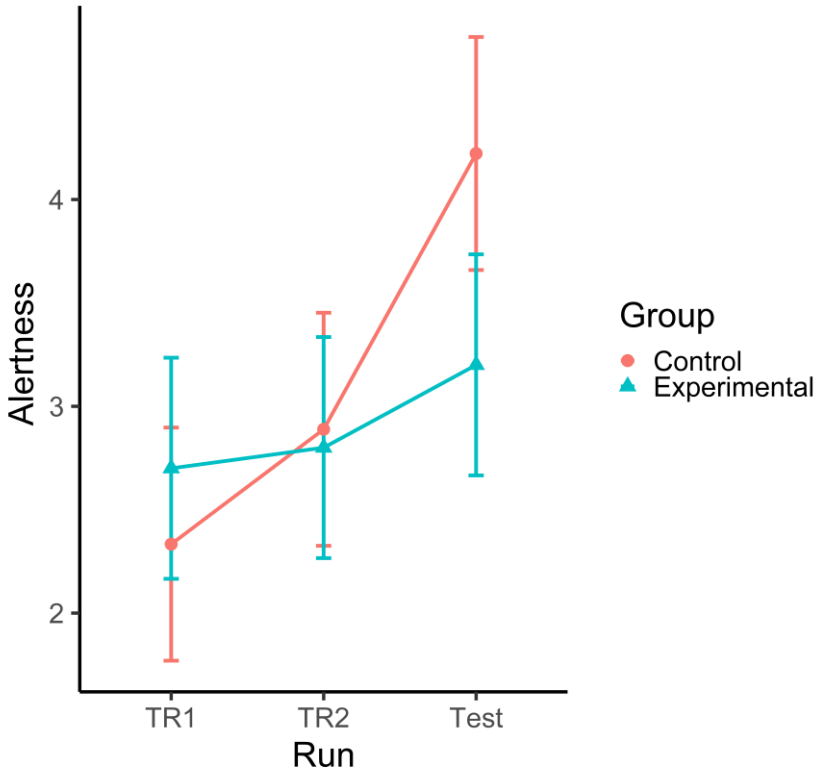

Alertness ~ Run*Group + motion + (1|Subj)

Figure S8: Linear mixed effect of alertness.

Control shows significant decrease of alertness. Otherwise, experimental does not show any significant alertness change.

Control group decreases significant alertness (Test compared to TR1 run in Control: dF=34, t=3.46, p=0.003). Otherwise, experimental group does not significantly decrease alertness (Test compared to TR1 run in Experimental: dF=34, t=0.97, p=0.53).

2. Comfortability

Comfortability is measured by Visual Analog Scale (VAS) of the Comfortability Questionnaire after each run. The higher scale the more comfort.

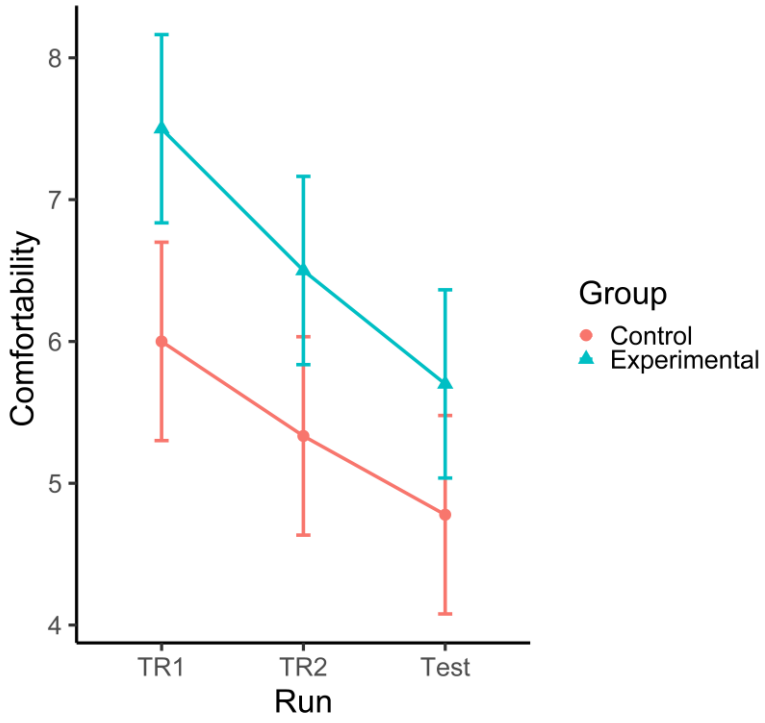

Figure S9: Linear mixed effect of comfortability.

Both groups decreased comfortability significantly across runs. However, the Control group lesser comfortable than the Experimental group in all runs.

Glossary of Terms

Term	Description
2D FFT	2-Dimensional Fast Fourier Transform
AFNI	Analysis of Functional NeuroImages
BEST	Bayesian Estimation Supersedes The t-Test
BOLD	Blood-Oxygen-Level-Dependent
CHM	computational head model
cm	Centimeter
dF	Degree of Freedom
DLPFC	Dorsolateral Prefrontal Cortex
ECN	Executive Control Network
EEG	Electroencephalography
EF	Electrical Field
EPI	Echo Planar Imaging
FC	Functional Connectivity
FDR	False Discovery Rate
FFC	Frontal-Frontal Connectivity
fMRI	Functional Magnetic Resonance Imaging
FOV	Field of View
FPS	Frontoparietal Synchronization
GLM	General Linear Model
HAM-D	Hamilton Depression Rating Scale

HD	High Definition
HDI	Highest Density Interval
HRF	Hemodynamic Response
IPA	Isopropyl Alcohol
KSS	Karolinska Sleepiness Scale
LME	Linear Mixed Effect
mA	Miliampere
MEG	Magnetoencephalography
MNI	Montreal Neurological Institute Space Standard
MR	Magnetic Resonance
MRCDI	Magnetic Resonance Current Density Imaging
NFR	Negative-Feeling-Reactivity
NG	Next Generation
NIBS	Non-Invasive Brain Stimulation
NIfTI	Neuroimaging Informatics Technology Initiative
POMS	Profile of Mood States Scale
PPI	Psychophysiological Interaction
RF	Radio Frequency
ROI	Region of Interest
ROPE	Region of Practical Equivalent
rsfMRI	Resting-State Functional Magnetic Resonance Imaging
SD	Standard Deviation
SENSE	Sensitivity Encoding

SimNIBS	Simulation Non-Invasive Brain Stimulation
SNR	Signal Noise Ratio
STAI-S	State-Trait Anxiety Inventory
SubjID	Subject Identity
tACS	Transcranial Alternating Current Stimulation
tDCS	Transcranial Direct Current Stimulation
TE	Time Echo
tES	Transcranial Electrical Stimulation
TR	Time Repetation
tRNS	Transcranial Random Noise Stimulation
TSNR	Temporal Signal-Noise Ratio
VAS	Visual Analog Scale
WIRB	Western Internal Review Board

References

Akam, T., & Kullmann, D. M. (2014). Oscillatory multiplexing of population codes for selective communication in the mammalian brain. *Nature Reviews Neuroscience*. https://doi.org/10.1038/nrn3668

Alam, M., Truong, D. Q., Khadka, N., & Bikson, M. (2016). Spatial and polarity precision of concentric high-definition transcranial direct current stimulation (HD-tDCS). *Physics in Medicine and Biology*. https://doi.org/10.1088/0031-9155/61/12/4506

Andersen, L. M., Jerbi, K., & Dalal, S. S. (2020). Can EEG and MEG detect signals from the human cerebellum? In NeuroImage (Vol. 215). Academic Press Inc. https://doi.org/10.1016/j.neuroimage.2020.116817

Antal, A., Alekseichuk, I., Bikson, M., Brockmöller, J., Brunoni, A. R., Chen, R., Cohen, L. G., Dowthwaite, G., Ellrich, J., Flöel, A., Fregni, F., George, M. S., Hamilton, R., Haueisen, J., Herrmann, C. S., Hummel, F. C., Lefaucheur, J. P., Liebetanz, D., Loo, C. K., … Paulus, W. (2017). Low intensity transcranial electric stimulation: Safety, ethical, legal regulatory and application guidelines. In *Clinical Neurophysiology* (Vol. 128, Issue 9).

Antal, A., Boros, K., Poreisz, C., Chaieb, L., Terney, D., & Paulus, W. (2008). Comparatively weak after-effects of transcranial alternating current stimulation (tACS) on cortical excitability in humans. *Brain Stimulation: Basic, Translational, and Clinical Research in Neuromodulation*, *1*(2), 97–105. https://doi.org/10.1016/J.BRS.2007.10.001

Antal, A., & Paulus, W. (2013). Transcranial alternating current stimulation (tACS). *Frontiers in Human Neuroscience*. https://doi.org/10.3389/fnhum.2013.00317

Bächinger, M., Zerbi, V., Moisa, M., Polania, R., Liu, Q., Mantini, D., … Wenderoth, N. (2017). Concurrent tACS-fMRI reveals causal influence of power synchronized neural activity on resting state fMRI connectivity. *Journal of Neuroscience*. https://doi.org/10.1523/JNEUROSCI.1756-16.2017

Beeli, G., Casutt, G., Baumgartner, T., & Jäncke, L. (2008). *Modulating presence and impulsiveness by external stimulation of the brain*. https://doi.org/10.1186/1744-9081-4-33

Benjamini, & Hochberg. (1995). Controlling the False Discovery Rate: A Practical and Powerful Approach to Multiple Testing. *Journal of the Royal Statistical Society. Series B (Methodological)*.

Bickel, W. K., Yi, R., Landes, R. D., Hill, P. F., & Baxter, C. (2011). Remember the future: Working memory training decreases delay discounting among stimulant addicts. *Biological Psychiatry*. https://doi.org/10.1016/j.biopsych.2010.08.017

Bikson, M., name, A., & Rahman, A. (2013). Origins of specificity during tDCS: anatomical, activity-selective, and input-bias mechanisms. *Frontiers in Human Neuroscience*, *7*(OCT), 688. https://doi.org/10.3389/fnhum.2013.00688

Bikson, M., Esmaeilpour, Z., Adair, D., Kronberg, G., Tyler, W. J., Antal, A., … Peterchev, A. V. (2019). Transcranial electrical stimulation nomenclature. *Brain Stimulation*. https://doi.org/10.1016/j.brs.2019.07.010

Bogler, C., Vowinkel, A., Zhutovsky, P., & Haynes, J. D. (2017). Default network activity is associated with better performance in a vigilance task. Frontiers in Human Neuroscience, 11, 623. https://doi.org/10.3389/FNHUM.2017.00623/BIBTEX

Borggaard, J. (2019). nelder_mead. Retrieved from Mathematics Department, Virginia Tech, Florida State University website: https://people.sc.fsu.edu/~jburkardt/m_src/nelder_mead/nelder_mead.html

Brooks, S. J., Wiemerslage, L., Burch, K., Maiorana, S., Cocolas, E., Schiöth, H., … Stein, D. (2017). The impact of cognitive training in substance use disorder: the effect of working memory training on impulse control in methamphetamine users. *Psychopharmacology*. https://doi.org/10.1007/s00213-017-4597-6

Buzsáki, & Draguhn, A. (2004). Neuronal oscillations in cortical networks. *Science*. https://doi.org/10.1126/science.1099745

Cabral-Calderin, Y., Williams, K. A., Opitz, A., Dechent, P., & Wilke, M. (2016). Transcranial alternating current stimulation modulates spontaneous low frequency fluctuations as measured with fMRI. *NeuroImage*. https://doi.org/10.1016/j.neuroimage.2016.07.005

Canolty, R. T., & Knight, R. T. (2010). The functional role of cross-frequency coupling. *Trends in Cognitive Sciences*. https://doi.org/10.1016/j.tics.2010.09.001

Chaieb, L., Antal, A., Pisoni, A., Saiote, C., Opitz, A., Ambrus, G. G., … Paulus, W. (2014). Safety of 5 kHz tACS. *Brain Stimulation*. https://doi.org/10.1016/j.brs.2013.08.004

Cohen, J. (1988). Statistical Power Analysis for the Behavioral Sciences. Statistical Power Analysis for the Behavioral Sciences. https://doi.org/10.4324/9780203771587

Cohen, J. D., Perlstein, W. M., Braver, T. S., Nystrom, L. E., Noll, D. C., Jonides, J., & Smith, E. E. (1997). Temporal dynamics of brain activation during a working memory task. *Nature*. https://doi.org/10.1038/386604a0

Datta, A., Bansal, V., Diaz, J., Patel, J., Reato, D., & Bikson, M. (2009). Gyri-precise head model of transcranial direct current stimulation: Improved spatial focality using a ring electrode versus conventional rectangular pad. *Brain Stimulation*. https://doi.org/10.1016/j.brs.2009.03.005

Datta, A., Elwassif, M., & Bikson, M. (2009). Bio-heat transfer model of transcranial DC stimulation: Comparison of conventional pad versus ring electrode. *Proceedings of the 31st Annual International Conference of the IEEE Engineering in Medicine and Biology Society: Engineering the Future of Biomedicine, EMBC 2009*. https://doi.org/10.1109/IEMBS.2009.5333673

Di, X., Biswal, B.B., 2017. Psychophysiological Interactions in a Visual Checkerboard Task: Reproducibility, Reliability, and the Effects of Deconvolution. Front Neurosci 11, 573.

Dmochowski, J. P., Datta, A., Bikson, M., Su, Y., & Parra, L. C. (2011). Optimized multi-electrode stimulation increases focality and intensity at target. *Journal of Neural Engineering*. https://doi.org/10.1088/1741-2560/8/4/046011

Ekhtiari, H., Nasseri, P., Yavari, F., Mokri, A., & Monterosso, J. (2016). Neuroscience of drug craving for addiction medicine: From circuits to therapies. In *Progress in Brain Research*. https://doi.org/10.1016/bs.pbr.2015.10.002

Fischer, A. S., Keller, C. J., & Etkin, A. (2016). The Clinical Applicability of Functional Connectivity in Depression: Pathways Toward More Targeted Intervention. *Biological Psychiatry: Cognitive Neuroscience and Neuroimaging*. https://doi.org/10.1016/j.bpsc.2016.02.004

Fischer, D. B., Fried, P. J., Ruffini, G., Ripolles, O., Salvador, R., Banus, J., Ketchabaw, W. T., Santarnecchi, E., Pascual-Leone, A., & Fox, M. D. (2017). Multifocal tDCS targeting the resting state motor network increases cortical excitability beyond traditional tDCS targeting unilateral motor cortex. *NeuroImage*, *157*, 34–44. https://doi.org/10.1016/j.neuroimage.2017.05.060

Frank, E., Wilfurth, S., Landgrebe, M., Eichhammer, P., Hajak, G., & Langguth, B. (2010). Anodal skin lesions after treatment with transcranial direct current stimulation. *Brain Stimulation*. https://doi.org/10.1016/j.brs.2009.04.002

Gbadeyan, O., Steinhauser, M., Mcmahon, K., & Meinzer, M. (2016). Safety, Tolerability, Blinding Efficacy and Behavioural Effects of a Novel MRI-Compatible, High-Definition tDCS Set-Up. *Brain Stimulation*. https://doi.org/10.1016/j.brs.2016.03.018

Glover, G. H. (2011). Overview of functional magnetic resonance imaging. In *Neurosurgery Clinics of North America* (Vol. 22, Issue 2, pp. 133–139). NIH Public Access. https://doi.org/10.1016/j.nec.2010.11.001

Goodin, P., Lamp, G., Hughes, M. E., Rossell, S. L., & Ciorciari, J. (2019). Decreased response to positive facial affect in a depressed cohort in the dorsal striatum during a working memory task—A preliminary fMRI study. *Frontiers in Psychiatry*, *10*(MAR), 60. https://doi.org/10.3389/fpsyt.2019.00060

Gregersen, F., Göksu, C., Schaefers, G., Xue, R., Thielscher, A., & Hanson, L. G. (2021). Safety evaluation of a new setup for transcranial electric stimulation during magnetic resonance imaging. *Brain Stimulation*, *14*(3), 488–497. https://doi.org/10.1016/j.brs.2021.02.019

Hansen, P., Kringelbach, M., & Salmelin, R. (2010). MEG: An introduction to methods. In *MEG: An Introduction to Methods*. Oxford University Press. https://doi.org/10.1093/acprof:oso/9780195307238.001.0001

Holmes, G. L., & Khazipov, R. (2007). Basic neurophysiology and the cortical basis of EEG. In *The Clinical Neurophysiology Primer*. https://doi.org/10.1007/978-1-59745-271-7_2

Huang, X. (2018). Robust simplex algorithm for online optimization. *Physical Review Accelerators and Beams*, *21*(10). https://doi.org/10.1103/PhysRevAccelBeams.21.104601

Hutchison, J. S., Ward, R. E., Lacroix, J., Hébert, P. C., Barnes, M. A., Bohn, D. J., … Skippen, P. W. (2008). Hypothermia therapy after traumatic brain injury in children. *New England Journal of Medicine*. https://doi.org/10.1056/NEJMoa0706930

Ieong, H. F. H., & Yuan, Z. (2017). Resting-state neuroimaging and neuropsychological findings in opioid use disorder during abstinence: A review. *Frontiers in Human Neuroscience*. https://doi.org/10.3389/fnhum.2017.00169

Ivry, R., Huang, Y., Liu, A. A., Lafon, B., Friedman, D., Dayan, M., Wang, X., Bikson, M., Doyle, W. K., Devinsky, O., & Parra, L. C. (2017). Measurements and models of electric fields in the in vivo human brain during transcranial electric stimulation. https://doi.org/10.7554/eLife.18834.001

Jaeggi, S. M., Buschkuehl, M., Perrig, W. J., & Meier, B. (2010). The concurrent validity of the N-back task as a working memory measure. *Memory*, *18*(4), 394–412. https://doi.org/10.1080/09658211003702171

Jaušovec, N., Jaušovec, K., & Pahor, A. (2014). The influence of theta transcranial alternating current stimulation (tACS) on working memory storage and processing functions. *Acta Psychologica*. https://doi.org/10.1016/j.actpsy.2013.11.011

Jefferys, J., Deans, J., Bikson, M., & Fox, J. (2003). Effects of weak electric fields on the activity of neurons and neuronal networks. Radiation Protection Dosimetry, 106(4), 321–323. https://doi.org/10.1093/OXFORDJOURNALS.RPD.A006367

Karabanov, A. N., Saturnino, G. B., Thielscher, A., & Siebner, H. R. (2019). Can transcranial electrical stimulation localize brain function? *Frontiers in Psychology*, Vol. 10, p. 213. https://doi.org/10.3389/fpsyg.2019.00213

Kessler, S. K., Turkeltaub, P. E., Benson, J. G., & Hamilton, R. H. (2011). *Differences in the Experience of Active and Sham Transcranial Direct Current Stimulation*. https://doi.org/10.1016/j.brs.2011.02.007

Klingberg, T., Fernell, E., Olesen, P. J., Johnson, M., Gustafsson, P., Dahlström, K., … Westerberg, H. (2005). Computerized training of working memory in children with ADHD - A randomized, controlled trial. *Journal of the American Academy of Child and Adolescent Psychiatry*. https://doi.org/10.1097/00004583-200502000-00010

Klingberg, T., Forssberg, H., & Westerberg, H. (2002). Training of working memory in children with ADHD. *Journal of Clinical and Experimental Neuropsychology*. https://doi.org/10.1076/jcen.24.6.781.8395

Kucyi, A., Hove, M. J., Esterman, M., Matthew Hutchison, R., & Valera, E. M. (2017). Dynamic Brain Network Correlates of Spontaneous Fluctuations in Attention. Cerebral Cortex, 27(3), 1831–1840. https://doi.org/10.1093/CERCOR/BHW029

Kunz, P., Antal, A., Hewitt, M., Neef, A., Opitz, A., & Paulus, W. (2017). 5 kHz transcranial alternating current stimulation: Lack of cortical excitability changes when grouped in a theta burst pattern. Frontiers in Human Neuroscience, 10, 683. https://doi.org/10.3389/FNHUM.2016.00683/BIBTEX

Kuo, M. F., & Nitsche, M. A. (2012). Effects of transcranial electrical stimulation on cognition. *Clinical EEG and Neuroscience*. https://doi.org/10.1177/1550059412444975

Kuo, M. F., Paulus, W., & Nitsche, M. A. (2014). Therapeutic effects of non-invasive brain stimulation with direct currents (tDCS) in neuropsychiatric diseases. In *NeuroImage* (Vol. 85, pp. 948–960). Academic Press Inc. https://doi.org/10.1016/j.neuroimage.2013.05.117

Kruschke, J. K. (2013). Bayesian estimation supersedes the t test. Journal of Experimental Psychology. General, 142(2), 573–603. https://doi.org/10.1037/A0029146

Lau-Zhu, A., Holmes, E. A., Butterfield, S., & Holmes, J. (2017). Selective Association Between Tetris Game Play and Visuospatial Working Memory: A Preliminary Investigation. https://doi.org/10.1002/acp.3339

Logothetis, N. K., Pauls, J., Augath, M., Trinath, T., & Oeltermann, A. (2001). Neurophysiological investigation of the basis of the fMRI signal. *Nature*, *412*(6843). https://doi.org/10.1038/35084005

Loo, C. K., Martin, D. M., Alonzo, A., Gandevia, S., Mitchell, P. B., & Sachdev, P. (2011). Avoiding skin burns with transcranial direct current stimulation: Preliminary considerations. *International Journal of Neuropsychopharmacology*. https://doi.org/10.1017/S1461145710001197

Lorenz, R., Simmons, L. E., Monti, R. P., Arthur, J. L., Limal, S., Laakso, I., … Violante, I. R. (2019). Efficiently searching through large tACS parameter spaces using closed-loop Bayesian optimization. *Brain Stimulation*. https://doi.org/10.1016/j.brs.2019.07.003

Luft, C. D. B., Zioga, I., & Bhattacharya, J. (2018). Anodal transcranial direct current stimulation (tDCS) boosts dominant brain oscillations. In *Brain Stimulation* (Vol. 11, Issue 3, pp. 660–662). Elsevier Inc. https://doi.org/10.1016/j.brs.2018.02.019

Mackowiak, P. A., Wasserman, S. S., & Levine, M. M. (1992). A Critical Appraisal of 98.6°F, the Upper Limit of the Normal Body Temperature, and Other Legacies of Carl Reinhold August Wunderlich. *JAMA: The Journal of the American Medical Association*. https://doi.org/10.1001/jama.1992.03490120092034

Mantini, D., Perrucci, M. G., Del Gratta, C., Romani, G. L., & Corbetta, M. (2007). Electrophysiological signatures of resting state networks in the human brain. *Proceedings of the National Academy of Sciences of the United States of America*. https://doi.org/10.1073/pnas.0700668104

Mathews, J. H., & Fink, K. K. (2004). Nelder-Mead method. In *Numerical Methods Using Matlab*.

McLaren, D.G., Ries, M.L., Xu, G., Johnson, S.C., 2012. A generalized form of context-dependent psychophysiological interactions (gPPI): A comparison to standard approaches. Neuroimage 61, 1277-1286.

MECMRI-Series. (2018). MECMRI-Series. Retrieved from BIOPAC Systems Inc website: https://www.biopac.com/wp-content/uploads/MECMRI-Series.pdf

Menon, V. (2011). Large-scale brain networks and psychopathology: A unifying triple network model. Trends in Cognitive Sciences, Vol. 15, pp. 483–506. https://doi.org/10.1016/j.tics.2011.08.003

Misaki, M., & Bodurka, J. (2021). The impact of real-time fMRI denoising on online evaluation of brain activity and functional connectivity. *Journal of Neural Engineering*, *18*(4), 046092. https://doi.org/10.1088/1741-2552/AC0B33

Misaki, M., Bodurka, J., & Paulus, M. P. (2022). A Library for fMRI Real-Time Processing Systems in Python (RTPSpy) With Comprehensive Online Noise Reduction, Fast and Accurate Anatomical Image Processing, and Online Processing Simulation. *Frontiers in Neuroscience, 16*. doi:10.3389/fnins.2022.834827

Moisa, M., Polania, R., Grueschow, M., & Ruff, C. C. (2016). Brain network mechanisms underlying motor enhancement by transcranial entrainment of gamma oscillations. *Journal of Neuroscience*. https://doi.org/10.1523/JNEUROSCI.2044-16.2016

Moliadze, V., Atalay, D., Antal, A., & Paulus, W. (2012). Close to threshold transcranial electrical stimulation preferentially activates inhibitory networks before switching to excitation with higher intensities. *Brain Stimulation: Basic, Translational, and Clinical Research in Neuromodulation*, *5*(4), 505–511. https://doi.org/10.1016/J.BRS.2011.11.004

Monti, R. P., Lorenz, R., Braga, R. M., Anagnostopoulos, C., Leech, R., & Montana, G. (2017).

Real-time estimation of dynamic functional connectivity networks. *Human Brain Mapping*. https://doi.org/10.1002/hbm.23355

Mulyana, B., Tsuchiyagaito, A., Smith, J., Misaki, M., Kuplicki, R., Soleimani, G., Rashedi, A., Shereen, D., Bergman, T. O., Cheng, S., Paulus, M., Bodurka, J., & Ekhtiari, H. (2021). Online Closed-Loop Real-Time tES-fMRI for Brain Modulation: Feasibility, Noise/Safety and Pilot Study. *BioRxiv*, 2021.04.10.439268. https://doi.org/10.1101/2021.04.10.439268

Nelder, J. A., & Mead, R. (1965). A Simplex Method for Function Minimization. *The Computer Journal*. https://doi.org/10.1093/comjnl/7.4.308

Neri, F., Mencarelli, L., Menardi, A., Giovannelli, F., Rossi, S., Sprugnoli, G., … Santarnecchi, E. (2020). A novel tDCS sham approach based on model-driven controlled shunting. *Brain Stimulation*. https://doi.org/10.1016/j.brs.2019.11.004

Nitsche, M. A., Boggio, P. S., Fregni, F., & Pascual-Leone, A. (2009). Treatment of depression with transcranial direct current stimulation (tDCS): A Review. In *Experimental Neurology* (Vol. 219, Issue 1, pp. 14–19). Academic Press. https://doi.org/10.1016/j.expneurol.2009.03.038

Noury, N., Hipp, J. F., & Siegel, M. (2016). Physiological processes non-linearly affect electrophysiological recordings during transcranial electric stimulation. *NeuroImage*, *140*, 99–109. https://doi.org/10.1016/j.neuroimage.2016.03.065

Noury, N., & Siegel, M. (2017). Phase properties of transcranial electrical stimulation artifacts in electrophysiological recordings. *NeuroImage*, *158*, 406–416. https://doi.org/10.1016/j.neuroimage.2017.07.010

O'connell, N. E., Cossar, J., Marston, L., Wand, B. M., Bunce, D., Moseley, G. L., & De Souza, L. H. (2012). Rethinking Clinical Trials of Transcranial Direct Current Stimulation: Participant and Assessor Blinding Is Inadequate at Intensities of 2mA. https://doi.org/10.1371/journal.pone.0047514

Owen, A. M., McMillan, K. M., Laird, A. R., & Bullmore, E. (2005). N-back working memory paradigm: A meta-analysis of normative functional neuroimaging studies. *Human Brain Mapping*, *25*(1), 46–59. https://doi.org/10.1002/hbm.20131

Ozen, S., Sirota, A., Belluscio, M. A., Anastassiou, C. A., Stark, E., Koch, C., & Buzsáki, G. (2010). Behavioral/Systems/Cognitive Transcranial Electric Stimulation Entrains Cortical Neuronal Populations in Rats. https://doi.org/10.1523/JNEUROSCI.5252-09.2010

Parks, E. L., & Madden, D. J. (2013). Brain connectivity and visual attention. Brain Connectivity, 3(4), 317–338. https://doi.org/10.1089/BRAIN.2012.0139

Piervirgili, G., Petracca, F., & Merletti, R. (2014). A new method to assess skin treatments for lowering the impedance and noise of individual gelled Ag-AgCl electrodes. *Physiological Measurement*. https://doi.org/10.1088/0967-3334/35/10/2101

Pillai, J. A., Hall, C. B., Dickson, D. W., Buschke, H., Lipton, R. B., & Verghese, J. (2011). *Association of Crossword Puzzle Participation with Memory Decline in Persons Who Develop Dementia*. https://doi.org/10.1017/S1355617711001111

Poreisz, C., Boros, K., Antal, A., & Paulus, W. (2007). Safety aspects of transcranial direct current stimulation concerning healthy subjects and patients. *Brain Research Bulletin*. https://doi.org/10.1016/j.brainresbull.2007.01.004

Prabhakaran, V., Narayanan, K., Zhao, Z., & Gabriel, J. D. E. (2000). Integration of diverse information in working memory within the frontal lobe. *Nature Neuroscience*. https://doi.org/10.1038/71156

Price, C. J., Coope, I. D., & Byatt, D. (2002). A convergent variant of the Nelder-Mead algorithm. *Journal of Optimization Theory and Applications*, *113*(1). https://doi.org/10.1023/A:1014849028575

Reato, D., Gasca, F., Datta, A., Bikson, M., Marshall, L., & Parra, L. C. (2013). Transcranial Electrical Stimulation Accelerates Human Sleep Homeostasis. *PLoS Computational Biology*, *9*(2). https://doi.org/10.1371/journal.pcbi.1002898

Reato, D., Rahman, A., Bikson, M., & Parra, L. C. (2010). Low-intensity electrical stimulation affects network dynamics by modulating population rate and spike timing. *Journal of Neuroscience*, *30*(45), 15067–15079. https://doi.org/10.1523/JNEUROSCI.2059-10.2010

Rosenberg, M. D., Scheinost, D., Greene, A. S., Avery, E. W., Kwon, Y. H., Finn, E. S., … Chun, M. M. (2020). Functional connectivity predicts changes in attention observed across minutes, days, and months. Proceedings of the National Academy of Sciences, 117(7), 3797–3807. https://doi.org/10.1073/PNAS.1912226117

Ruffini, G., Fox, M. D., Ripolles, O., Miranda, P. C., & Pascual-Leone, A. (2014). Optimization of multifocal transcranial current stimulation for weighted cortical pattern targeting from realistic modeling of electric fields. *NeuroImage*. https://doi.org/10.1016/j.neuroimage.2013.12.002

Saiote, C., Turi, Z., Paulus, W., & Antal, A. (2013). Combining functional magnetic resonance imaging with transcranial electrical stimulation. *Frontiers in Human Neuroscience*. https://doi.org/10.3389/fnhum.2013.00435

Saturnino, G. B., Puonti, O., Nielsen, J. D., Antonenko, D., Madsen, K. H., & Thielscher, A. (2019). SimNIBS 2.1: A Comprehensive Pipeline for Individualized Electric Field Modelling for Transcranial Brain Stimulation. In *Brain and Human Body Modeling*. https://doi.org/10.1007/978-3-030-21293-3_1

Saturnino, Madsen, K. H., Siebner, H. R., & Thielscher, A. (2017). How to target inter-regional phase synchronization with dual-site Transcranial Alternating Current Stimulation. *NeuroImage*. https://doi.org/10.1016/j.neuroimage.2017.09.024

Saturnino, Madsen, K., & Thielscher, A. (2019). Efficient Electric Field Simulations for Transcranial Brain Stimulation. *BioRxiv*. https://doi.org/10.1101/541409

Sauseng, P., Klimesch, W., Schabus, M., & Doppelmayr, M. (2005). Fronto-parietal EEG coherence in theta and upper alpha reflect central executive functions of working memory. *International Journal of Psychophysiology*. https://doi.org/10.1016/j.ijpsycho.2005.03.018

Shafi, M. M., Westover, M. B., Fox, M. D., & Pascual-Leone, A. (2012). Exploration and modulation of brain network interactions with noninvasive brain stimulation in combination with neuroimaging. *European Journal of Neuroscience*, Vol. 35, pp. 805–825. https://doi.org/10.1111/j.1460-9568.2012.08035.x

Singer, S., & Nelder, J. (2009). Nelder-Mead algorithm. *Scholarpedia*. https://doi.org/10.4249/scholarpedia.2928

Singh, S. P. (2014). Magnetoencephalography: Basic principles. *Annals of Indian Academy of Neurology*, *17*(SUPPL. 1), S107. https://doi.org/10.4103/0972-2327.128676

Soleimani, G., Kupliki, R., Bodurka, J., Paulus, M., & Ekhtiari, H. (2021). fMRI Informed Montage Selection for Transcranial Electrical Stimulation: Frontoparietal Synchronization for Drug Cue Reactivity. *BioRxiv*.

Splittgerber, M., Suwelack, J. H., Kadish, N. E., & Moliadze, V. (2020). The Effects of 1mA tACS and tRNS on Children/Adolescents and Adults: Investigating Age and Sensitivity to Sham Stimulation. https://doi.org/10.1155/2020/8896423

Stagg, C. J., & Nitsche, M. A. (2011). Physiological basis of transcranial direct current stimulation. In *Neuroscientist* (Vol. 17, Issue 1, pp. 37–53). Neuroscientist. https://doi.org/10.1177/1073858410386614

Tan, J., Wansbrough, K., Williams, A. G., Nitsche, M. A., Vallence, A. M., & Fujiyama, H. (2020a). The importance of model-driven approaches to set stimulation intensity for multi-channel transcranial alternating current stimulation (tACS). In *Brain Stimulation* (Vol. 13, Issue 4, pp. 1002–1004). Elsevier Inc. https://doi.org/10.1016/j.brs.2020.04.001

Tan, J., Wansbrough, K., Williams, A. G., Nitsche, M. A., Vallence, A. M., & Fujiyama, H. (2020b). The importance of model-driven approaches to set stimulation intensity for multi-channel transcranial alternating current stimulation (tACS). In *Brain Stimulation* (Vol. 13, Issue 4, pp. 1002–1004). Elsevier Inc. https://doi.org/10.1016/j.brs.2020.04.001

Teplan, M. (2002). Fundamentals of EEG measurement. *Measurement Science Review*.

Thielscher, A., Antunes, A., & Saturnino, G. B. (2015). Field modeling for transcranial magnetic stimulation: A useful tool to understand the physiological effects of TMS? *Proceedings of the Annual International Conference of the IEEE Engineering in Medicine and Biology Society, EMBS*. https://doi.org/10.1109/EMBC.2015.7318340

Villamar, M. F., Volz, M. S., Bikson, M., Datta, A., Dasilva, A. F., & Fregni, F. (2013). Technique and considerations in the use of 4x1 ring high-definition transcranial direct current stimulation (HD-tDCS). *Journal of Visualized Experiments: JoVE*. https://doi.org/10.3791/50309

Violante, I. R., Li, L. M., Carmichael, D. W., Lorenz, R., Leech, R., Hampshire, A., … Sharp, D. J. (2017). Externally induced frontoparietal synchronization modulates network dynamics and enhances working memory performance. *ELife*. https://doi.org/10.7554/eLife.22001

Vosskuhl, J., Huster, R. J., & Herrmann, C. S. (2016). BOLD signal effects of transcranial alternating current stimulation (tACS) in the alpha range: A concurrent tACS–fMRI study. *NeuroImage*. https://doi.org/10.1016/j.neuroimage.2015.10.003

Wagner, T. A., Zahn, M., Grodzinsky, A. J., & Pascual-Leone, A. (2004). Three-dimensional head model simulation of transcranial magnetic stimulation. *IEEE Transactions on Biomedical Engineering*. https://doi.org/10.1109/TBME.2004.827925

Weinrich, C. A., Brittain, J. S., Nowak, M., Salimi-Khorshidi, R., Brown, P., & Stagg, C. J. (2017). Modulation of Long-Range Connectivity Patterns via Frequency-Specific Stimulation of Human Cortex. *Current Biology*. https://doi.org/10.1016/j.cub.2017.08.075

Weiss, F., Zamoscik, V., Schmidt, S. N. L., Halli, P., Kirsch, P., & Gerchen, M. F. (2020). Just a very expensive breathing training? Risk of respiratory artefacts in functional connectivity-based real-time fMRI neurofeedback. NeuroImage, 210, 116580. https://doi.org/10.1016/J.NEUROIMAGE.2020.116580

Whitman, J. C., Ward, L. M., & Woodward, T. (2013). Patterns of cortical oscillations organize neural activity into whole-brain functional networks evident in the fMRI BOLD signal. *Frontiers in Human Neuroscience*. https://doi.org/10.3389/fnhum.2013.00080

Williams, K. A., Cabral-Calderin, Y., Schmidt-Samoa, C., Weinrich, C. A., Dechent, P., & Wilke, M. (2017). Simultaneous transcranial alternating current stimulation and functional magnetic resonance imaging. *Journal of Visualized Experiments*. https://doi.org/10.3791/55866

Womelsdorf, T., Schoffelen, J. M., Oostenveld, R., Singer, W., Desimone, R., Engel, A. K., & Fries, P. (2007). Modulation of neuronal interactions through neuronal synchronization. *Science*. https://doi.org/10.1126/science.1139597

Yavari, F., Nitsche, M. A., & Ekhtiari, H. (2017). Transcranial electric stimulation for precision

medicine: A spatiomechanistic framework. *Frontiers in Human Neuroscience, 11*. https://doi.org/10.3389/fnhum.2017.00159

Yuan, H., Ding, L., Zhu, M., Zotev, V., Phillips, R., & Bodurka, J. (2016). Reconstructing Large-Scale Brain Resting-State Networks from High-Resolution EEG: Spatial and Temporal Comparisons with fMRI. *Brain Connectivity*, *6*(2), 122–135. https://doi.org/10.1089/brain.2014.0336

Yuan, H., Zotev, V., Phillips, R., Drevets, W. C., & Bodurka, J. (2012). Spatiotemporal dynamics of the brain at rest - Exploring EEG microstates as electrophysiological signatures of BOLD resting state networks. *NeuroImage*, *60*(4), 2062–2072. https://doi.org/10.1016/j.neuroimage.2012.02.031

Zoefel, B., Archer-Boyd, A., & Davis, M. H. (2018). Phase Entrainment of Brain Oscillations Causally Modulates Neural Responses to Intelligible Speech. *Current Biology*. https://doi.org/10.1016/j.cub.2017.11.071